NAVAL POSTGRADUATE SCHOOL
Monterey, California

THESIS

A LABVIEW© BASED WIND TUNNEL DATA ACQUISITION SYSTEM

by

Michael R. Huff

September 1998

Thesis Advisor: Conrad F. Newberry

Approved for public release; distribution is unlimited.

REPORT DOCUMENTATION PAGE

Form Approved
OMB No. 0704-0188

1. AGENCY USE ONLY *(Leave blank)*	2. REPORT DATE	3. REPORT TYPE AND DATES COVERED
	September 1998	Master's Thesis

4. TITLE AND SUBTITLE
A LABVIEW© BASED WIND TUNNEL DATA ACQUISITION SYSTEM

5. FUNDING NUMBERS

6. AUTHOR(S)
Huff, Michael R.

7. PERFORMING ORGANIZATION NAME(S) AND ADDRESS(ES)
Naval Postgraduate School
Monterey, CA 93943-5000

8. PERFORMING ORGANIZATION REPORT NUMBER

9. SPONSORING / MONITORING AGENCY NAME(S) AND ADDRESS(ES)

10. SPONSORING/MONITORING AGENCY REPORT NUMBER

11. SUPPLEMENTARY NOTES
The views expressed in this thesis are those of the author and do not reflect the official policy or position of the Department of Defense or the U.S. Government.

12a. DISTRIBUTION / AVAILABILITY STATEMENT
Approved for public release; distribution unlimited.

12b. DISTRIBUTION CODE

13. ABSTRACT ***(Maximum 200 words)***

The NPS Aerolab® Low Speed Wind Tunnel located in Halligan Hall of the Naval Postgraduate School has been in operation since 1953. Although the tunnel is well maintained, its data acquisition system has not kept pace with modern technology. An effective but affordable solution for acquiring data was needed. It was determined that a software package known as LabVIEW© provides a low cost, data acquisition solution that will enhance the capabilities of the wind tunnel, while at the same time making it more user friendly to faculty and students. The focus of this thesis is the design of a LabVIEW© program that will collect and plot force and moment data from a six-component strain gauge balance and yield real time, non-dimensional, force and moment coefficients in six degrees of freedom. Wind tunnel tests consisting of α sweeps in the NPS Aerolab® low-speed wind tunnel were conducted to verify $(L/D)I_{sp}$ optimized, $M_\infty = 6$, conical-flow waverider data obtained in 1994 using a different data acquisition system. Results of current testing substantiate the validity of the 1994 test data. Analysis of the current data set resolved pitching moment concerns related to the 1994 data.

14. SUBJECT TERMS
LabVIEW©, VI, Data Acquisition, Strain Gauge Balance, Wind Tunnel, Waverider, Lift, Drag, Aeromoments.

15. NUMBER OF PAGES
131

16. PRICE CODE

17. SECURITY CLASSIFICATION OF REPORT	18. SECURITY CLASSIFICATION OF THIS PAGE	19. SECURITY CLASSIFICATION OF ABSTRACT	20. LIMITATION OF ABSTRACT
Unclassified	Unclassified	Unclassified	UL

Approved for public release; distribution is unlimited

A LABVIEW© BASED WIND TUNNEL DATA ACQUISITION SYSTEM

Michael R. Huff
Lieutenant, United States Navy
B.S., University of Illinois, 1989

Submitted in partial fulfillment of the
requirements for the degree of

MASTERS OF SCIENCE IN AERONAUTICAL ENGINEERING

from the

NAVAL POSTGRADUATE SCHOOL
September 1998

Author: _____
Michael R. Huff

Approved by: _____
Conrad F. Newberry, Thesis Advisor

_____
Richard M. Howard, Second Reader

_____
Gerald H. Lindsey, Chairman
Department of Aeronautics and Astronautics

ABSTRACT

The NPS Aerolab® Low Speed Wind Tunnel located in Halligan Hall of the Navy Postgraduate school has been in operation since 1953. Although the tunnel is well maintained, its data acquisition system has not kept pace with modern technology. An effective but affordable solution for acquiring data was needed. It was determined that a software package known as LabVIEW© would provide a low cost, data acquisition solution that will enhance the capabilities of the wind tunnel, while at the same time making it more user friendly to faculty and students. The focus of this thesis is the design of a VI that will collect and plot force and moment data from a six component strain gauge balance and yield real time, non-dimensional, force and moment coefficients in six degrees of freedom. Wind tunnel tests consisting of angle-of-attack sweeps in the NPS Aerolab® low-speed wind tunnel were conducted to verify $(L/D)I_{sp}$ optimized, $M_\infty = 6$, conical-flow waverider data obtained in 1994 using a different data acquisition system. Results of current testing substantiate the LabVIEW© code and the validity of the 1994 test data. Analysis of the current wind tunnel test data resolved pitching moment concerns related to the 1994 data.

TABLE OF CONTENTS

LIST OF TABLES

LIST OF FIGURES

LIST OF ABBREVIATIONS AND ACRONYMS

α	Angle Of Attack
AOA	Angle Of Attack (used when α font unavailable)
AX	Axial Force Strain Gauge Element
b	Wingspan (13.9375 in)
c	Root chord (length of model, 15 in)
$\bar{c}$	Mean Aerodynamic Chord (12.05 in)
C_A	Non-dimensional Axial Force Coefficient
C_D	Non-dimensional Drag Force Coefficient
C_L	Non-dimensional Lift Force Coefficient
C_M	Non-dimensional Pitching Moment Coefficient
C_N	Non-dimensional Normal Force Coefficient
DAQ	Data Acquisition Board
Δp	Static pressure difference (cm H_20)
ε	Wind Tunnel Blockage Correction Factor
K	NPS wind tunnel calibration constant.
L/D	Lift to Drag ratio
LoFLYTE	Low Observable Flight Test Equipment (A waverider)
NI	National Instruments©
N1, N2	Normal Force Strain Gauge Elements
q	Dynamic pressure (lbf/ft^2)
ρ_∞	Freestream density ($slugs/ft^3$)
RM	Rolling Moment Strain gauge Element
S	Model Planform Area
S1, S2	Side Force Strain Gauge Elements
SC-2043-SG	Signal Conditioning (SC) Board
V_∞	Freestream velocity (ft/s)
VI	Virtual Instrument

ACKNOWLEDGEMENTS

It is with the utmost appreciation that I wish to thank the following individuals for the assistance given me during this endeavor. First I must thank Professor Newberry for the knowledge, support and patience he displayed during the development of this thesis. He was thoroughly professional in giving me guidance when needed, yet allowed me to venture forth and learn without spoon-feeding. I can not imagine choosing a better thesis advisor. Much the same can be said for Professor Howard, whose advice pointed me in the right direction on numerous occasions. His understanding of stability and control issues was certainly a great asset. Next I wish to thank Dr. Anthony Dietz from NASA Ames for the superb help he gave me during the creation of the LabVIEW© program. His expertise and willingness to help proved invaluable and will always be remembered. Finally, my greatest appreciation goes to my wife Stacy, whose love and support kept me going during the times when I most needed inspiration. It is to her that I give the most credit for completion of this project.

I. INTRODUCTION

A. THE NEED FOR AN IMPROVED DATA ACQUISITION SYSTEM

Perhaps the most challenging part of wind tunnel experimentation is acquiring data that can be easily processed and analyzed. The wind tunnel data acquisition system in use prior to this thesis utilized an IBM© PS2 computer with an installed data acquisition card for obtaining the data. In this manner it was similar to a typical PC based system, but in other areas its differences were readily apparent.

The operating system of the IBM PS2 is not compatible with today's PC, complicating data retrieval into existing spreadsheet and computational programs. This incompatibility carried over to the data acquisition program, Microsoft Quick Basic, used by the PS2. Quick Basic is a programming language not familiar to most faculty and students using the wind tunnel nor typical of a modern data acquisition system. The output of the program yielded only dimensional forces and moments. The user would then have to non-dimensionalize the results off-line using another software application, which also meant that real time results could not be displayed during the data acquisition process in order to compare test values with expected results.

Most important however, the PS2's hard drive was no longer functioning (it was broken). With the above factors in mind, it was thought more beneficial to develop another data acquisition system for the wind tunnel rather than try to repair the existing one, if costs could be kept reasonable. Developing a new system would create an

opportunity to update data acquisition methods for the wind tunnel and eliminate the negative aspects germane to the previous system. A software package known as LabVIEW© was found to have the attributes most needed to overcome the previous system's inadequacies, and had already been purchased for another application. What remained would be to develop an application that would fulfill the requirements of a wind tunnel data acquisition system.

The goals kept in mind when developing a LabVIEW© application for the wind tunnel were to provide the user with a well-documented and easily manipulated program. The program is fully compatible with and functions under the Windows© operating system, allowing data retrieval onto portable media that can be processed on any home/office PC. Even more important, however, was the need to make results available to the user while the data is being acquired. Real time display of all intermediate steps, as well as final results, allows the user to troubleshoot areas of concern and pinpoint sources of technical problems regarding the testing. Having all intermediate steps available also allows the user to determine how various aspects of the data contribute to the final non-dimensionalized results.

B. LABVIEW© GRAPHICAL INSTRUMENTATION PROGRAM

LabVIEW© is a program development application, much like various commercial development systems such as C or BASIC. However, LabVIEW© is different from those applications in one important respect. Other programming systems use *text-based* languages to create lines of code, while LabVIEW© uses a *graphical* programming

language, G, to create programs in block diagram form [Ref. 1]. The implication is that once designed, a LabVIEW© program will offer a simple method for acquiring and processing data obtained from the wind tunnel or other devices.

LabVIEW© relies on graphical symbols rather than textual language to describe programming actions. There are extensive libraries of functions and subroutines included with the software package for many programming tasks. LabVIEW© contains application specific libraries for data acquisition, instrument control and analysis. Also included in the software are many conventional program development tools to set breakpoints, animate program execution to see how data passes through the program, and single-step through the program to make debugging and program development easier.

LabVIEW© programs are called *virtual instruments (VIs)* because their appearance and operation imitate actual instruments. VIs have both an interactive user interface and a source code equivalent, and accept parameters from higher-level VIs. The following are descriptions of these VI features as taken from the LabVIEW© User Manual [Ref. 1].

1. VIs contain an interactive interface between the user and software which is called the *front panel* because it simulates the panel of a physical instrument. The front panel can contain knobs, push buttons, graphs, and other controls and indicators. Data is acquired by the front panel via the keyboard and mouse; the results can be viewed on the computer screen.

2. VIs receive instructions from a *block diagram,* which is constructed in LabVIEW©'s programming language, "G." The block diagram supplies a pictorial

solution to a programming problem, and depicts graphically the written code familiar to most programmers, e.g., "while loops," "for loops," "if/then cases," "formula nodes," etc. The means whereby the front panel items are wired to the rest of the program are also displayed. In other words, the block diagram contains the source code for a given VI.

3. VIs use a hierarchical and modular structure. They can be developed and used as top-level programs, or as subprograms within other programs or subprograms. When a VI is encapsulated within another VI it is called a *subVI.* The *icon and connector pane* of a VI work like a graphical parameter list so that other VIs can pass data to it as a *subVI.* The above descriptions collectively comprise what is known as *modular programming.* Modularity in this case leads to dividing an application into a series of tasks, which can be further broken down in a hierarchical manner again until a complicated application comprises a number of simple subtasks. In the present case, the overarching VI's task is to acquire, process, display and save force and moment data. Various *subVIs* acquire the voltages, perform the interactions, plot the graphs, append to spreadsheets, etc. Many of the more complicated *subVIs* contain *subVIs* of their own. Note that it is not mandatory to create *subVIs.* The program could execute as one very large and cumbersome VI. However, since each *subVI* can be executed by itself apart from the rest of the application, debugging is much easier.

C. TESTING MOTIVATION

Two major aspects were covered in this thesis; validating the LabVIEW© program and verifying the accuracy of data obtained through the LabVIEW© methodology as compared to the previous data acquisition program. With regard to the LabVIEW© program, the first step was to confirm that the VI correctly yields the desired results when known values are inputted. A comparison was made to the Quick Basic code used by the former data acquisition system to confirm similarity of results. Full validation of the code was accomplished when the VI demonstrated the capability to correctly acquire and process the data from the wind tunnel.

The second aspect concerns verifying the results obtained on the Price Waverider by Cedrun [Ref. 2]. Based upon the theoretical potential of Price's design, NASA Ames constructed two aluminum models for testing Price's design at the Naval Postgraduate School. A 15-inch long aluminum model was developed for wind tunnel testing and an 8-inch long model was made for water tunnel testing. Cedrun tested the wind tunnel model in 1994. General results agreed favorably with HAVOC predicted values for the Price waverider and previous wind tunnel testing of Vanhoy's waverider and conventional delta wing configurations [Ref. 2]. Questions did arise concerning pitching moment instability and flow separation, both of which occurred at an AOA lower than expected. In addition, axial forces were often negative, even at low angles of attack. Therefore this thesis will attempt to validate Cedrun's results with the improved data acquisition techniques available using LabVIEW©.

D. WHY LOW-SPEED TESTING

The Naval Postgraduate School (NPS) Aerolab® wind tunnel is only capable of up to 200 mph maximum speed. In addition, the hardware used in the tunnel to acquire data is capable of handling only limited forces and would be damaged by the forces generated by a higher speed tunnel. Either of these constraints limits the testing conditions to low subsonic flight, but this is still sufficient to validate the performance of the LabVIEW© VI.

Waverider configurations are the result of "on-design" optimization; that is, they are typically optimized for flight at specific design Mach number. Theoretical flight performance results are thus based upon a specified set of operational conditions including altitude, flight speed and α. Reality dictates that aircraft flight is a dynamic process. Included in this process are maneuvers or flight conditions that require low flight speed, at the very minimum, takeoffs and landings. In general, there is very little knowledge of how well suited the hypersonic derived, geometrical characteristics of waveriders are for acceptable subsonic performance. This provides a further rationale for testing a hypersonic configuration at lower subsonic speeds.

II. EXPERIMENTAL APPARATUS

A. WIND TUNNEL

The NPS horizontal low-speed wind tunnel located in Halligan Hall was used for conducting all experiments. Manufactured by Aerolab® Development Company in the early 1950s, it is a single return, closed circuit tunnel [Ref. 3]. Air flow through the tunnel is provided by a 100-hp electric motor that drives a three-blade, variable pitch fan. A four-gear transmission and a 10:1 contraction ratio allow for test section speeds of up to 200 miles per hour.

Closed circuit wind tunnels require special considerations to reduce turbulence intensity in the test section. The NPS tunnel accomplishes this through use of stator blades located directly behind the fan, two fine wire mesh screens six inches apart in the settling chamber and turning vanes located at each corner of the tunnel. As a result, a test section ambient turbulence intensity of 0.2 % is achieved [Ref. 4].

The wind tunnel test section has an area of 8.75ft^2 (45 inches wide by 28 inches in height) and is therefore approximately 1/10th the cross sectional area of the settling chamber. The test section walls are slightly divergent fore to aft to compensate for the effective contraction caused by longitudinal boundary layer growth. Typical of most low speed tunnels, leakage occurs through the duct walls, which uncorrected would drop pressure below atmospheric in the test section. A breather slot located immediately downstream of the tunnel test section helps provide a return mechanism for lost air.

Adequate illumination, visualization and access to the test model are provided by frosted glass corner fillet fluorescent lights and movable window tunnel sidewalls located on either side of the test section. A schematic of the tunnel is presented in Figure 2.1 and a complete description of all wind tunnel characteristics is covered in the NPS Wind Tunnel Lab Manual [Ref. 3].

Wind tunnel air temperature is measured by use of a dial thermometer extended into the settling chamber. The test section dynamic pressure, $q = \frac{1}{2}\rho_\infty V_\infty^2$, is determined from the static pressure difference, Δp, between four manifold-flush static taps in the test section and a similar set of four taps in the settling chamber. Both sets of taps are connected to a common manifold and the value for Δp is presented on a micromanometer. The Δp is converted into dynamic pressure using equation (2.1) and a calibration constant calculated from a 1998 wind tunnel calibration experiment.

$$q = \frac{1}{2}\rho_\infty V_\infty^2 = 2.046\ K\ \Delta p \qquad (2.1)$$

where: q = dynamic pressure (lbf/ft^2)

ρ_∞ = freestream density ($slugs/ft^3$)

V_∞ = freestream velocity (ft/s)

K = NPS wind tunnel calibration constant.

= 1/0.9012 = 1.109632

2.046 = conversion factor (cm H_2O to lbf/ft^2)

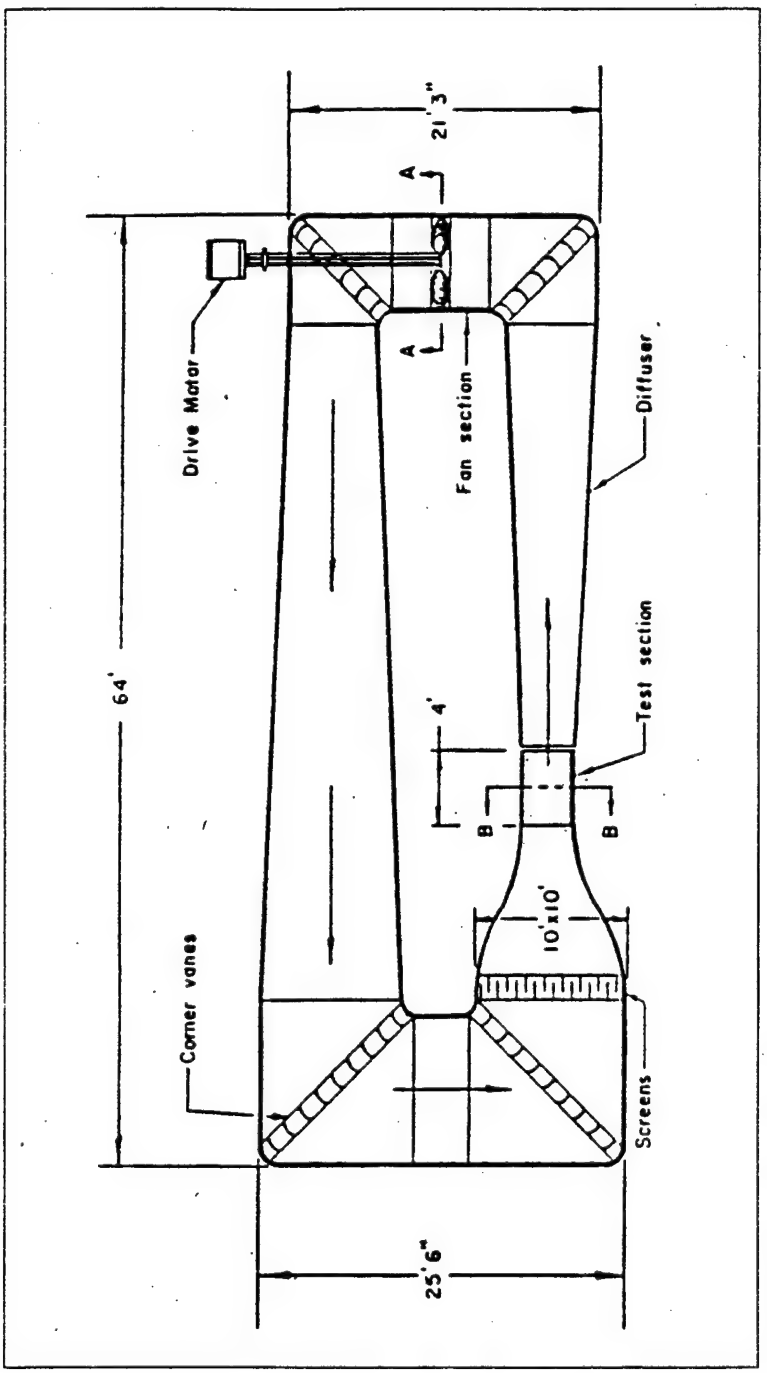

Figure 2.1 NPS Low Speed Wind Tunnel

B. STRAIN GAUGE BALANCE AND ASSEMBLY

Force and moment measurements were obtained by means of a six component internal strain gauge balance. The balance, on loan from NASA Ames and manufactured by Task Corporation, measures .75 inches in diameter and is a floating-frame type as pictured in Figure 2.2 on the following page. This frame consists of an inner rod that is fastened to the support sting and an outer casing that is inserted into the waverider model. Forces and moments are obtained by measuring the resistance of the elements connected between the inner rod and outer casing.

All gauged sections of the balance used during experimentation utilize bending, 4-active foil type, epoxy bonded, 350 ohm (Ω) strain gauges. The two normal force elements (N1 and N2) use 350 Ω bridge resistance for determining normal force and pitching moment, as do the two side force elements (S1 and S2) for side force and yawing moment. The dual axial element (AX) and dual rolling element (RM) each use two full wheatstone bridges wired in parallel with a corresponding resistance of 175 Ω for determining drag and rolling moment respectfully. The coordinate system within which these forces are defined is shown in Figure 2.3. Wiring for each channel consists of four, 36 gauge wires, two for the excitation voltage to the balance and two for output voltage from the balance to the strain gauge signal conditioner.

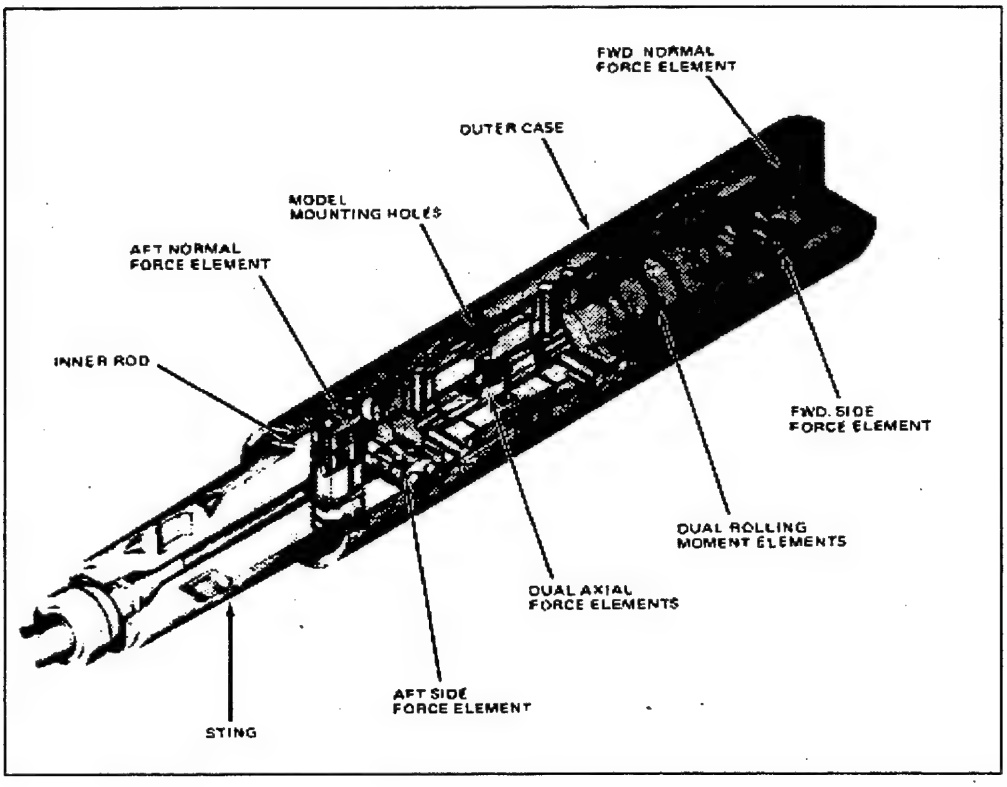

Figure 2.2 Sting Balance

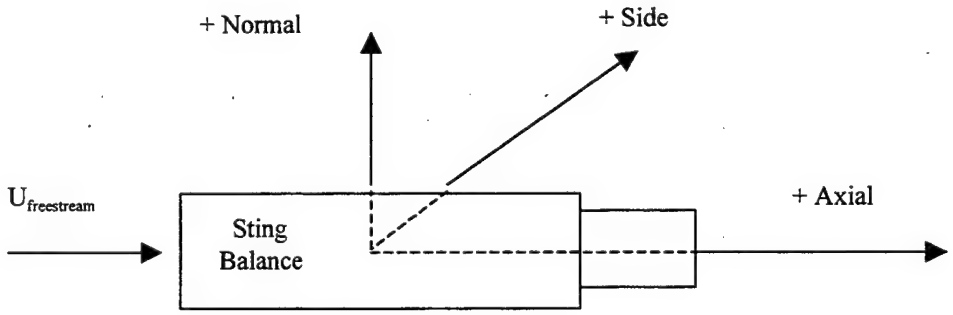

Figure 2.3 Sting Balance Coordinate System

The six output channels of the strain gage balance; N1, N2, S1, S2, AX and RM, were calibrated at the NASA Ames Calibration Laboratory prior to release of the balance to the Naval Postgraduate School. The excitation voltage for the calibration procedure was 5 volts direct current (V_{DC}) with interaction constants determined iteratively during calibration. The interaction coefficients determined by the NASA Ames calibration are presented in Appendix A. This calibration can be verified by placing known loads on the balance and comparing them to results displayed on the front panel (computer screen).

The balance is attached via a 6.875 inch extender sleeve to a yoke assembly that, in turn, is mounted in the wind tunnel test section as shown in Figure 2.4. Four machine screws secure the bottom of the assembly to a turntable mechanism in the test section. Depending on the orientation of the model, the turntable facilitates measurement of yaw and angle-of-attack (AOA). The top of the yoke fits through a circular cutout in the ceiling of the test section, allowing rotation by the turntable but restricting any other unwanted movement. All 24 wires from the strain gauge balance are fed through the sleeve, yoke assembly and then out of the tunnel though the breather (or ventilation) slot at the end of the test section. Enough slack in the wire bundle was allowed for $\pm$ 90° angle of rotation.

C. STRAIN GAUGE SIGNAL CONDITIONING BOARD

Once outside the wind tunnel, the 24 wires from the strain gauge balance are routed to a National Instruments Strain Gauge Signal Conditioning (SC) Board, model # SC-2043-SG. The purpose of signal conditioning is to interface and properly prepare the

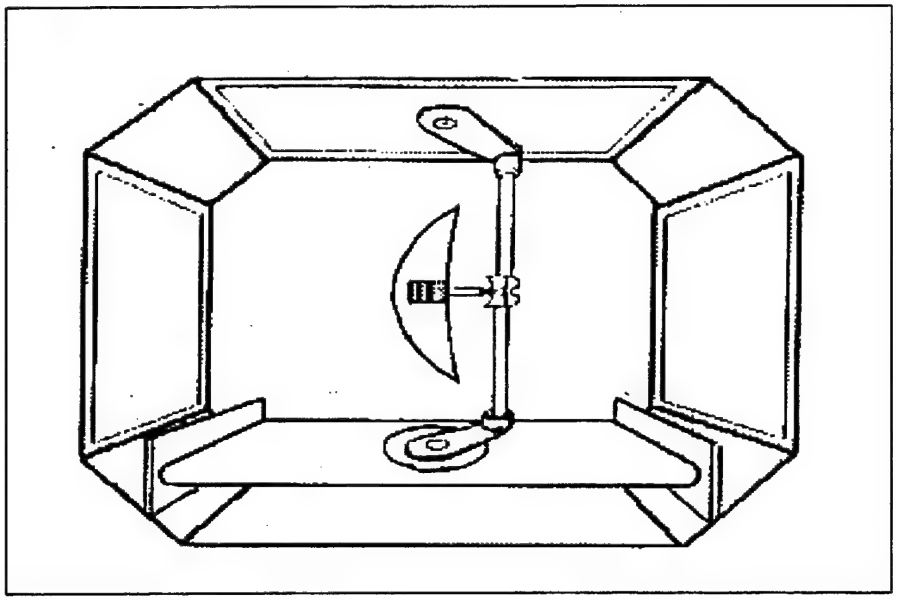

Figure 2.4 Aircraft Model Mounting.

strain gauge signals for the data acquisition (DAQ) board installed in the computer. The SC-2043-SG provides for up to eight channels of signal conditioning with a selection of three wheatstone bridge configurations (half, full and quarter). On-Board excitation of $2.5V_{DC}$ is provided; however, it was decided to use an external excitation source of $5V_{DC}$ since 5 V_{DC} was used by NASA to determine the interaction coefficients.

Voltage excitation leads and input signal leads (i.e. connections with the strain gauge balance) are accomplished via a screw terminal block. The conditioned signals

from the SC-2043-SG are transferred to the DAQ board via a 50 pin connector and cable. The cable connection also serves as a power cable, providing power to the SC board from the DAQ board. A green Light Emitting Diode (LED) indicates that the SC board is on.

Proper configuration of the SC board is accomplished through one slide switch and 12 jumpers (jumper leads). The slide switch (SW1) selects the power supply for the SC board, in this setup the internal (INT) position is chosen to acquire power via the DAQ board. Jumpers JW1 and JW3 are used to select onboard or external voltage excitation to the strain gauge balance. In this case, the EXT position is selected. Jumpers JW2 and JW8 provide for the option of excitation voltage sensing on the DAQ board. The remaining eight jumpers configure the onboard (full, half or quarter wheatstone) bridge completion network for each of the eight channels that may be used. For further details regarding configuring the SC Board consult the SC-2043-SG User Manual [Ref. 5]. Figure 2.5 shows a block diagram that illustrates the key functional components of the SC-2043-SG.

D. AT-MIO-16E-10 DATA ACQUISITION (DAQ) BOARD

The AT-MIO-16E-10 is a completely "Plug and Play-compatible," multifunction analog, digital, and timing I/O boards for use with IBM PCs and compatible computers. The DAQ board is the interface between LabVIEW© and the strain gauge signal conditioning board. It is capable of acquiring analog signals from thermocouples, strain gauges, voltage sources, and current sources. It can also acquire or generate digital signals for communication and control. The board includes a 12-bit Analog to Digital

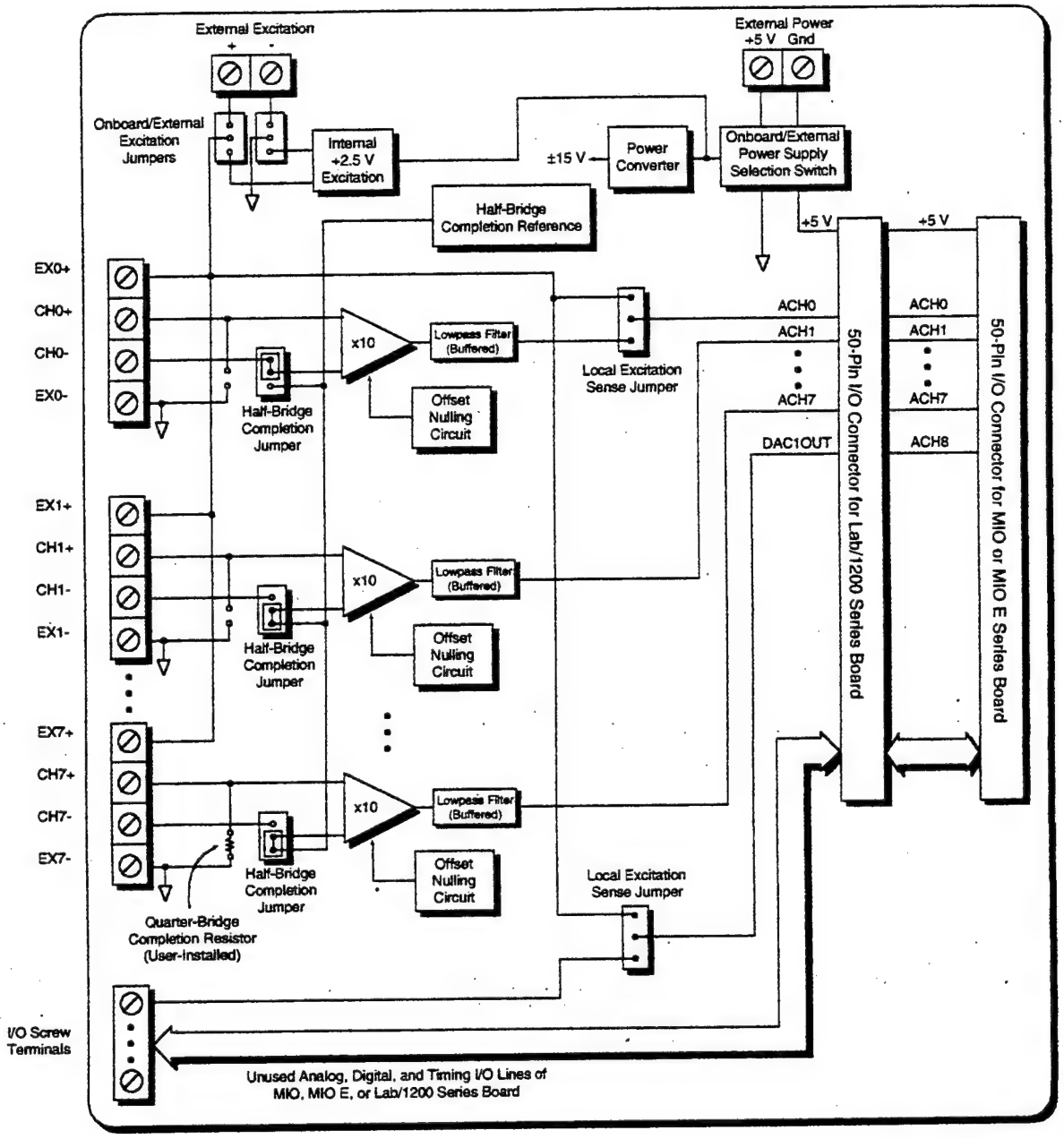

Figure 2.5 SC-2043-SG Block Diagram

Converter (ADC) with 16 analog inputs, 12-bit Digital to Analog Converters (DACs) with voltage outputs, eight lines of TTL-compatible digital I/O, and two 24-bit counter/timers for timing I/O [Ref. 6]. Because the DAQ board has no DIP switches, jumpers, or potentiometers, it was easily configured and calibrated using the NI-DAQ software.

A completely switchless and jumperless DAQ board is made possible by the National Instruments DAQ-PnP bus interface chip which connects the board to the AT I/O bus. The DAQ-PnP implements the "Plug and Play" ISA Specification so that the DMA, interrupts, and base I/O addresses are all software configurable. The primary benefit of this is that the board configuration can be easily changed without having to remove the board from the computer.

Timing related functions are handled by the National Instruments DAQ-STC system timing controller. The DAQ-STC consists of three timing groups that include a total of seven 24-bit and three 16-bit counters and a maximum timing resolution of 50 ns. The three groups control analog input, analog output, and general-purpose counter/timer functions.

III. EXPERIMENTAL PROCEDURE

A. HISTORICAL PERSPECTIVE

Since the early 1940s, the difficulty in designing aircraft configurations that develop high lift-to-drag (L/D) ratios at high supersonic and hypersonic speeds has resulted in much research. Even in the late 1990s, the challenge to develop realizable hypersonic aircraft persists, with many top designers and engineers pursuing alternative solutions. One plausible concept that has evolved from hypersonic flight research is the waverider configuration. Though primarily based on theory, the configuration shows high L/D potential and is the focus of considerable aerodynamic research in both Europe and the United States. In particular, ongoing waverider research is taking place at NASA Ames, NASA Langley, University of Maryland, University of Oklahoma, and the Naval Postgraduate School. The following paragraphs give a brief description of the waverider concept and a historical synopsis detailing its evolution. This provides a background for the remainder of the paper.

A waverider is a supersonic or hypersonic vehicle that, at the design point, has an attached shock wave all along its leading edge. Because of this, the vehicle appears to be riding on top of its shock wave - hence the term "waverider" [Ref. 7]. This is in contrast to a more conventional hypersonic vehicle, where the shock wave is usually detached from the leading edge. The aerodynamic advantage of the waverider, as shown operating at its design point in Figure 3.1a, is "that the high pressure behind the shock wave under the vehicle does not "leak" around the leading edge to the top surface" [Ref. 7].

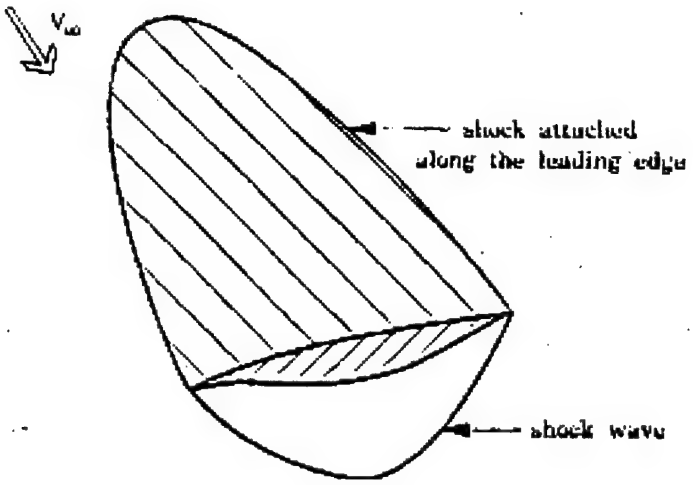

(a) WAVERIDER

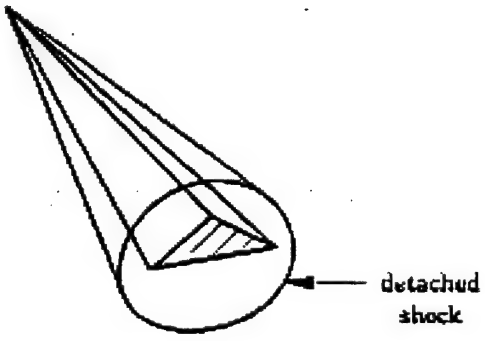

(b) GENERIC VEHICLE

Figure 3.1 Waverider vs. a generic hypersonic configuration.

Thus "the flow field over the bottom surface is contained and the high pressure is preserved" [Ref. 7]. In contrast, for the vehicle shown in Figure 3.1b, there is communication between the flows over the bottom and top surfaces. In this case the high pressure air "leaks" around the leading edge and the level of pressure on the bottom surface is reduced, resulting in less lift. Because of this leakage, the conventional vehicle in Figure 3.1b must fly at a larger AOA to produce the same lift as the waverider in Figure 3.1a. This yields a secondary benefit, which is that because the waverider generates the same lift at a smaller α, drag is significantly reduced and the L/D for the waverider is considerably higher than that of a conventional supersonic or hypersonic configuration. Typically the wave drag for the weak attached shock is also lower than the wave drag induced by conventional aircraft with a detached shock.

"Another characteristic of waveriders is that they are generated from known flow fields established by other basic shapes different from that of the waverider itself" [Ref. 7]. If we restrict this consideration to a 3D wing-body or lifting body, such as the Price configuration that will be introduced later, then the lower and upper surfaces of the waverider are usually derived from stream surfaces in the disturbed flow generated by a cone (or other shape). Even though cone-flow derived configurations are not conical, the flow field in the shock layer between the conical shock and the non-conical body will remain conical. The surfaces of the waverider thus become *stream surfaces* that exists behind a conical shock wave, stream surfaces that are generated by streamlines that begin on the shock surface itself. Hence, the shock wave is, by definition, attached to the leading edge of the waverider. Alternatively, it can be said that the lateral edges of the waverider ride on the captured shock wave [Ref. 8].

Eggers at NASA Ames initiated preliminary research into the waverider concept in 1955. During this time, Eggers designed and studied a flat-top wing-body combination in which the body is situated entirely below the wing [Ref. 9]. This design was based on the principle that the wing could be tapered to follow its own shock wave.

A bomber was actually developed by North American Aviation that took advantage of Egger's research (the B-70 Valkyrie) although it was not inversely derived from a known flowfield [Ref. 10]. In this case the configuration allowed the shock wave created by the tapering underbody of the airplane to sweep back parallel to the leading edge of the wing, just behind it on the lower surface. A natural phenomenon of a shock wave is that it is a compression wave across which a large buildup of positive pressure occurs. This positive pressure field behind the shock wave was superimposed on the underside of the B-70 wing. The pressure field is augmented by the positive pressure on the tapered fuselage and tends to be contained by the B-70's folding wingtips. The pressure field thus created and contained supports approximately 30% of the weight of the air vehicle at cruise conditions. This means the airplane can fly at lower angle of attack for a given weight, thereby decreasing the drag [Ref. 10]. This indeed is very similar to the waverider concept.

In 1959, Nonweiler introduced what was probably the first true waverider design. The design was based on the idea of a three dimensional body derived from the flow field behind a planar shock [Ref. 11]. The resulting configuration was a delta wing planform top view with a caret (named after the dictionary symbol "^") shaped cross section. While flying at the design Mach number, the shock would be attached to the leading

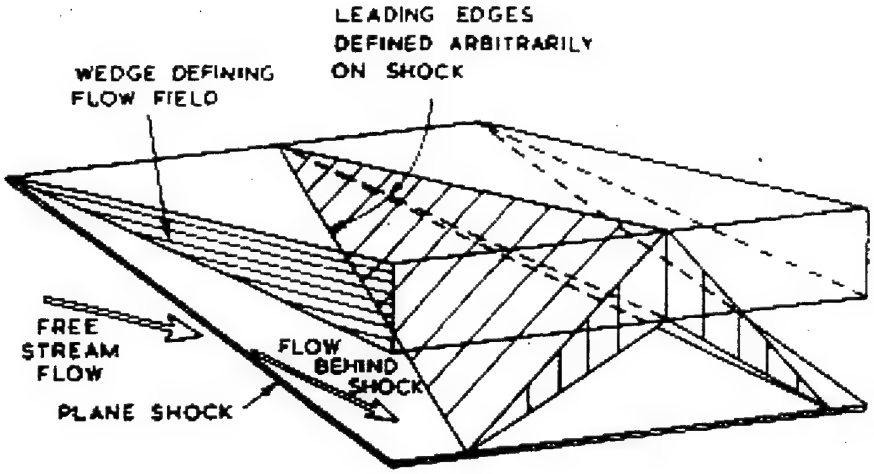

a. CONSTRUCTION FROM KNOWN FLOW FIELD

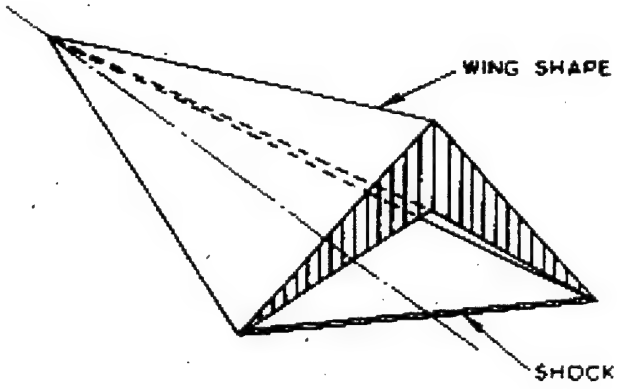

b. RESULTING WING AND SHOCK

Figure 3.2 Nonweiler's Caret Wing

edges preventing spanwise flow and spillage from the lower to upper surface [Ref. 11]. Figure 3.2 shows Nonweiler's configuration.

From the 1960s through the 1980s, waverider designers expanded upon Nonweiler's research by exploring known flow fields generated by right circular and elliptic cones. A conical flow waverider is shown in Figure 3.3 [Ref. 12]. In the late 1980's, Bowcutt and Anderson continued development of waverider designs based upon L/D optimization which included viscous effects [Ref. 13]. Including viscous effects in the design analysis was an essential step for turning theory into practical application.

The rationale behind including viscous effects in the optimization is based on the fact that previous configurations using only inviscid analysis tended to be less realistic than those configurations based on viscous flows. The skin friction drag associated with the large surface area greatly reduces the predicted L/D ratio, which led many researchers to lose interest in the waverider concept [Ref. 7]. Including viscous effects in the L/D optimization allows for the determination of a waverider with maximum L/D and takes into account tradeoffs between wave drag and skin friction drag during the process.

Bowcutt and Anderson's configuration obtained the lower surface of their design from stream surfaces in the disturbed flow generated by a cone. This is typical of previous designs. The upper surface differed in that it used the stream surfaces of a contracting cylinder in its derivation [Ref. 13]. In 1988 Vanhoy contributed more research to including viscous effects in the optimization process of waverider design by performing low speed wind tunnel comparisons of his own Mach 6 L/D optimized waverider with a sharp edged delta wing platform [Ref. 14]. Boycutt/Anderson and Vanhoy's optimized Mach 6 waverider designs are shown in Figure 3.4.

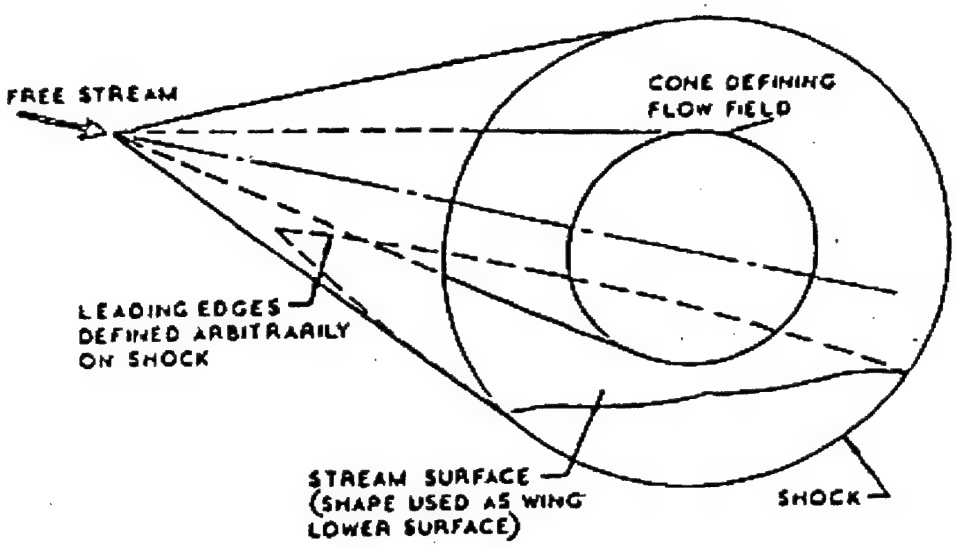

a. CONSTRUCTION FROM KNOWN FLOW FIELD

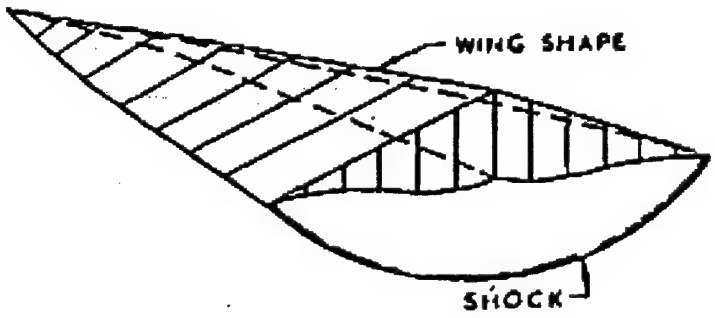

b. RESULTING WING AND SHOCK

Figure 3.3 Conical Flow Waverider Design

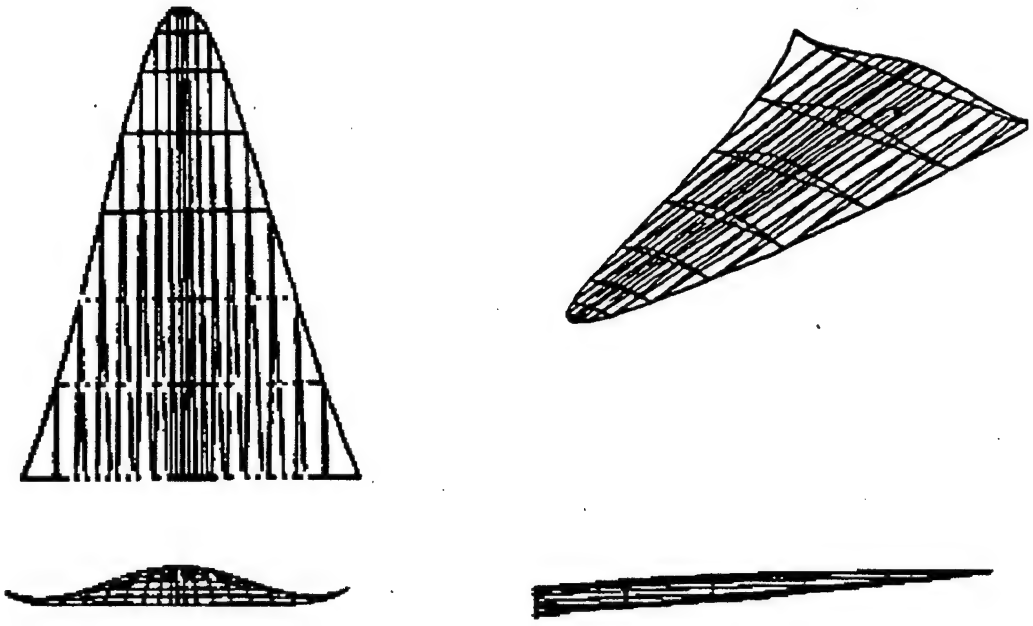

A. BOWCUTT AND ANDERSON'S OPTIMIZED WAVERIDER

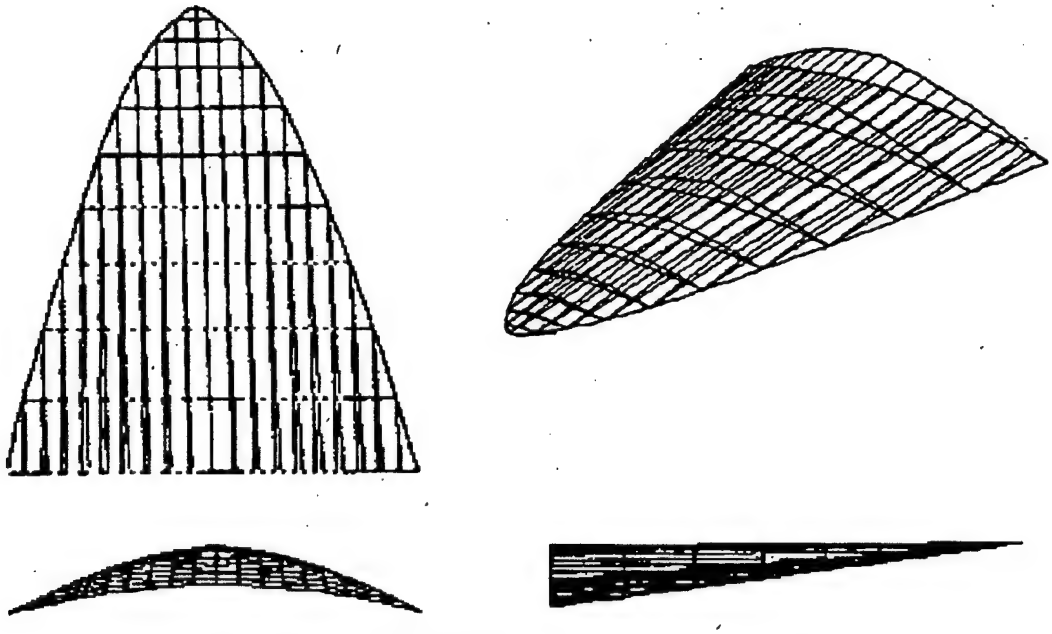

B. VANHOY'S MACH 6 OPTIMIZED WAVERIDER

Figure 3.4 Mach 6 Optimized Waveriders

One further step taken in waverider design was the development of a mission specific waverider configuration. In 1993, LT David Price, USN, with assistance from the NASA Ames Research Center, completed the optimization and performance analysis of a hypersonic (Mach 6) conical-flow waverider for a deck-launched intercept mission [Ref. 15]. Using the Waverider Code and Hypersonic Aircraft Vehicle Optimization Code (HAVOC) developed by the Systems Analysis Branch of NASA Ames, and taking into account the practical considerations of optimum waveriders discussed by Schindel [Ref. 16], a hydrocarbon-scramjet powered waverider optimized for mission performance was designed by Price. The configuration is unique in that it not only includes viscous effects but is optimized to maximize the product of L/D and I_{sp} [Ref. 15]. Figure 3.5 shows Price's optimum configuration.

B. WAVERIDER MODEL

The Price Waverider model was manufactured in 1994 by the NASA Ames Machine Shop to accept the strain gauge (sting) balance. 7075 aluminum alloy was chosen as the material for the model due to its weight, rigidity and ability to maintain an edge. Properties of the aluminum alloy are listed in Table 3.1. To avoid any misinterpretation in reading the table, the value given for ultimate strength equals 578,000,000 N/m^2. The sting balance is mounted via a 3/4 inch diameter hole drilled in the base of the model. It is secured to the model by a 1/8 inch set screw. This set screw is located along the centerline of the model 10.25 inches aft of the nose and corresponds to the sting balance focal point when the sting is mounted in the model. Model parameters are listed in Table 3.2.

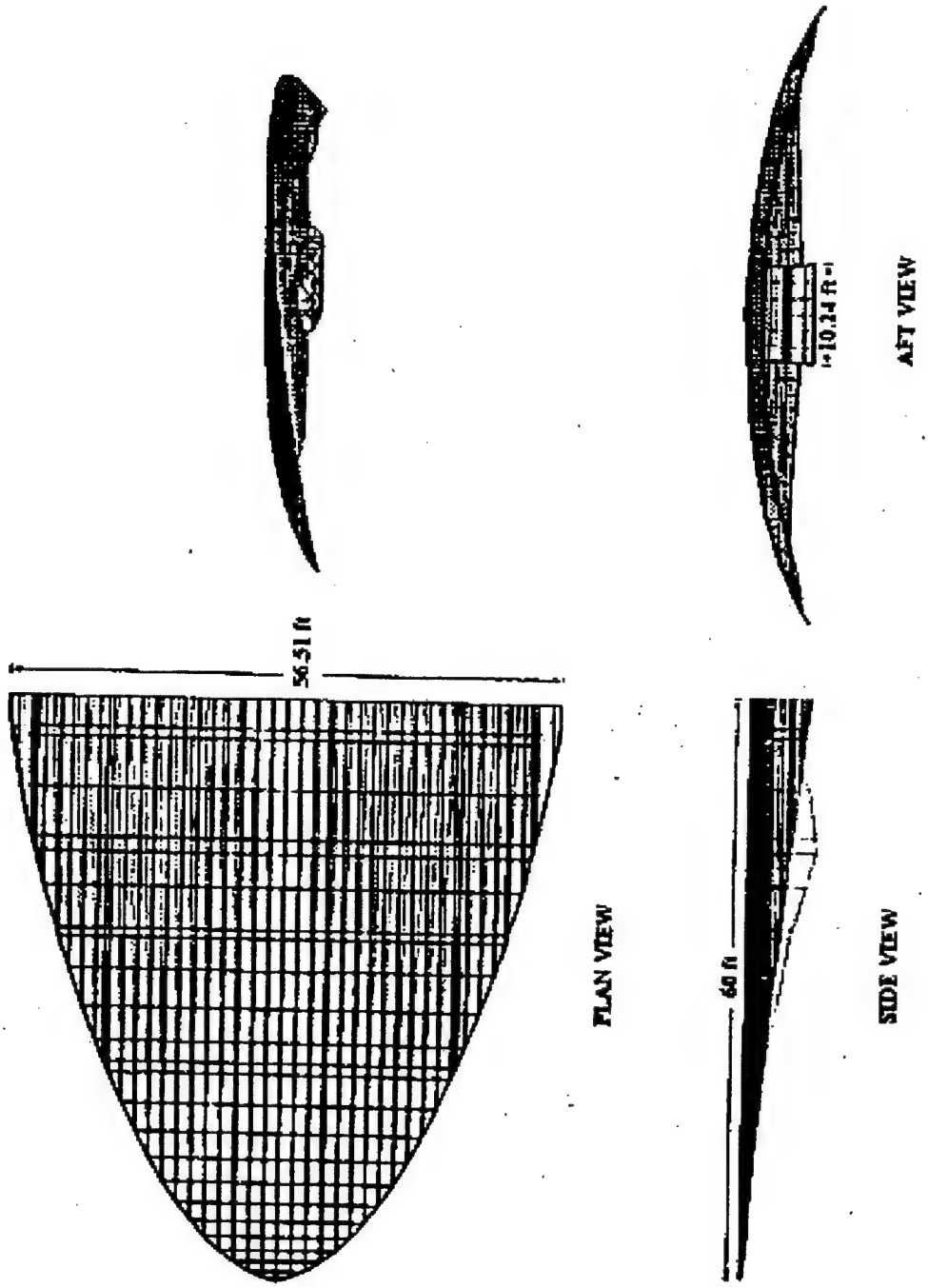

Figure 3.5 Price Mach 6 Waverider

Figure 3.5 Price Mach 6 Waverider

TABLE 3.1

7075 ALUMINUM PROPERTIES

Property	density	Ultimate Strength	Yield Strength	Young's Modulus	Shear Modulus
Units	kg/m^3	N/m^2	N/m^2	N/m^2	N/m^2
Value	$2.8*10^3$	$578*10^6$	$469*10^6$	$71*10^9$	$26.9*10^9$

TABLE 3.2

MODEL PARAMETERS

Length	15 in
Span	13.9375 in
Weight	7.65445 lb
Planform Area	0.991623 ft^2
AR	1.41
Material	7075 Al

C. DATA ACQUISITION PREPARATION

1. Strain Gauge Signal Conditioning Board Preparation

With no power to the signal conditioning board, a connection was made between it and the DAQ board installed in the computer. A 50 to 22 pin connector cable made by National Instruments was used to make the connection. Setup and recognition of the conditioning board required running the NI-DAQ installation setup program included with LabVIEW©. Under "configure accessories" the SC-2043-SG was selected with voltage sensing chosen as channel eight. (Allowable strain gauge channels are numbered

0-7, while channel 8 is provided to sense and display the excitation voltage on the front panel of the LabVIEW© VI.) The DAQ board was further configured as "nonreferenced single-ended" as required by the conditioning board [Ref. 4].

Switch #1 (SW1) was set to the internal (INT) position to provide power to the conditioning board from a $+5V_{DC}$ line on the DAQ board. This voltage source powers the board only and is not used to provide excitation to the strain gauges. The board does provide a fixed excitation of $2.5V_{DC}$ but this is insufficient for excitation as the sting balance was calibrated at $5V_{DC}$, therefore an external excitation source was used. This required setting jumpers W1 and W3 to the external (EXT) position and connecting the excitation source to connector J7. Setting jumper W8 to the EXT position allowed the previously mentioned voltage sensing.

Wheatstone bridge completion was the next item that required configuration, although this was simply verification since the factory default settings were for a full-bridge setup; the same as the strain gauge balance. Choices are possible for full, half or quarter-bridge completion, so it was necessary to ensure that default settings were selected. Jumpers W4-W7 and W10-W13 were verified to be in the full-bridge configuration.

The final connections involved connecting the 24 wires from the sting balance to the screw terminal block mounted on the signal conditioning board. Six of the eight channels of the board were required for the sting balance connections. Each channel of the sting has four wires each, two for +/- excitation (EX) and two for the +/- return (CH) signal. Since the channels provided for this purpose are numbered 0-7 on the board it was arbitrarily decided to use channels 1-6 to keep things simple. They were wired in

the following order: N1, N2, S1, S2, AX, and RM. Two channels on the board remained unused. To prevent these unused channels from saturating, causing significant power consumption and possible loss of accuracy, the screw terminals of the CH +/- inputs were shorted to their respective negative excitation screw terminal [Ref. 4].

The calibration of the conditioning board setup required having the LabVIEW© program activated. Each channel used by the sting balance required nulling, which amounts to setting the strain gauge, return signal voltages to zero when no load is applied to the balance. To provide for nulling, each channel on the board has its own circuit with a trimming potentiometer (pot) to adjust the voltage. While viewing the voltage level on the monitor, the pots were rotated until zero voltage on all six channels was obtained.

2. LabVIEW© VI Development

The most time consuming process during the evolution of this thesis involved creating the Virtual Instrument for performing experimentation. With very little LabVIEW© experience among the faculty, it was known from the outset that there would be a steep learning curve for the writer in developing a program that would not only work, but would be easily used by the rest of the department. To realize the greatest benefit from using a graphical program, the user should be able to get a "full solution" in real time and not have to go "off-line" to process the data taken during experimentation. In this particular example there was a desire to determine, in real time, the non-dimensional values of C_L, C_D, and C_M as a function of the angle-of-attack as the data is taken. This was achieved, and in addition, plots of C_L vs. α, C_D vs. α, C_M vs. α and C_L vs. C_D were also rendered as the data was taken. Finally the data is appended, via the

LabVIEW© VI, to any spreadsheet or text program desired, e.g., Excel, for future analysis. The general procedure for developing this program will be discussed in the next paragraphs.

The first step in the procedure was simply to acquire the voltages from the sting balance and display them on the front panel. This was accomplished using a pre-designed VI from the built in library. There were several acceptable choices but the one copied to the block diagram was the *AcquireNscans.vi*. This VI automatically determines the number of channels being scanned and acquires the voltages for each. Front panel controls allow tailoring the length of time the channels are scanned, the number of samples taken and the gain adjustment of the DAQ board, among others. Appendix A depicts the Front panel and Block Diagram. In this case, six channels were scanned from the sting balance and one extra channel (CHN 8) for verifying the excitation voltage. Default values are currently set at 10,000 scans over 10 seconds with gain set to 1000 via high and low limit selections

Discounting the excitation sensing, what were acquired were 60,000 voltage signals. Each of the six channels is a column array of 10,000 values. What was needed was a time average of the columns, which yields six voltage values for N1 through RM. This was accomplished by transposing the [10,000 X 6] matrix and then using a subVI to calculate the mean value of each row. A "For Loop" performs the mean calculation for each row sequentially. The results of this calculation are displayed on the front panel under the title "Mean." When no load is applied to the sting balance the mean values should read zero; therefore, nulling the system requires monitoring these values as discussed in the previous section.

The next step in the block diagram requires a calculation of the direct force nonlinear values and the force interaction values. Two separate subVIs were created to accomplish this, *preinteract.vi* and *interact1.vi*. For the first subVI, the six mean values described in the paragraph above were sent to individual formula nodes that execute calculations for both positive and negative voltages. A "True/False" case structure is "wired" in the subVI to the incoming signal from each channel to determine if it is positive or negative, which determines which equation to calculate. This yields 12 equations, two per channel. Appendix B lists the constants for the direct force nonlinear equations.

The calculations from the *preinteract.vi* are then sent to *interact1.vi* to account for force interactions between the strain gauge elements in the sting balance. This VI executes calculations in much the same way, with a formula node for each channel again surrounded by a "True/False" case structure to account for positive or negative voltage cases. This again yields 12 equations. However, since the VI is checking for convergence due to interactions, each calculated signal is routed back as an input to the five other channels. Including the initial signal from the *preinteract.vi* there are six voltage signals routed in and one voltage signal routed out for each channel. A For Loop surrounds the *interact1.vi* to perform the iterations with the default number of iterations set to 20 on the front panel. This seems enough to ensure convergence to the actual value, as iterations greater than 10 effected no change on the calculated values during testing.

The six resulting values from the interaction convergence yield the actual forces felt by the strain gauge elements. These forces are displayed on the front panel as XN1,

XN2, XS1, XS2, XAX and XRM. The next step is to convert these individual element forces into forces that the model "feels." This is accomplished by yet another formula node in the block diagram. It is also at this point that one final "True/False" case is needed. The "true" case will select the "Tare reading," which is simply the weight of the model with no external forces applied. The "false" case will select the forces on the model when the wind tunnel is running and execute the remainder of the program.

The Tare reading is selected prior to running the tunnel. This is achieved simply enough by selecting "ON" for the "TARE" button on the front panel. The formula node then computes the normal, side, axial and rolling (moment) forces on the model. These forces should be negligible except for the side force. (Recall that the model is mounted sideways as shown in Figure 2.4 and Appendix E.) The calculated values are saved as local variables so they will be remembered during wind tunnel testing. Additionally, these values are displayed on the front panel as "Tare Readings".

After the tunnel is running and stabilized, data collection is initiated by selecting OFF for the Tare reading. This changes the "True/False" case allowing force calculations to be made. Other required selections at this time include entering AOA, manometer Δp, chord length, temperature, atmospheric pressure and planform area, as well as selecting a file to save the data to for future retrieval. Selecting the run program allows the formula node to execute again, this time calling the local variables from the Tare readings and subtracting them from the force calculations. The adjusted force calculations are then collected as an array and displayed on the front panel below the Tare readings. They consist of normal, axial and side force, as well as pitch, yaw and rolling moments. Monitoring the force calculations on the front panel serves as a useful tool in avoiding

overloading the balance. Warning indicators turn red on the front panel when forces exceed 80% of rated strain gauge loads to further reduce the possibility of overload.

As stand alone values, the force calculation values are not too useful to the aerodynamicist until they are nondimensionalized. The next two formula nodes accomplish this; the first calculating C_N, C_A and C_M from the normal force, axial force and pitching moment. Included in the first formula node are the user's inputs for chord length and planform area, as well as the value for dynamic pressure calculated from the manometer Δp. The second formula node uses the values of C_N and C_A, along with the user's input for AOA, to calculate C_L and C_D.

The calculated values from the two formula nodes used by this program are AOA, C_L, C_D and C_M. These outputs are then collected into an array in the order stated above and sent to another subVI that appends the data by row to a spreadsheet file. Other data appended automatically to the spreadsheet includes C_N, C_A, Normal, Axial and Side forces, Pitch, Yaw and Rolling moments, IAS, True wind tunnel speed, Reynolds number and dynamic pressure. Each successive run adds another row to the spreadsheet. It is worth noting here that other values based on the force/moment calculations can be calculated and displayed with little effort if desired.

Finally, the results are graphically displayed on the front panel as plots of C_L vs. α, C_D vs. α, C_M vs. α and C_L vs. C_D. A buffer subVI is placed in front of each graph icon on the block diagram to retain each data point taken. Otherwise each successive run would overwrite the previous data point. The benefit of creating plots in real time, in addition to saving the data, is a major advantage of the program. The user can monitor the plots and verify that the model is behaving as predicted. Unexpected results can be

immediately determined, and if possible, corrected on the spot, eliminating repeat tests due to faulty data collection or procedures.

D. STING BALANCE WIND TUNNEL EXPERIMENTS

1. Test plan

Following calibration of the signal conditioning board and sting balance [App. A], the model was secured on the yoke in the wind tunnel. The determined schedule of testing was six data runs at different tunnel speeds, varying the AOA during each run. The sweep ranges of α were dictated by the rated load of the balance. To ensure a margin of safety, applied loads were not allowed to exceed 80% of the rating. To further reduce the possibility of damage to the balance, each test run was begun at the lowest practical tunnel speed. Tunnel speed was increased gradually for each run, with the force equations continuously monitored for near overload conditions. A synopsis of the runs is listed in Table 3.1.

2. Tare Values

Prior to taking wind tunnel measurements, the tare values representing forces and moments due to the weight of the model were determined. A discussion of how this is accomplished is covered under LabVIEW© VI development. In short this simply means selecting the "ON" button for the TARE reading. Subsequent runs will automatically subtract this amount from the "tunnel on" data points. It was found that the nulling range of the circuit board allowed nulling the Tare values down to zero.

TABLE 3.3

TEST CONDITIONS

Test	q (lb/ft^2)	IAS (mph)	Sweep range (deg)
0	3.61	45	0 to 45
1	3.65	45	-90 to 90
2	7.74	60	-25 to 22
3	13.74	75	-18 to 13
4	20.29	90	-13 to 8
5	25.92	100	-11 to 6
6	31.94	110	-10 to 4

3. Preliminary Test

A preliminary test (test 0) was performed neglecting the use of the interaction equations. This was done to isolate any problems with data acquisition using the LabVIEW© program. Preliminary procedures before beginning the test were performed to ensure integrity of the tunnel [Ref. 3]. Tunnel speed was brought up to 45 mph, with a corresponding dynamic pressure of 3.61 lbf/ft^2. Angle-of-attack was varied from 0-45° while maintaining a constant vigil on the monitor to check balance loads. All loads were significantly below warning levels, indicating much higher speed was possible. Data acquisition performed as expected, with both real time plots and spreadsheet data created. Negative sweeps were to be performed but the turntable drive mechanism that controls changing AOA failed. This temporarily halted further testing until repairs could be made on 29 August 1998.

4. Subsequent Tests:

Tests one through six comprised the formal testing of the model with force interaction coefficients included. For each run, the model was initially placed at 0° α then moved incrementally to locate the angle-of-attack that yielded forces equaling or exceeding the 80% limit load criteria. It was found in all cases that N1 reached its load limit first, and higher negative α settings were achievable than positive. Once the limiting negative AOA was determined the model was moved incrementally (via the turntable) through the allowable angle of attack range. Data points were taken statically after moving the turntable to each desired AOA location.

5. Data reduction

Data files of all tests were collected, as previously mentioned in spreadsheet format, and are presented in Appendix D. The LabVIEW© program calculated values of the force coefficients from the dimensional forces in the following manner. The normal and axial force coefficients ($C_{N \text{ and }} C_A$) were calculated using the appropriate form of equation (3.1).

$$C_F = \frac{F}{qS} \tag{3.1}$$

Where: C_F = force coefficient

F = force (lbf)

q = dynamic pressure (lbf/ft^2)

S = planform area (ft^2)

Using equations (3.2) and (3.3), the values for C_N and C_A were inputted to calculate the coefficients for lift and drag. Figure 3.6 depicts the use of these equations.

$$C_L = C_N \cos \alpha - C_A \sin \alpha \quad (3.2)$$

$$C_D = C_N \sin \alpha + C_A \cos \alpha \quad (3.3)$$

Where: C_N = normal force coefficient

C_A = axial force coefficient

α = angle of attack (degrees)

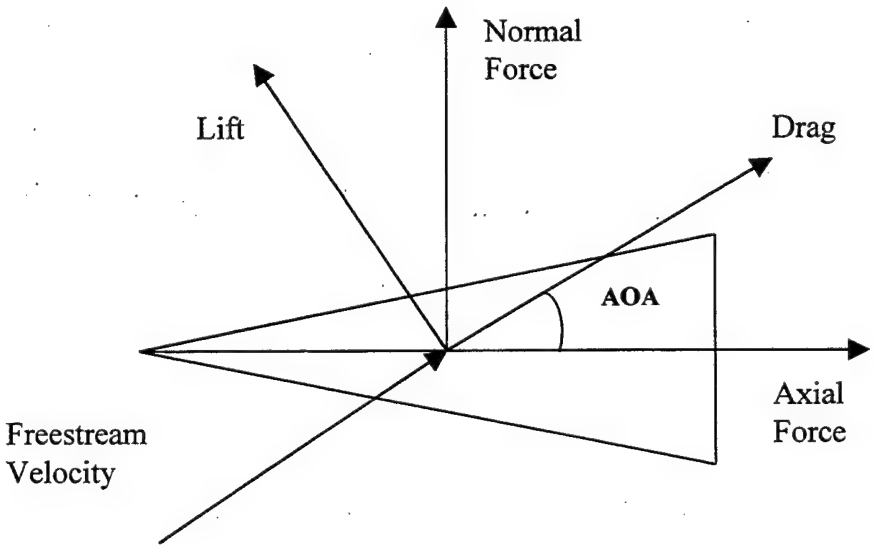

Figure 3.6 Calculation of C_L and C_D

The pitching moment coefficient was calculated using equation (3.4).

$$C_M = \frac{M}{qS\,c} \tag{3.4}$$

Where: C_M = moment coefficient

M = moment (ft-lbf)

c = root aerodynamic chord (ft)

The length of the model, i.e. root chord of 1.25 ft, was used as the reference chord length. Plots obtained from these calculations include C_L, C_D and C_M vs. α, C_L vs. C_D, C_M vs C_L and C_L/C_D vs α. The results of these plots are summarized in the next chapter.

IV. RESULTS AND DISCUSSION

A. VALIDATION OF LABVIEW© PROGRAM

Before obtaining results from the wind tunnel testing, it was necessary to validate the code that was written to acquire and process the data. This was accomplished by first running the program offline and inserting known values in the calculations, then by acquiring data via the strain gauge balance and comparing results to expected values.

1. Offline Validation

A version of the Quick Basic code used by Cedrun [Ref. 2] was obtained and converted to PC format, allowing manual input of dummy voltage values to be entered. Dummy voltages for the six strain gauge channels (N1-RM) were entered yielding Normal, Side and Axial "force" results and Pitch, Yaw and Rolling "moment" results. These same dummy voltages were inputted into the LabVIEW© program and identical results were obtained when using Cedrun's interaction coefficients.

2. Acquiring Data

With setup accomplished in the wind tunnel, known loads were applied in weight increments of one to ten pounds on the strain gauge balance as discussed in Appendix B. Results displayed on the front panel confirmed that accurate data was obtained for the weights applied. This served a secondary purpose of verifying the NASA Ames calibration of the balance.

B. WIND TUNNEL DATA

Results of the wind tunnel testing are decomposed into two areas. Lift and Drag comprising the first part of the discussion and pitching moment the second part. In both cases tunnel wall corrections were applied to the data. These corrections were made to account for the change in flow properties caused by the walls of the wind tunnel's closed test section. Corrections were included for solid blocking, wake blocking and streamline curvature. A brief discussion regarding these corrections and why they were needed is included in Appendix D. For more information, [Ref. 21] provides a detailed analysis of wind tunnel wall corrections and the theory behind them.

1. Lift and Drag

The graphs of C_L versus angle of attack for all six test runs are shown in Figures 4.1 through 4.6. The graphs show little variation in C_L with respect to dynamic pressure. The graph for C_L in Figure 1 is worth special note due to the large amount of difference between uncorrected values and corrected after 20° AOA. Applying the tunnel wall corrections yields a significant loss of C_L for AOAs greater than 20°. Tunnel wall corrections for values under 20° AOA were minor in comparison, which was also true for all other coefficients plotted. A maximum loss of 0.5 (C_L drops from 1.5 to 1.0) occurs at approximately 30° AOA, at which point the waverider stalls. Figure 4.1 substantiates Cedrun's conclusion that the waverider continues to generate lift at higher angles of attack after stall [Ref. 14].

Figures 4.7 through 4.12 display graphs for C_D versus AOA. It can be seen that minimum drag ($C_D = 0.03$) occurs at 0° AOA, therefore $C_{DMIN} = C_{D0}$. Drag is somewhat higher than results previously obtained by Cedrun, which is later shown to be a result of

the corrections made to the interaction coefficients. These corrections led to a larger positive axial force for all results that in turn led to higher drag values. The higher drag characteristics at positive vice negative AOA do agree with Cedrun and are explained by the corresponding higher lift characteristics also observed at positive AOA. C_L/ C_D versus AOA plots are shown in Figures 4.13 through 4.18. As can be seen, L/D is not much affected by tunnel wall corrections. A maximum value of approximately (L/D) = 4 occurred at 6^o AOA. C_L versus C_D plots are shown in Figures 4.25 through 4.30. Again, it can be seen that applying tunnel wall corrections has a significant effect at higher angles of attack, as shown by Figure 4.25. From 0 to +/- 20^o, the differences in C_L versus C_D are much less apparent.

A graph of C_L versus AOA attack with Reynolds number as a parameter is provided in Figure 4.37. The graph clearly shows that C_L is virtually unaffected by a change in the Reynolds number, also agreeing with previous results obtained by Cedrun.

2. Pitch

The graphs of C_M versus AOA for all six tests are shown in Figures 4.19 through 4.24. As with C_L, there was minimal variation in pitching moment with respect to changing dynamic pressure or Reynolds number. The point at which the pitching moments were initially taken is located 10.25 inches from the nose on centerline. Prior to applying wind tunnel boundary corrections, a moment transfer to the 1/4 root chord was necessary due to formula requirements [Ref. 21]. This involved a transfer of 6.5 inches, locating the 1/4 chord at 3.75 inches aft of the nose (0.3125 ft).

Additional plots of C_M versus AOA were created to show pitching moment about the leading edge in Figures 4.31 through 4.36. This location was chosen primarily to

compare with results contained in an AIAA paper by Miller and Argrow on a high-speed civil transport (HSCT) waverider, which was compared to the Price Waverider among others [Ref.22]. It is suggested that the authors did not transfer Cedrun's moment location [Ref. 2], which was at 68% aft of the LE of the root chord, before making the comparison. Figure 4.41 displays a correct comparison of the Price and HSCT waverider for C_M versus α.

In any case, the Price waverider appears longitudinally stable when referenced to the quarter chord and leading edge, but neither are particularly useful values for determining the longitudinal stability of an aircraft. In order to determine longitudinal stability the aerodynamic center (or neutral point), and the aircraft's center of gravity (c.g.) must be located. Since this is a model, the location of the c.g. is not likely to represent a real aircraft, but the aerodynamic center of the Price waverider model was located at 4.8 in (32%) aft of the leading edge. For static stability, this will require a c.g. location less than 32% aft the leading edge of the model; hence it appears unlikely that a representative aircraft will be statically stable. Figure 4.38 displays a plot of C_M versus AOA with zero slope, thereby indicating that the neutral point is at approximately $C_{M(c/3)}$.

The location of the neutral point can also be verified using the following formula if the location of the mean aerodynamic chord is known.

$$\left(\frac{\bar{x}}{c}\right)_{n.p.} = \overline{c_{ref}} - \frac{C_{M\alpha(ref)}}{C_{L\alpha}} \qquad (4.1)$$

The mean aerodynamic chord was found by determining the equation of the line fitting the perimeter of the waverider model as shown in Figure 4.39, then applying equation

4.2. This defined the length of the mean aerodynamic chord to be 12.05 inches.

$$\bar{c} = \frac{\int_{-b/2}^{b/2} c^2 dy}{\int_{-b/2}^{b/2} c dy} \tag{4.2}$$

With reference to the MAC of 12.05 inches, its origin is 2.95 inches aft of the centerline leading edge and the 1/4 chord is located 5.96 inches from the centerline leading edge. Taking C_M versus C_L about the MAC 1/4 chord location yields the result seen in Figure 4.40 when applying the data from the IAS of 75 mph. The slope of a linear fit to the C_M vs C_L plot is 0.0978, which yields $\frac{x}{\bar{c}} = 0.25 - 0.0978 = 0.1522$. To find the location of the neutral point with respect to the MAC, 0.1522 was multiplied by $\bar{c}$ yielding an x location 1.83 inches aft of the leading edge of the mean aerodynamic chord. When referenced back to the root chord, 1.83 + 2.95 = 4.78 inches from the leading edge on centerline as can be seen in Figure 4.39. This closely agrees with the 4.8 inches found from the previous method.

C. ACCURACY OF DATA

Figures 4.42 through 4.46 compare data obtained from Cedrun's work [Ref. 2] with current results. It was previously noted that Cedrun obtained lower drag and therefore higher L/D values, believed due to corrections made to the interaction coefficients during the current testing. In addition, for reasons perhaps also due to the incorrect interaction coefficients, many of the axial force values obtained by Cedrun were slightly negative, which would also lead to lower drag values. However, his method of

converting dynamic pressure from cm H_2O to lbf/ft^2 yielded values of q that were 3.1% lower than current values. This q discrepancy would tend to increase values for both C_D and C_L. With these many differences, it was decided to perform an additional test in the wind tunnel in an attempt to exactly duplicate Cedrun's results.

Interaction coefficients identical to Cedrun's were used and testing was performed using a q obtained by his method. Results of this final test match almost exactly with results Cedrun obtained. Closeness of fit is particularly apparent in Figures 4.43 and 4.45. The curve fit of Cedrun's data in Figure 4.46 is somewhat deceiving as it does not fall exactly on line with the LabVIEW© result. This is due to the limited number of data points for Cedrun's test run. In any case, this latest test supports the validity of current values obtained during runs one through six. The differences between these current values and those obtained during the 1994 test data are clearly due to corrections made to the interaction coefficients and the method previously used by Cedrun in obtaining q.

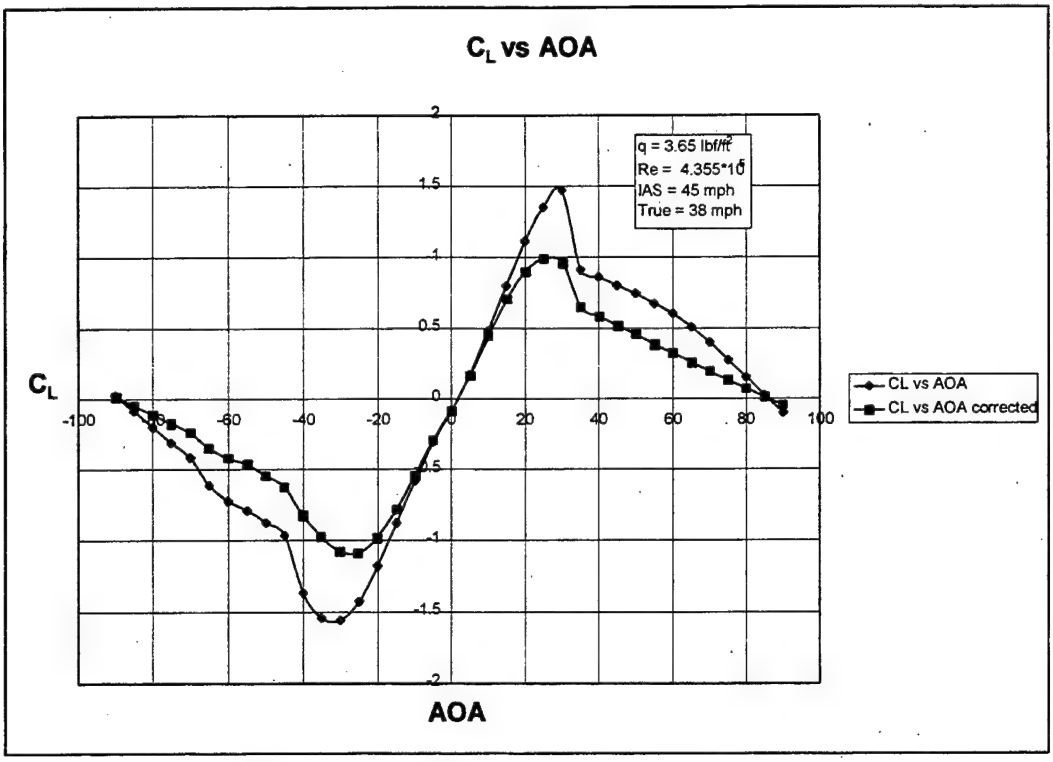

Figure 4.1 CL vs. AOA, IAS =45 mph

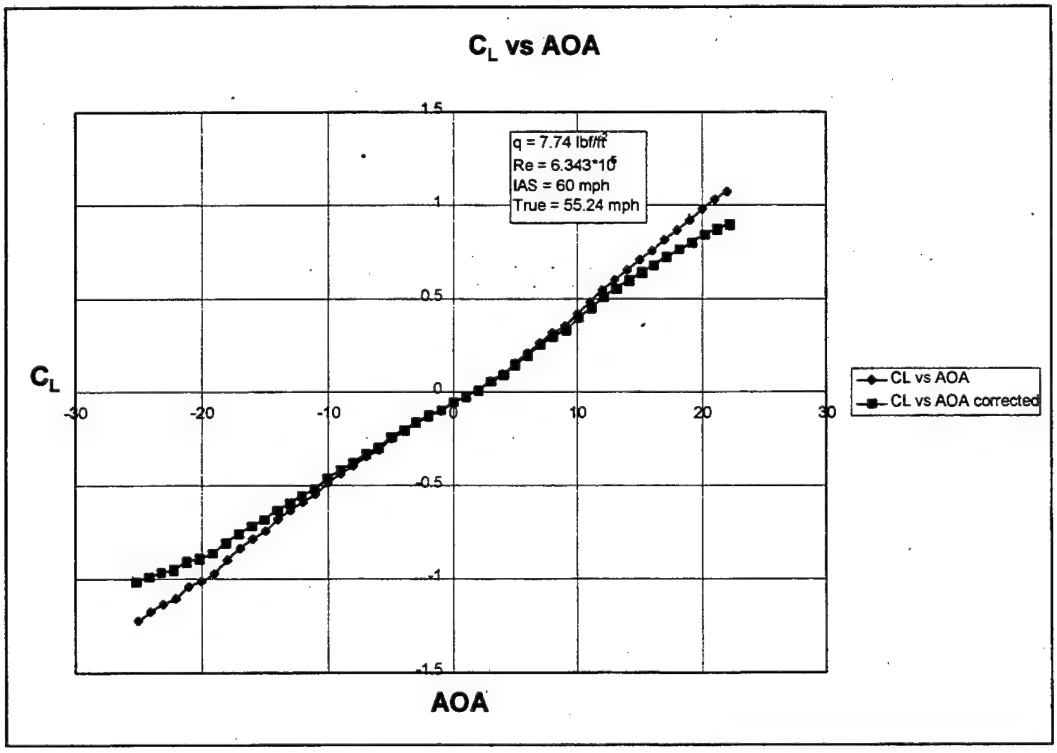

Figure 4.2 CL vs. AOA, IAS = 60 mph

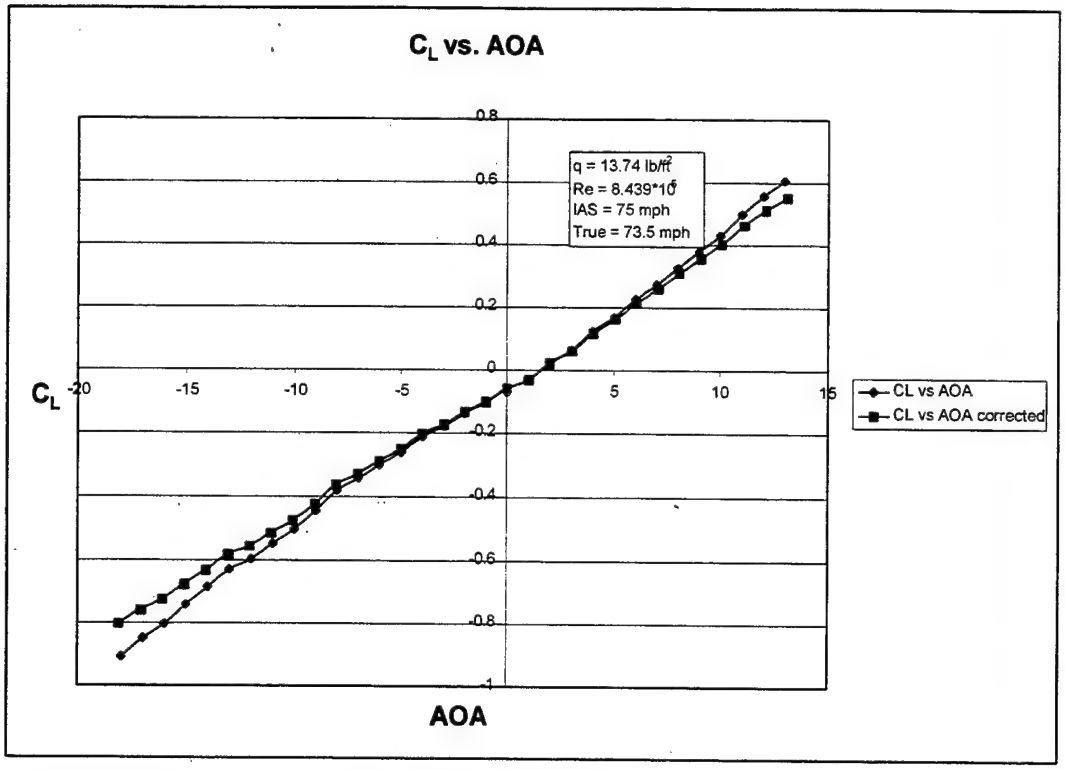

Figure 4.3 C_L vs. AOA, IAS = 75 mph

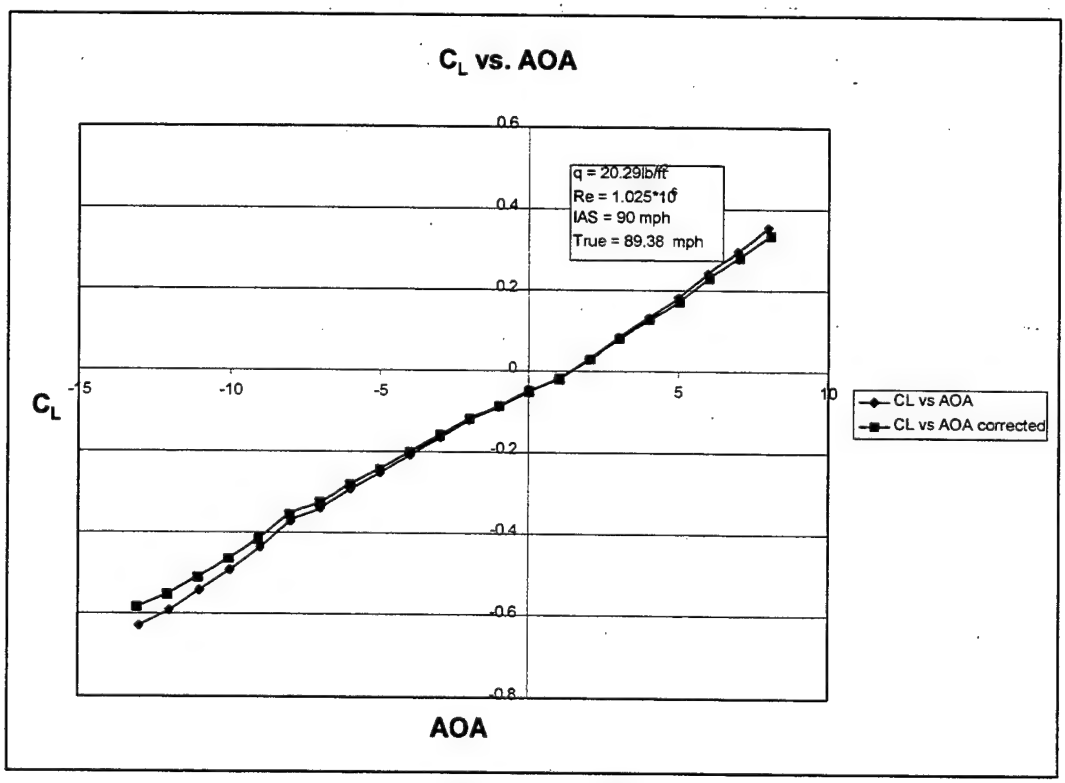

Figure 4.4 C_L vs. AOA, IAS = 90 mph

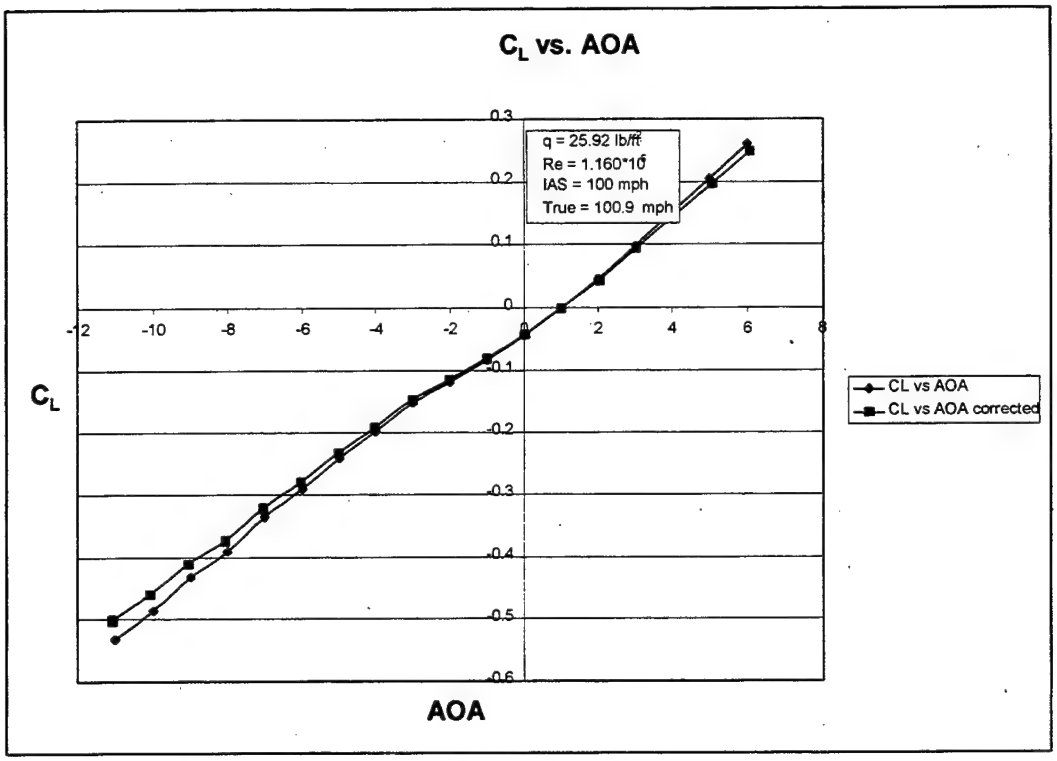

Figure 4.5 C_L vs. AOA, IAS = 100 mph

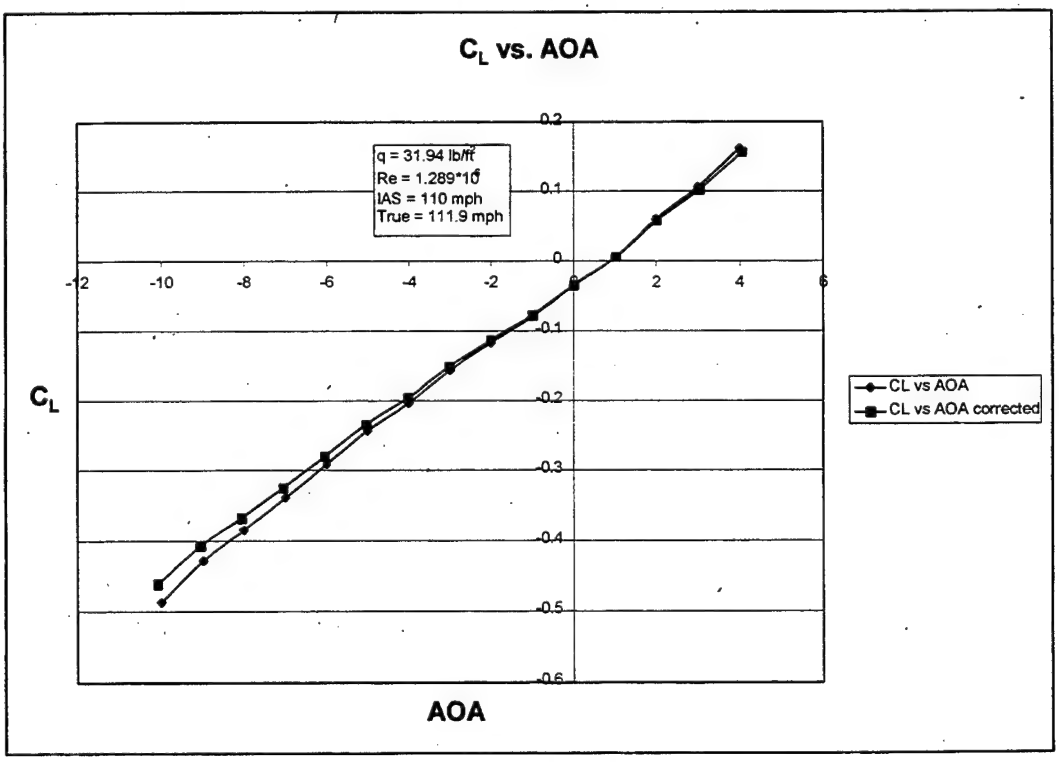

Figure 4.6 C_L vs. AOA, IAS = 110 mph

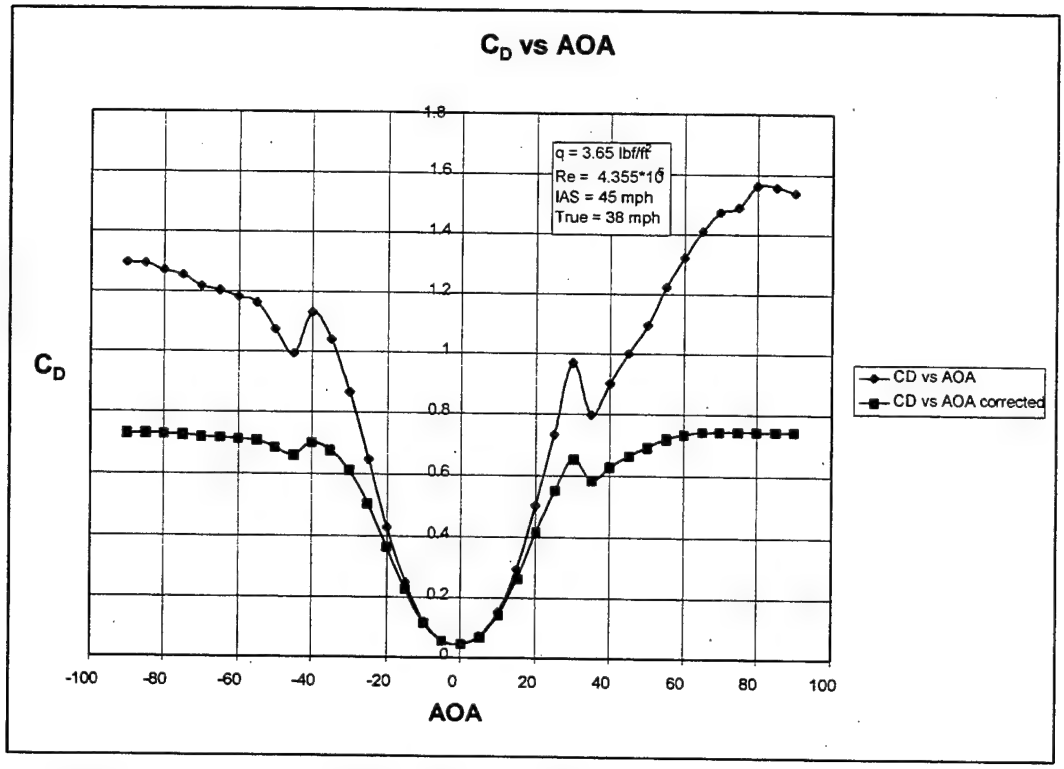

Figure 4.7 C_D vs. AOA, IAS = 45 mph

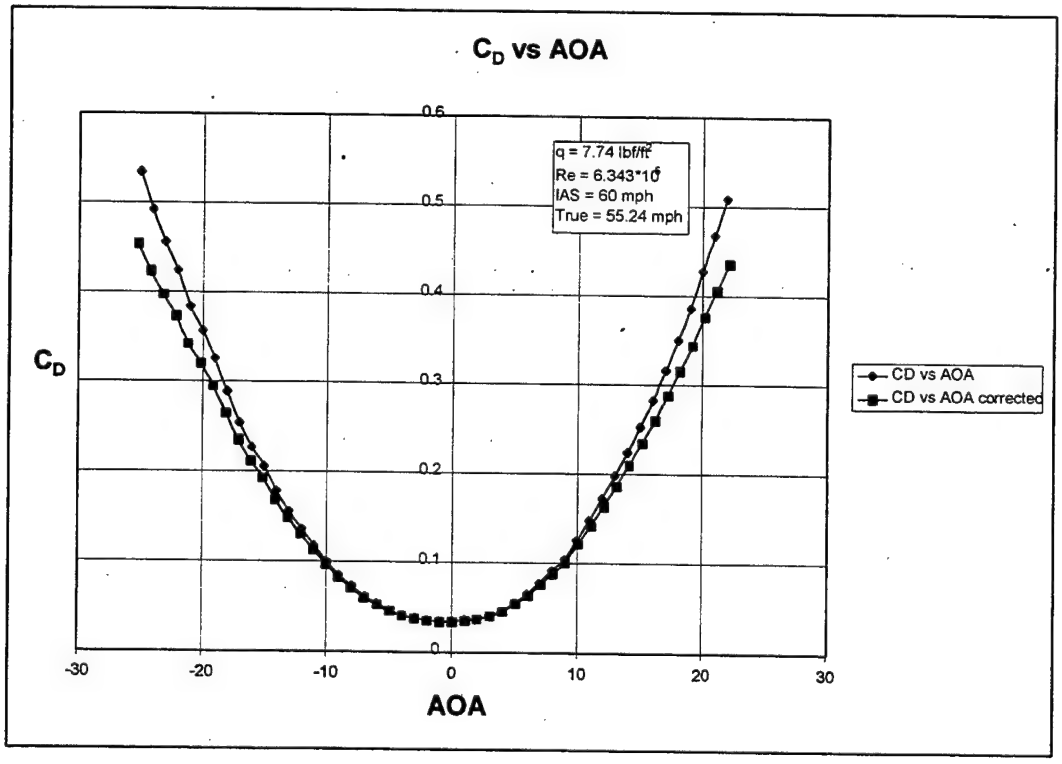

Figure 4.8 C_D vs. AOA, IAS = 60 mph

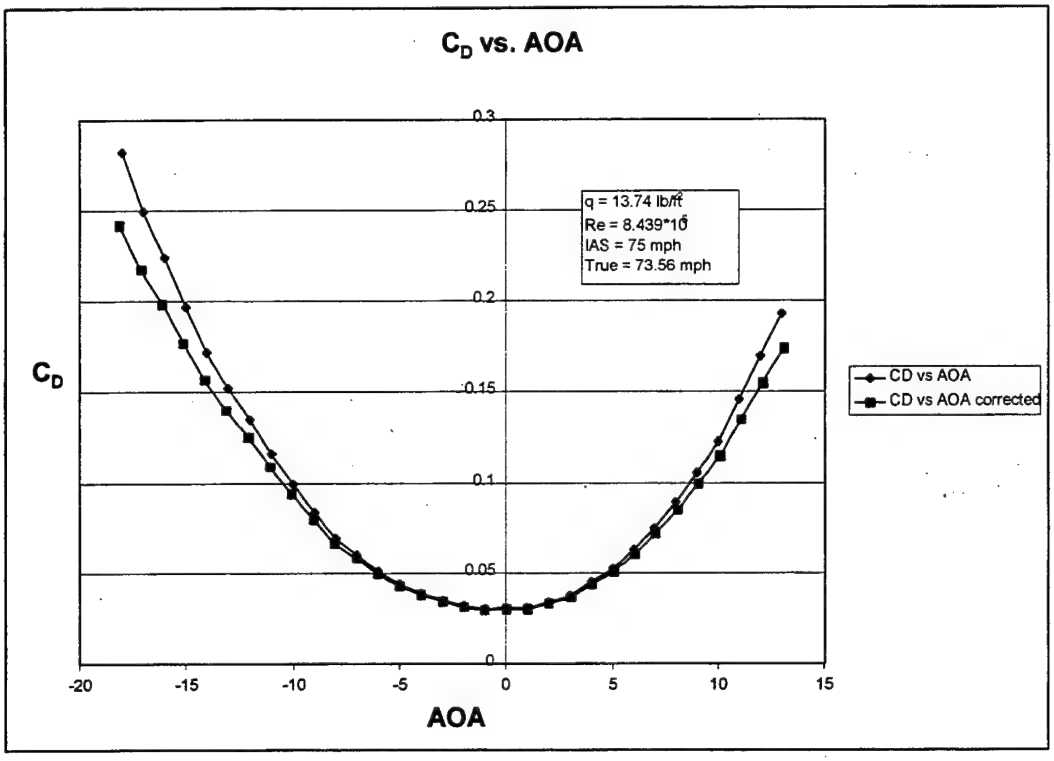

Figure 4.9 C_D vs. AOA, IAS = 75 mph

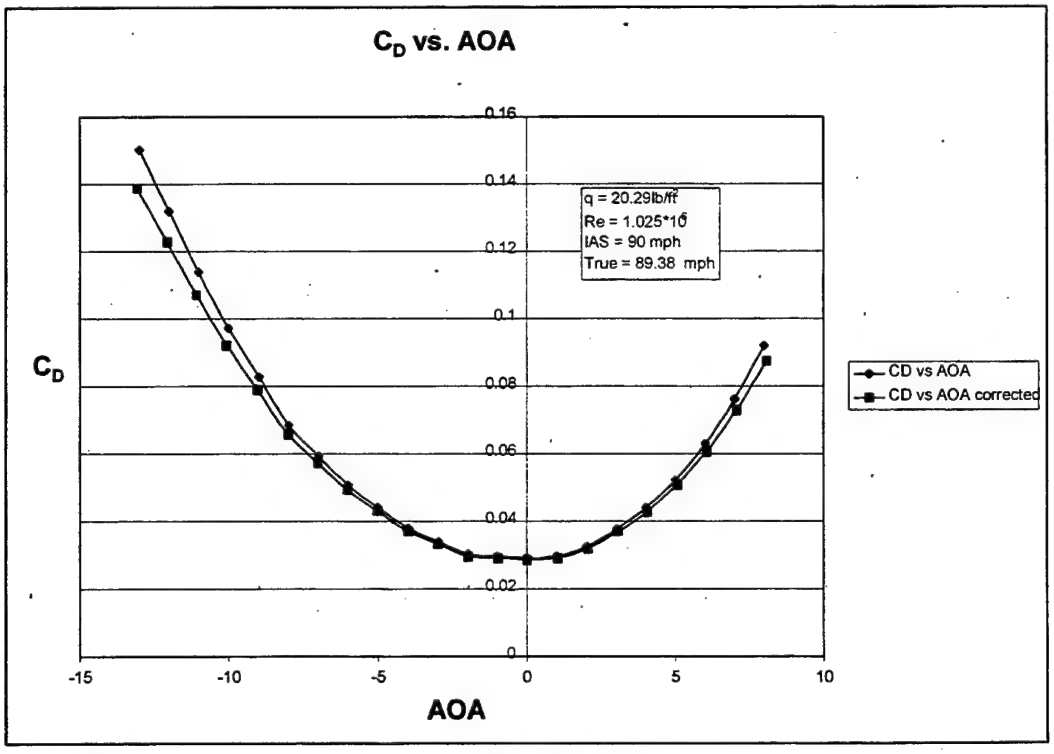

Figure 4.10 C_D vs. AOA, IAS = 90 mph

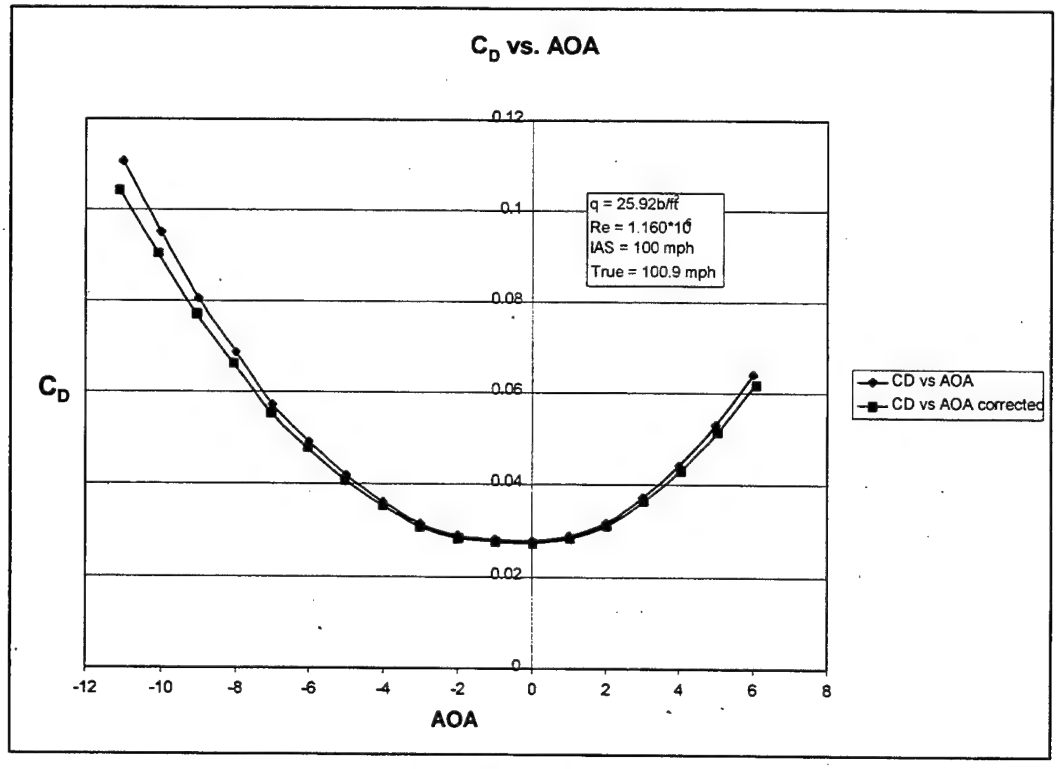

Figure 4.11 C_D vs. AOA, IAS = 100 mph

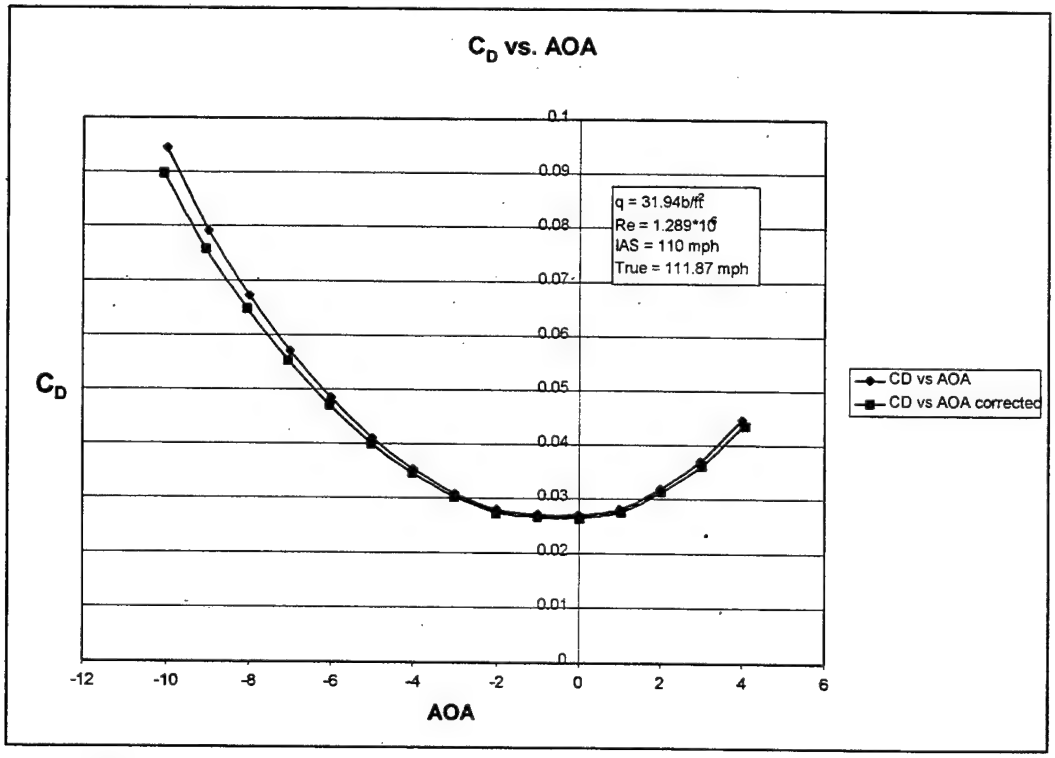

Figure 4.12 C_D vs. AOA, IAS = 110 mph

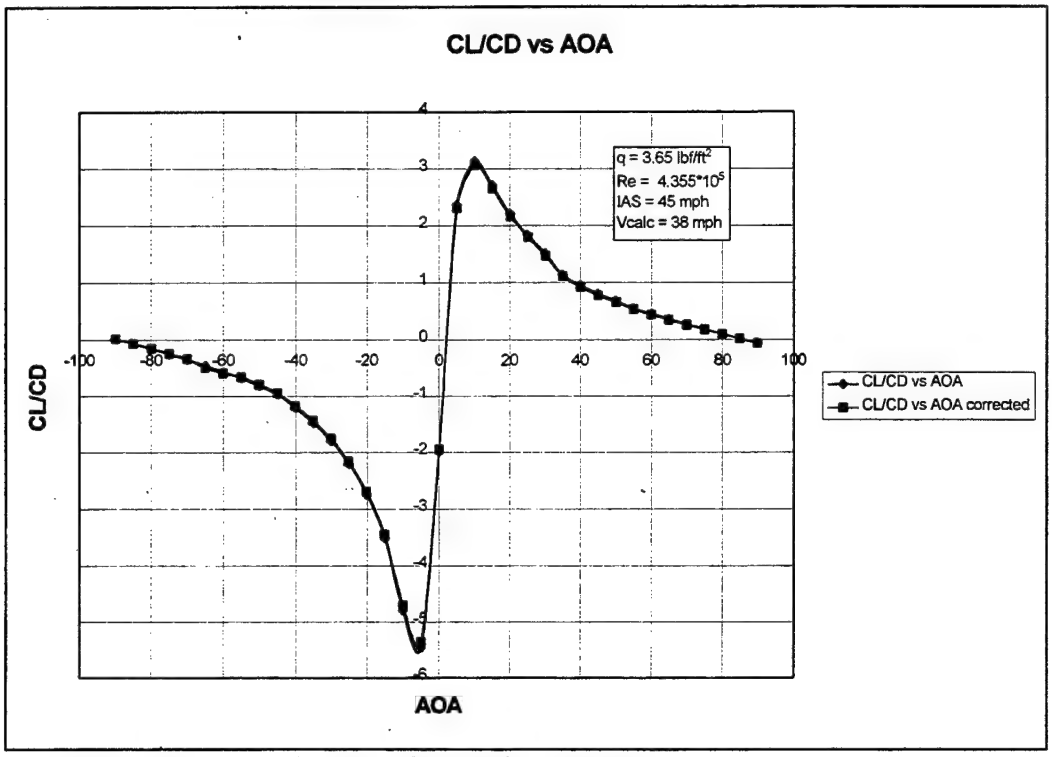

Figure 4.13 C_L/C_D vs. AOA, IAS = 45 mph

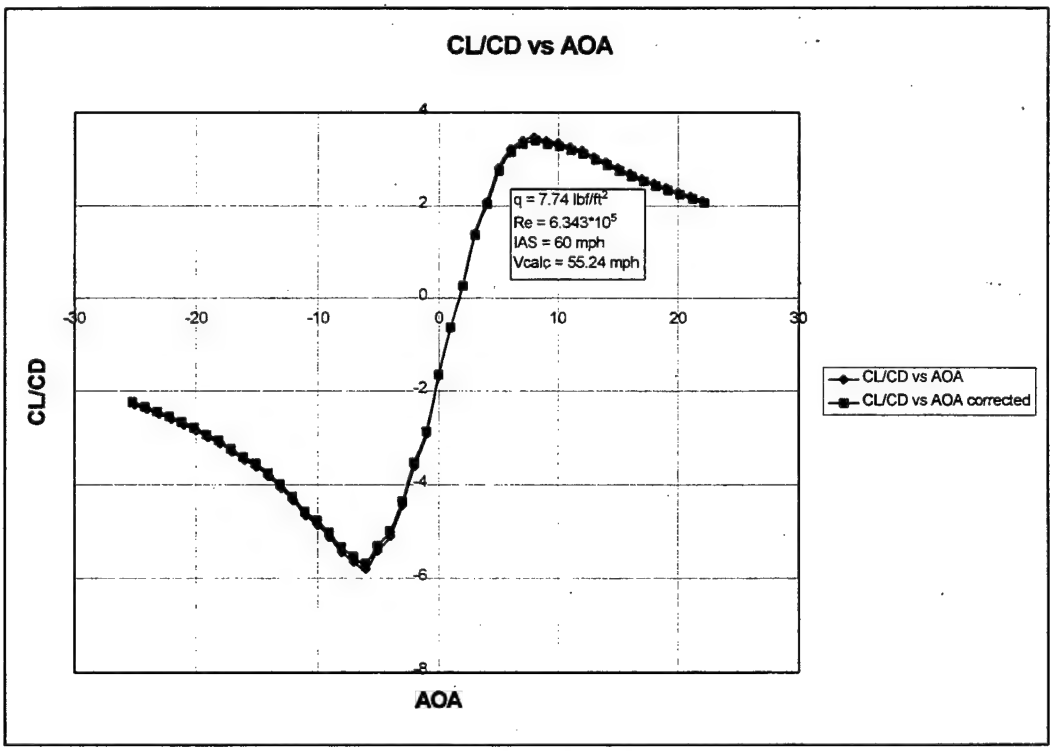

Figure 4.14 C_L/C_D vs. AOA, IAS = 60 mph

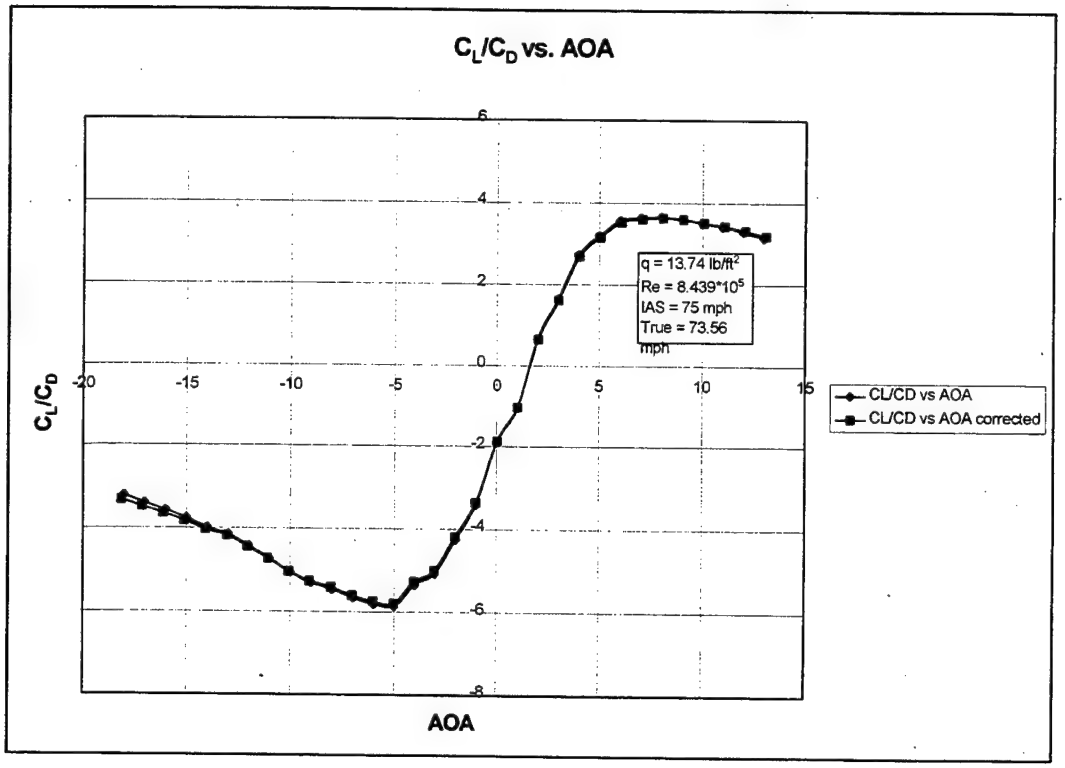

Figure 4.15 C_L/C_D vs. AOA, IAS = 75 mph

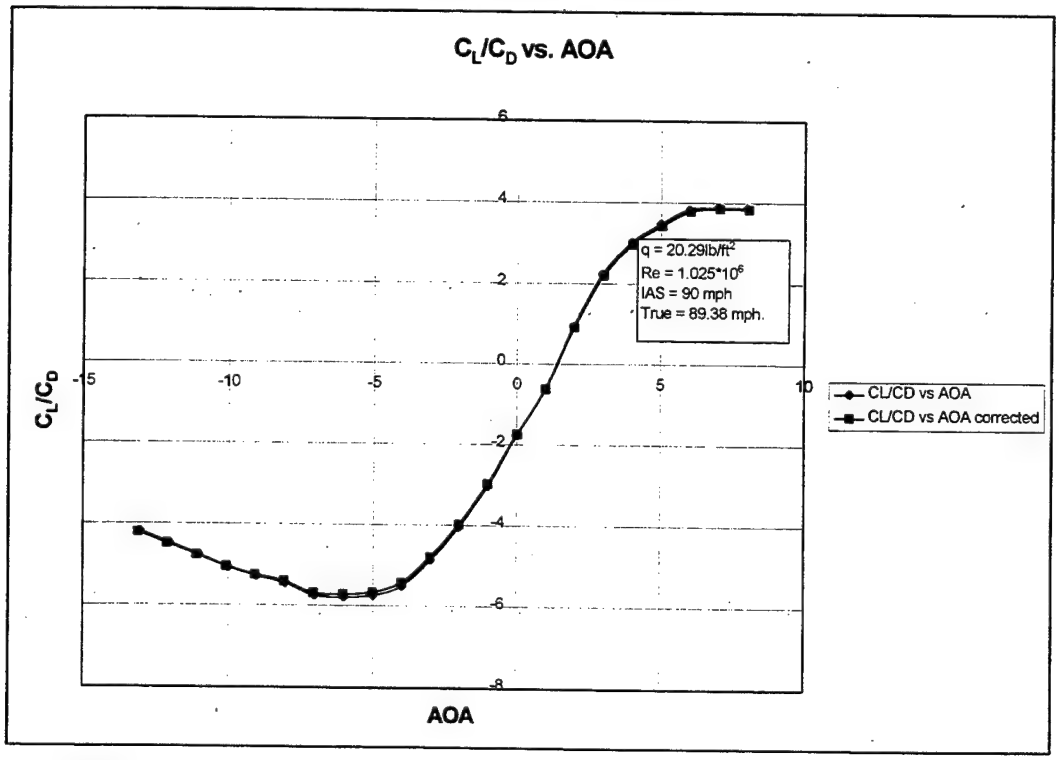

Figure 4.16 C_L/C_D vs. AOA, IAS = 90 mph

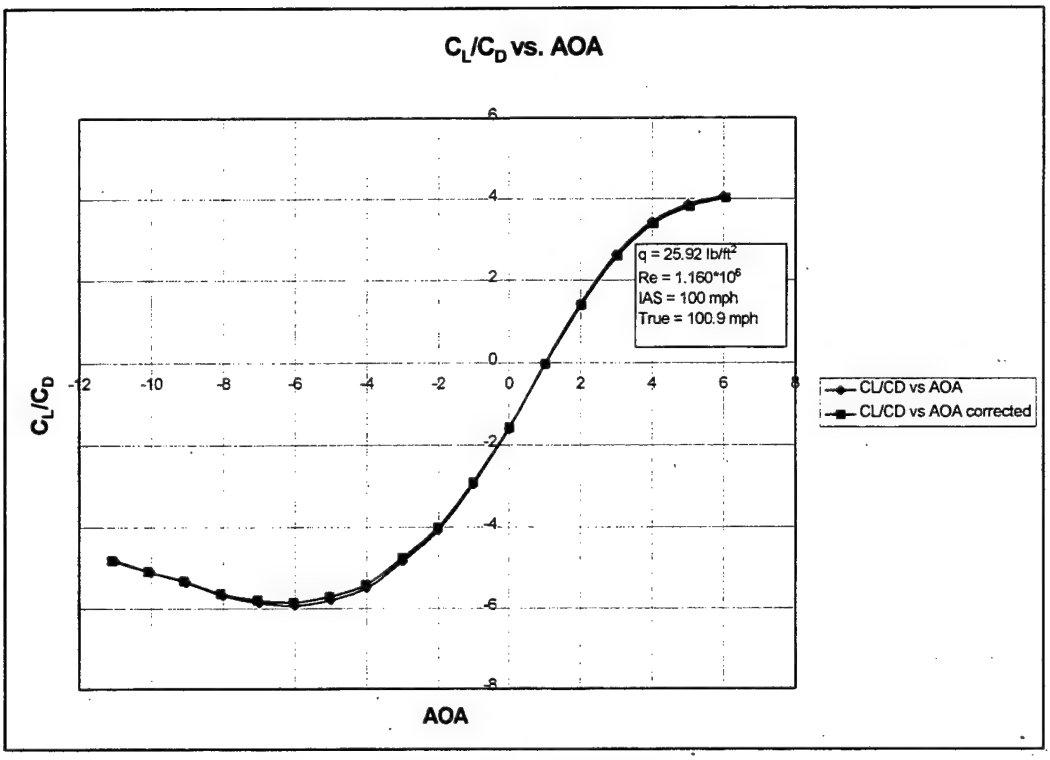

Figure 4.17 C_L/C_D vs. AOA, IAS = 100 mph

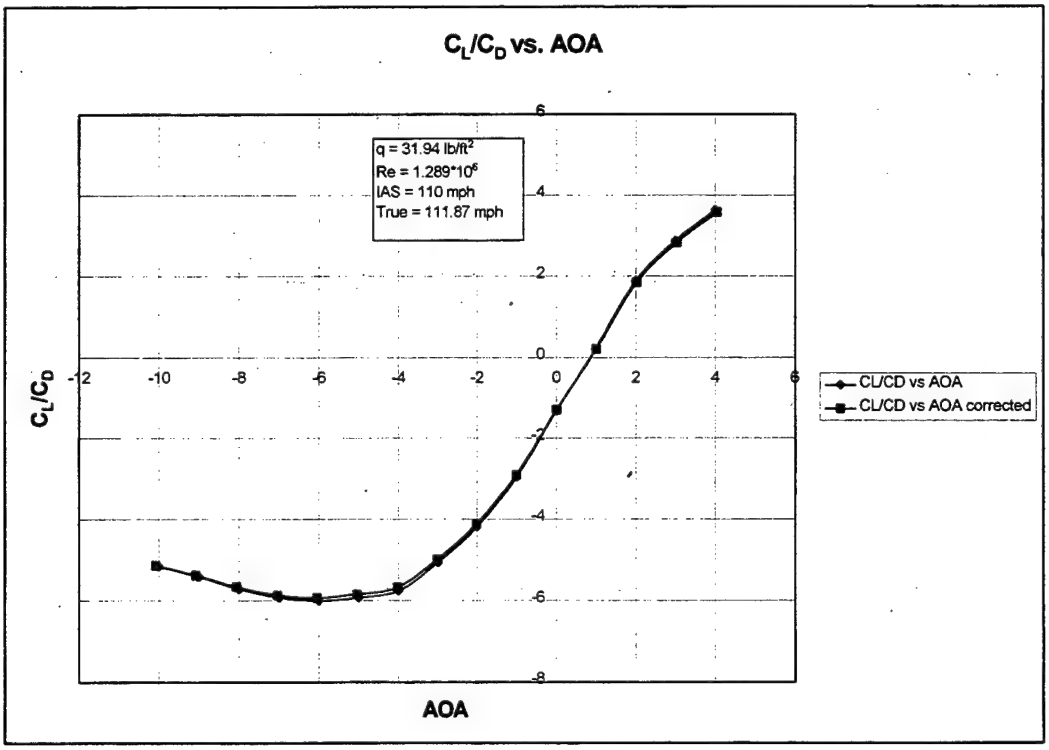

Figure 4.18 C_L/C_D vs. AOA, IAS = 110 mph

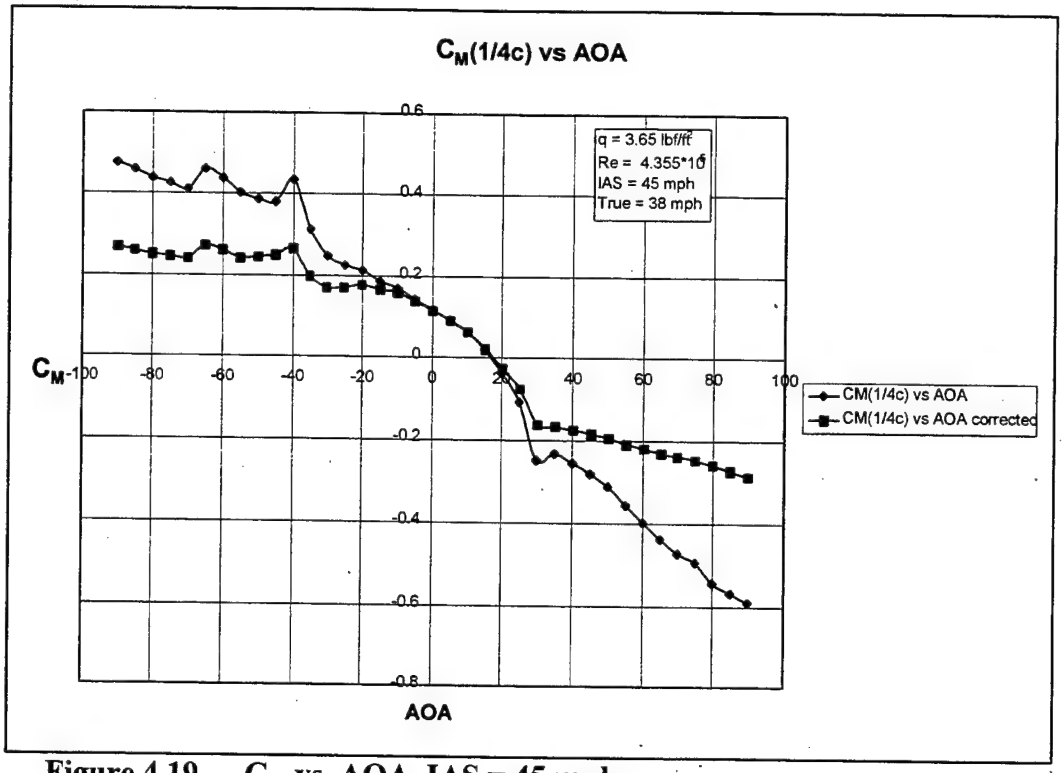

Figure 4.19 C_M **vs. AOA, IAS = 45 mph**

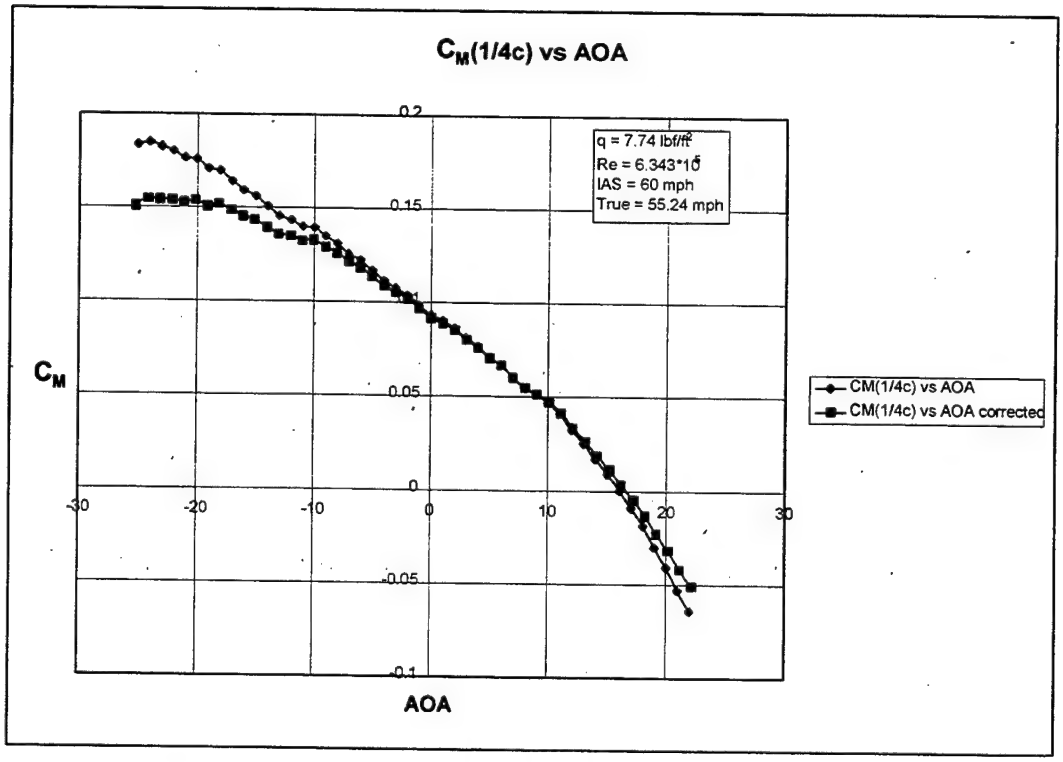

Figure 4.20 C_M **vs. AOA, IAS = 60 mph**

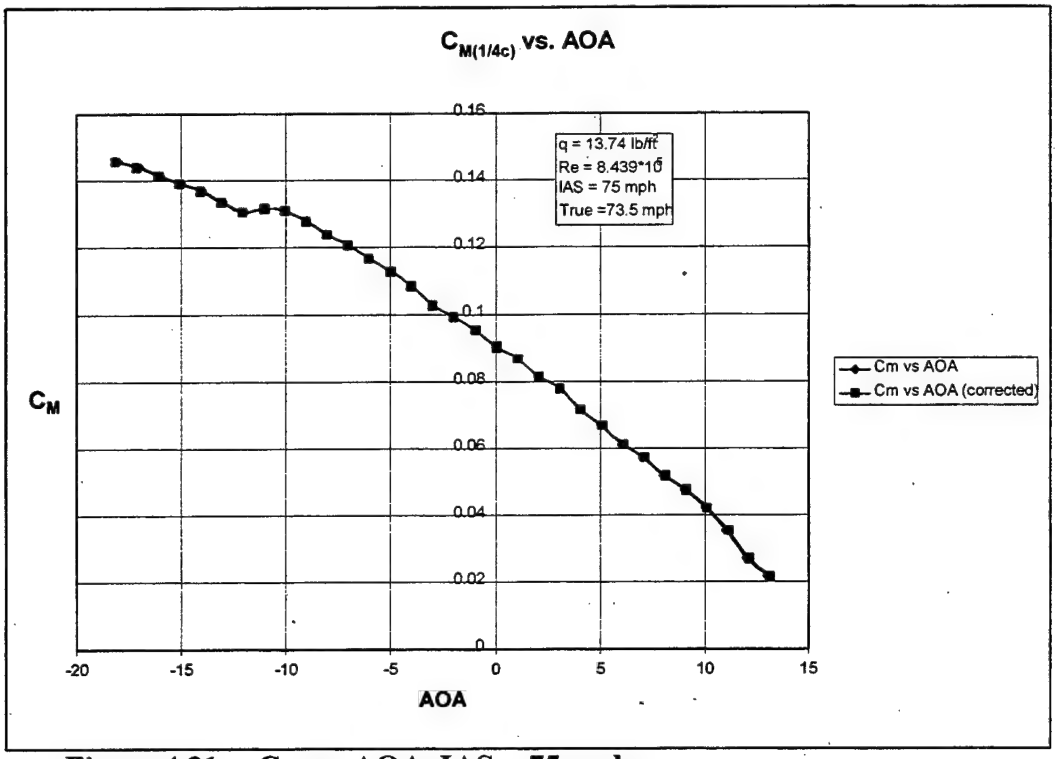

Figure 4.21 C_M vs. AOA, IAS = 75 mph

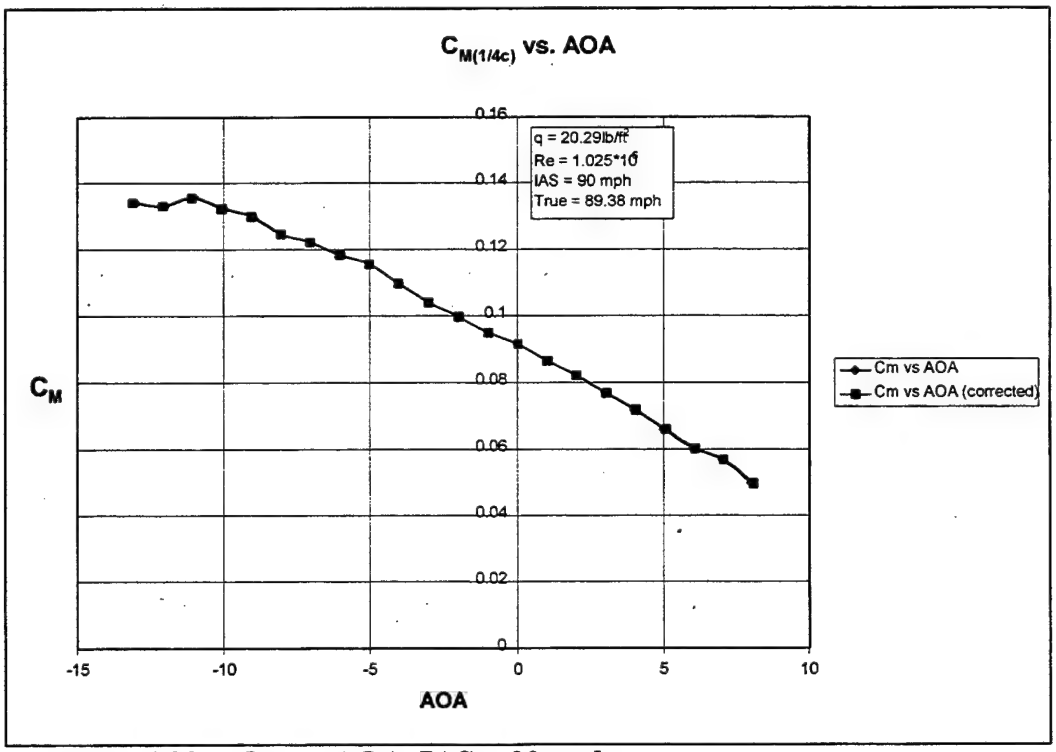

Figure 4.22 C_M vs. AOA, IAS = 90 mph

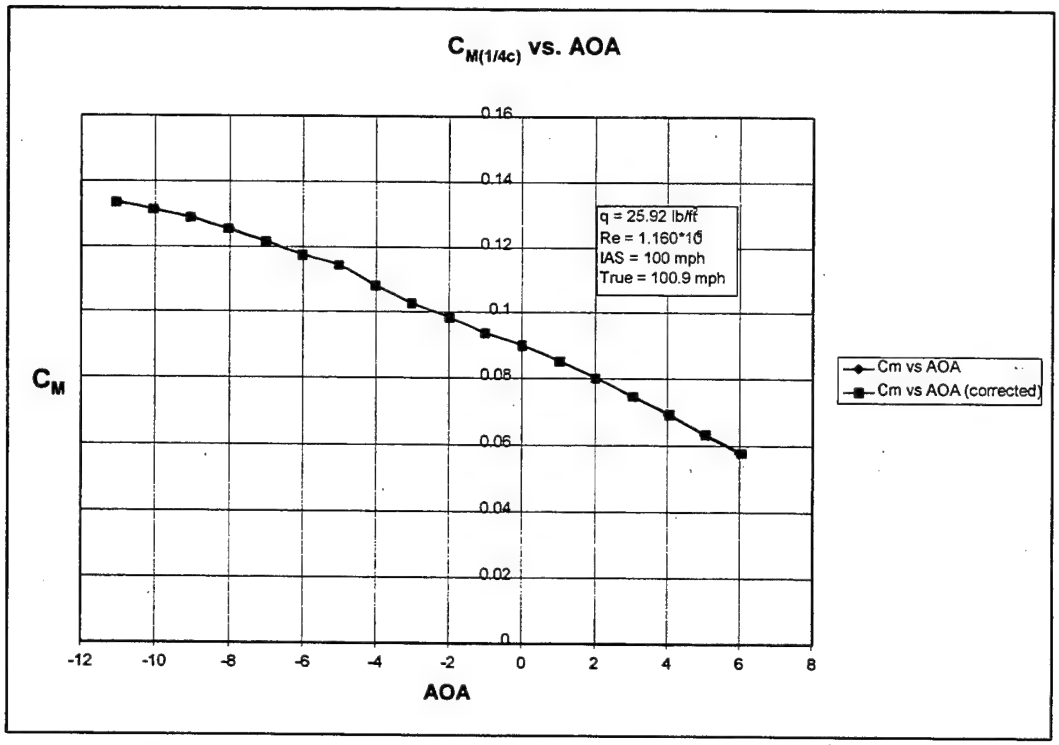

Figure 4.23 C_M vs. AOA, IAS = 100 mph

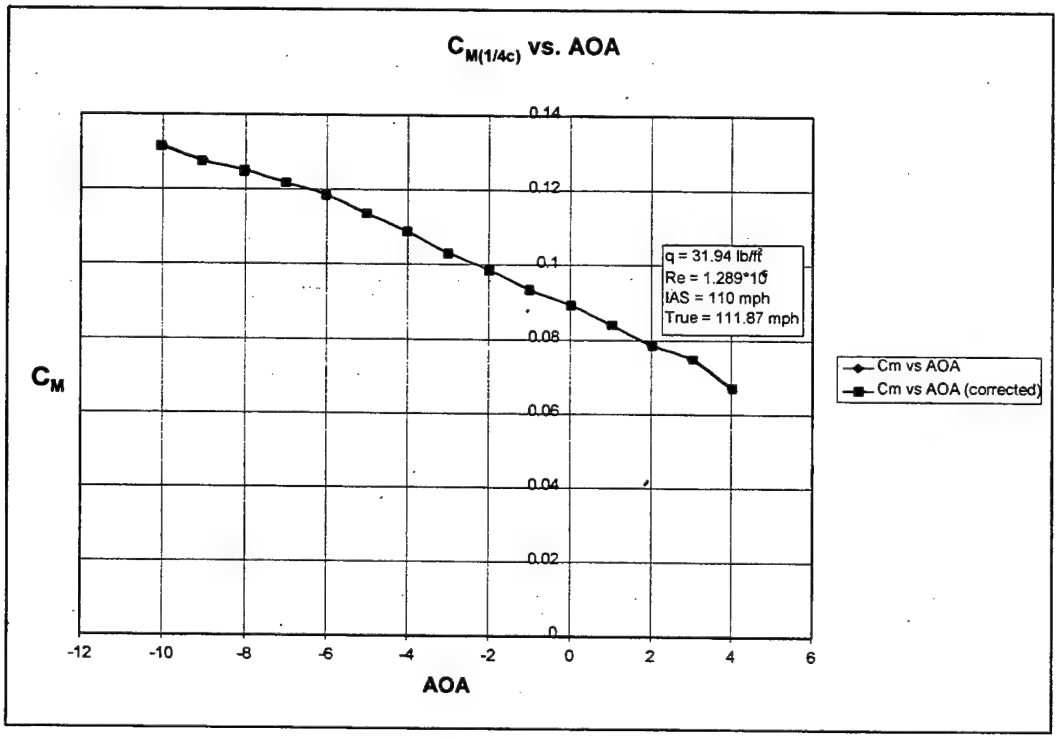

Figure 4.24 C_M vs. AOA, IAS = 110 mph

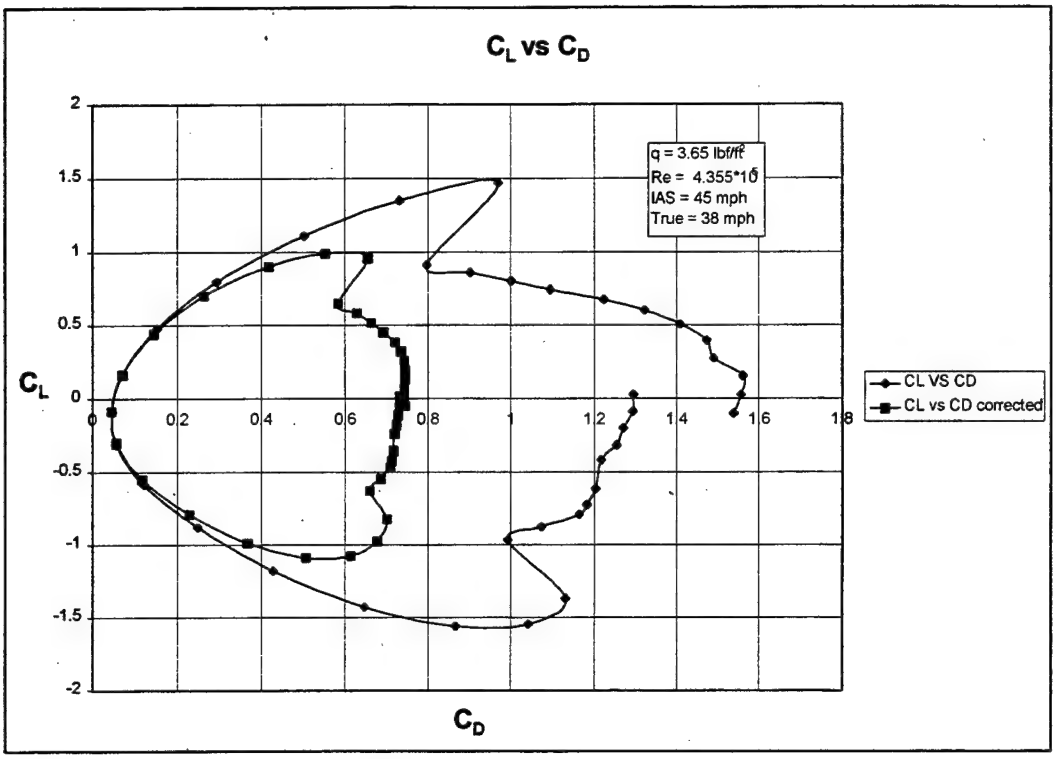

Figure 4.25 C_L vs. C_D, IAS = 45 mph

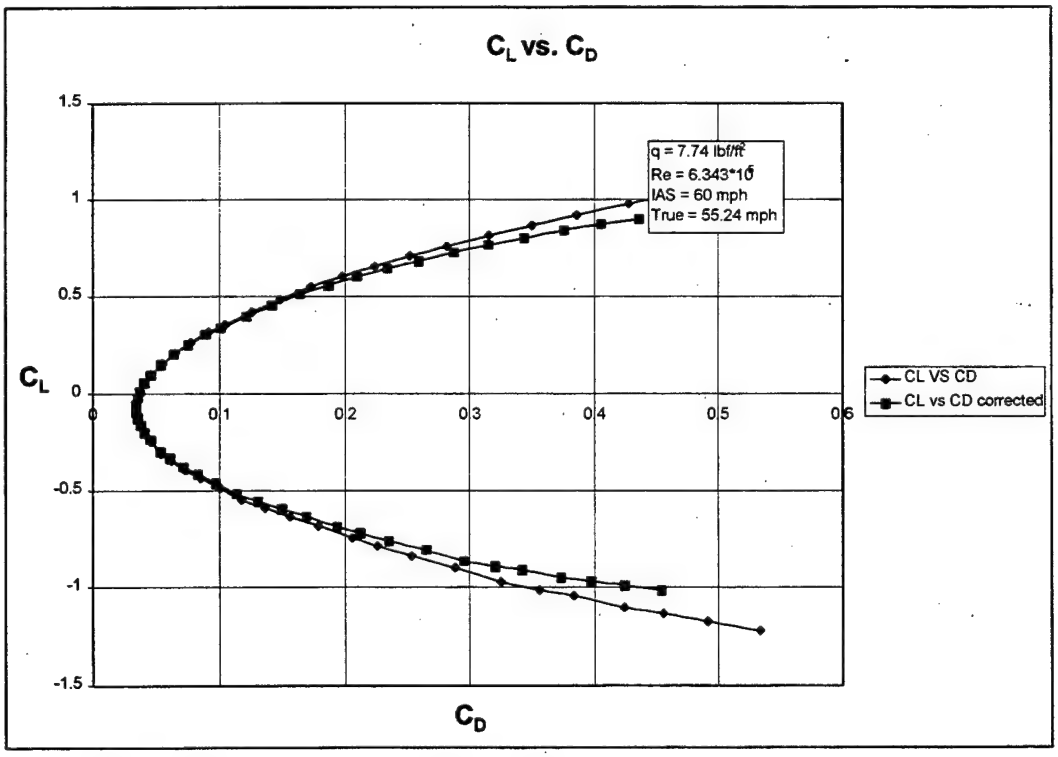

Figure 4.26 C_L vs. C_D, IAS = 60 mph

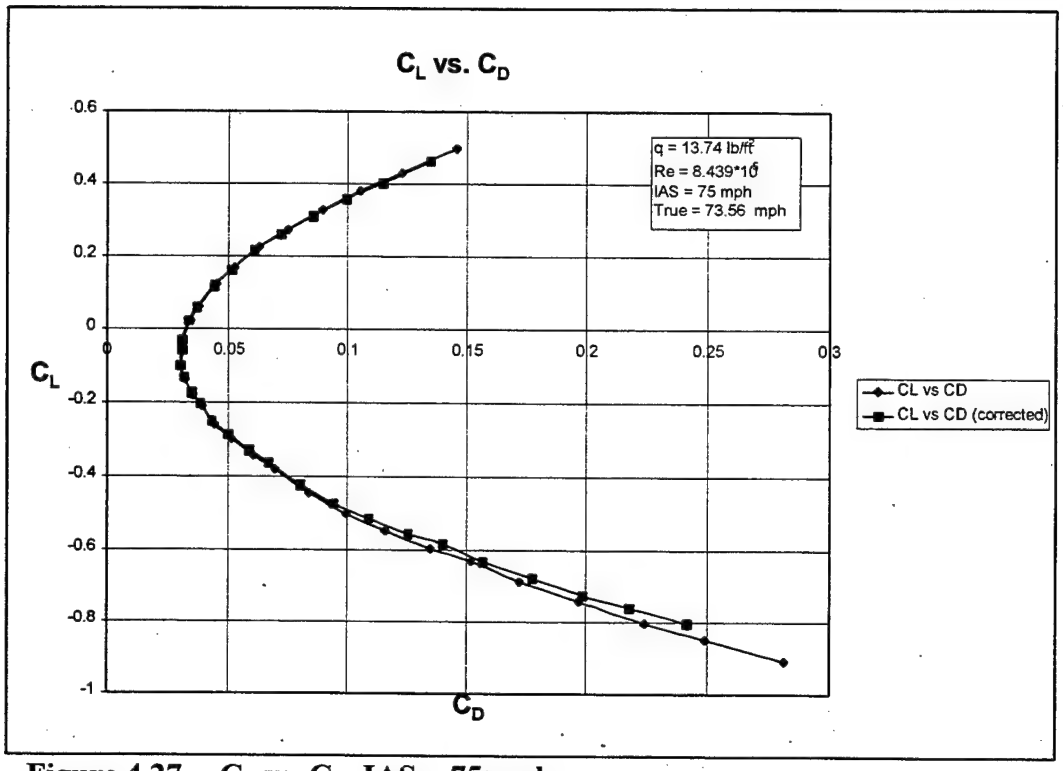

Figure 4.27 C_L vs. C_D, IAS = 75 mph

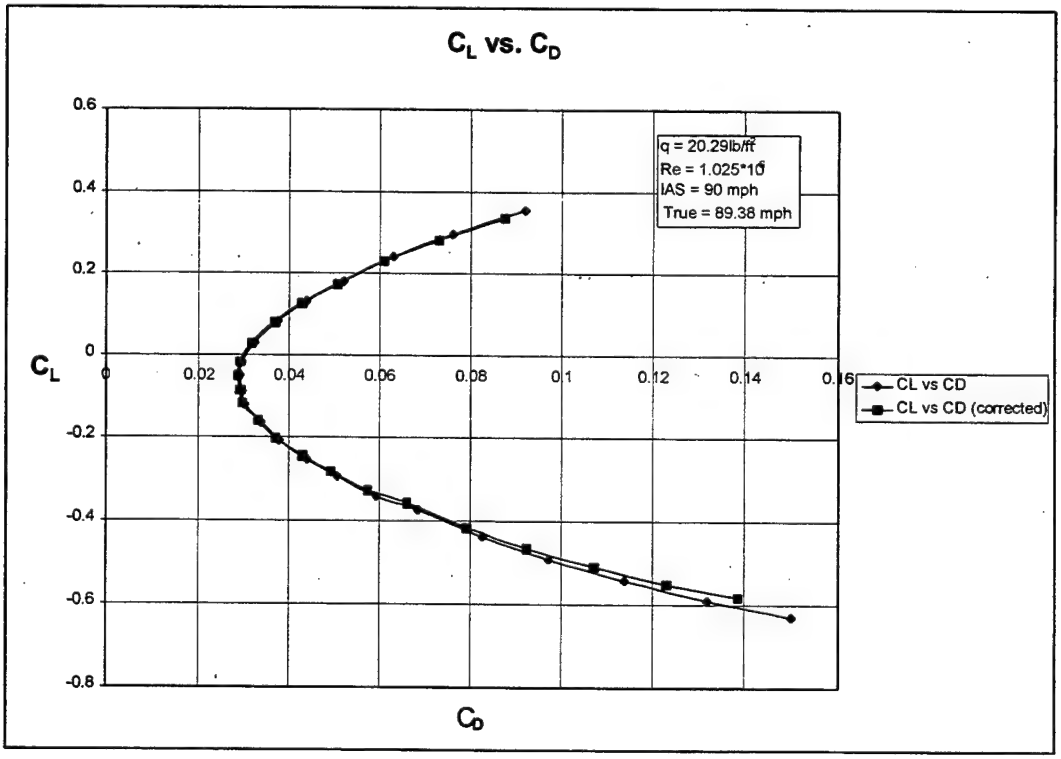

Figure 4.28 C_L vs. C_D, IAS = 90 mph

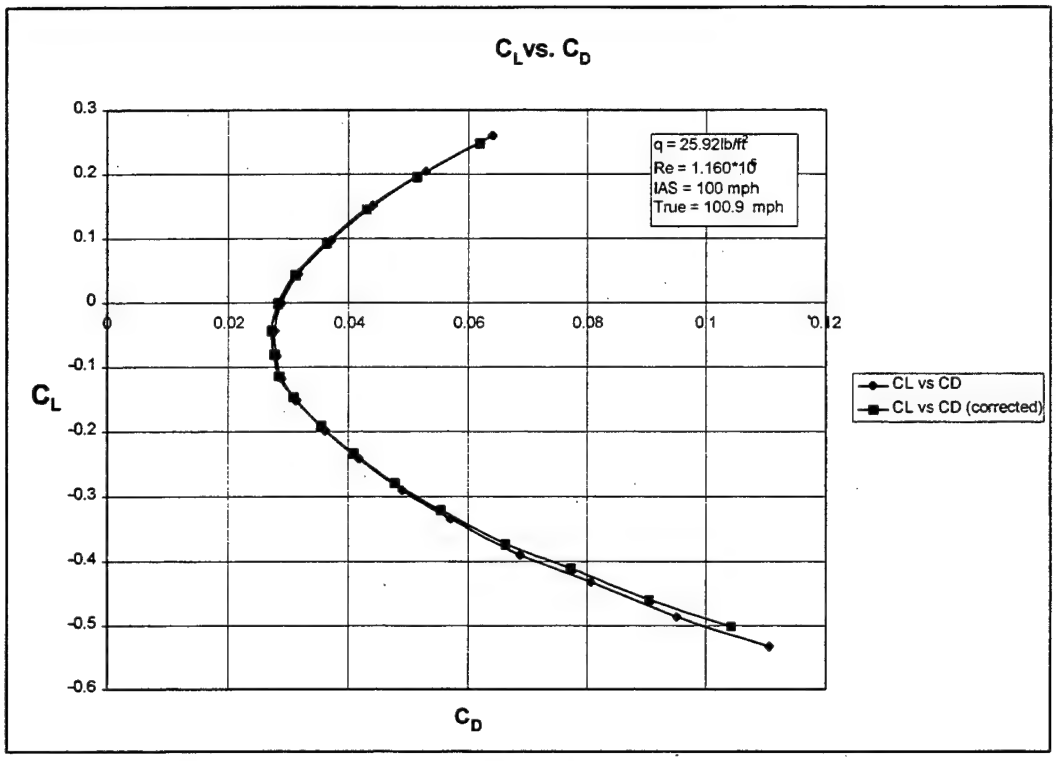

Figures 4.29 C_L vs. C_D, IAS = 100 mph

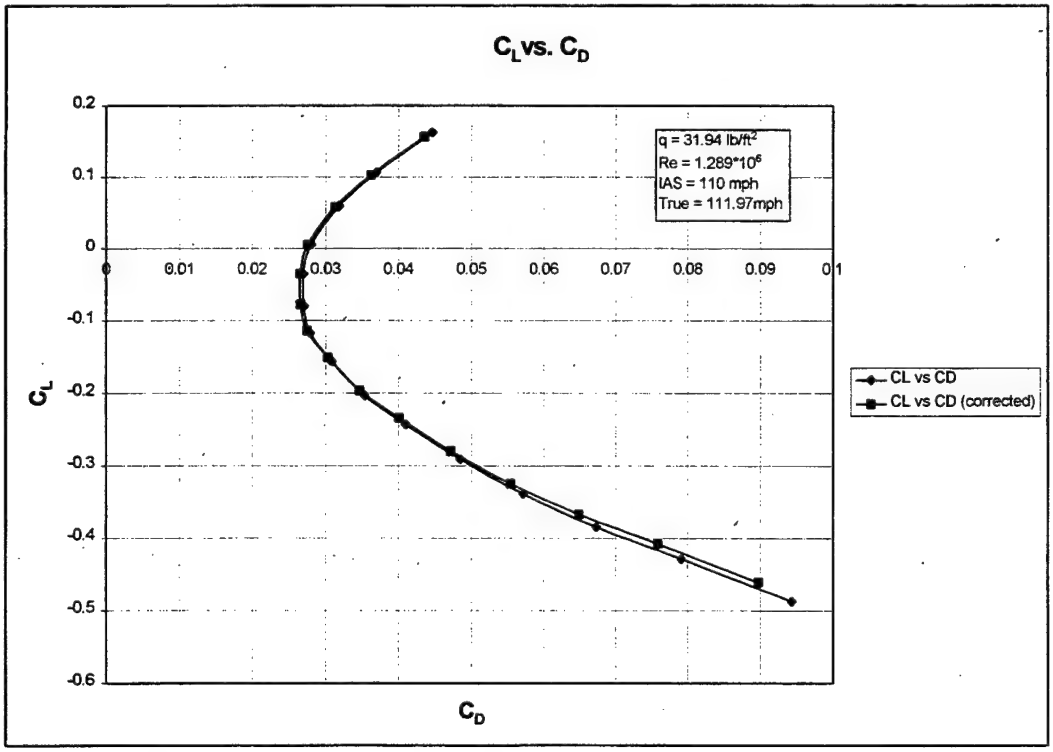

Figure 4.30 C_L vs. C_D, IAS = 110 mph

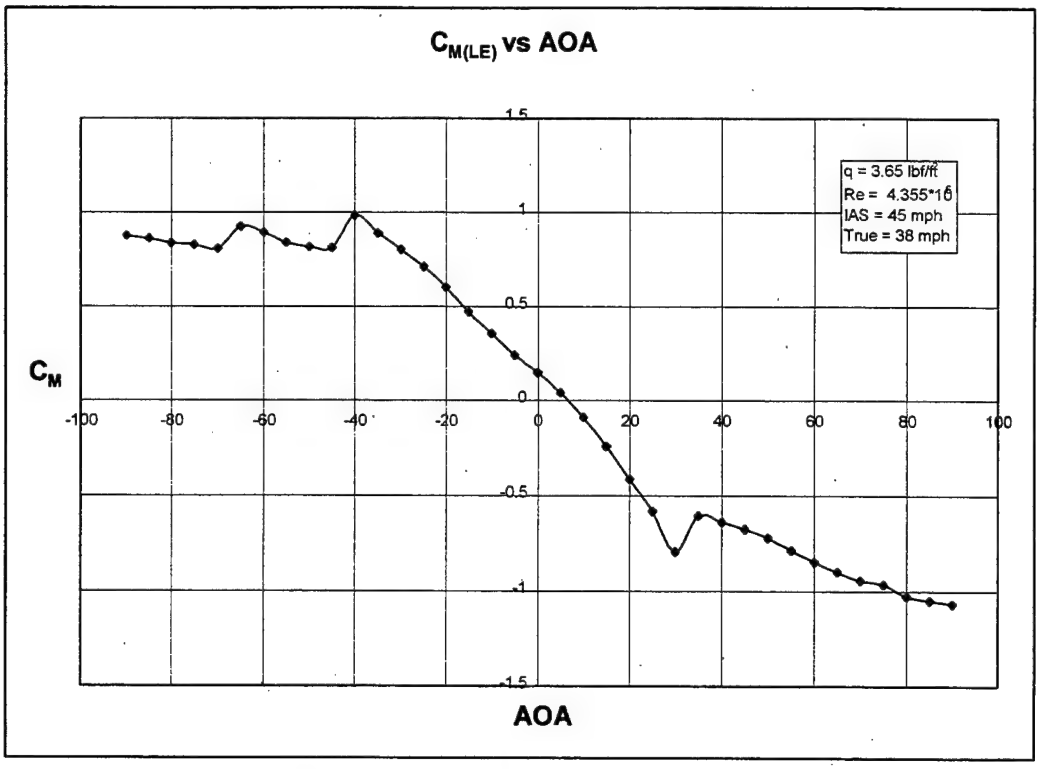

Figure 4.31 $C_{M(LE)}$ vs. AOA, IAS = 45 mph

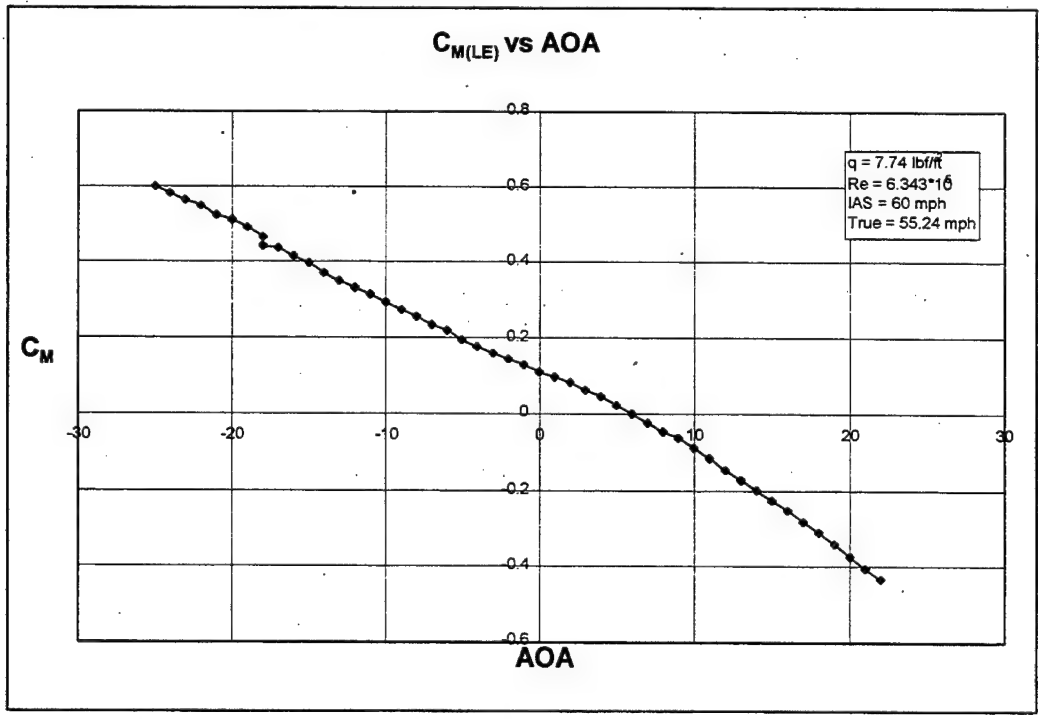

Figure 4.32 $C_{M(LE)}$ vs. AOA, IAS = 60 mph

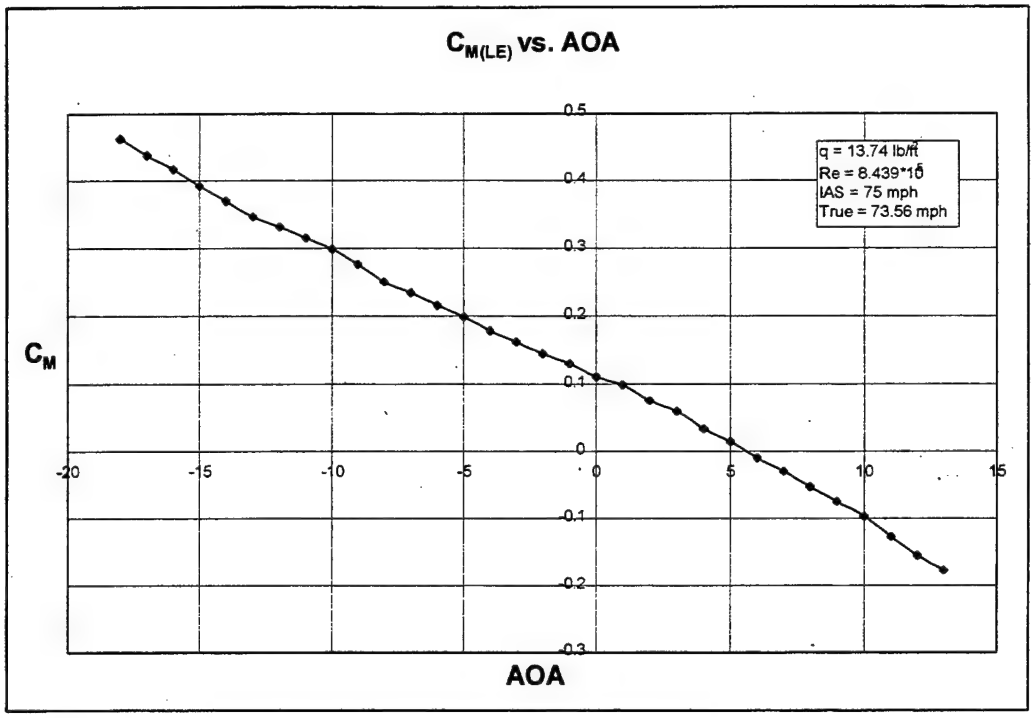

Figure 4.33 $C_{M(LE)}$ **vs. AOA, IAS = 75 mph**

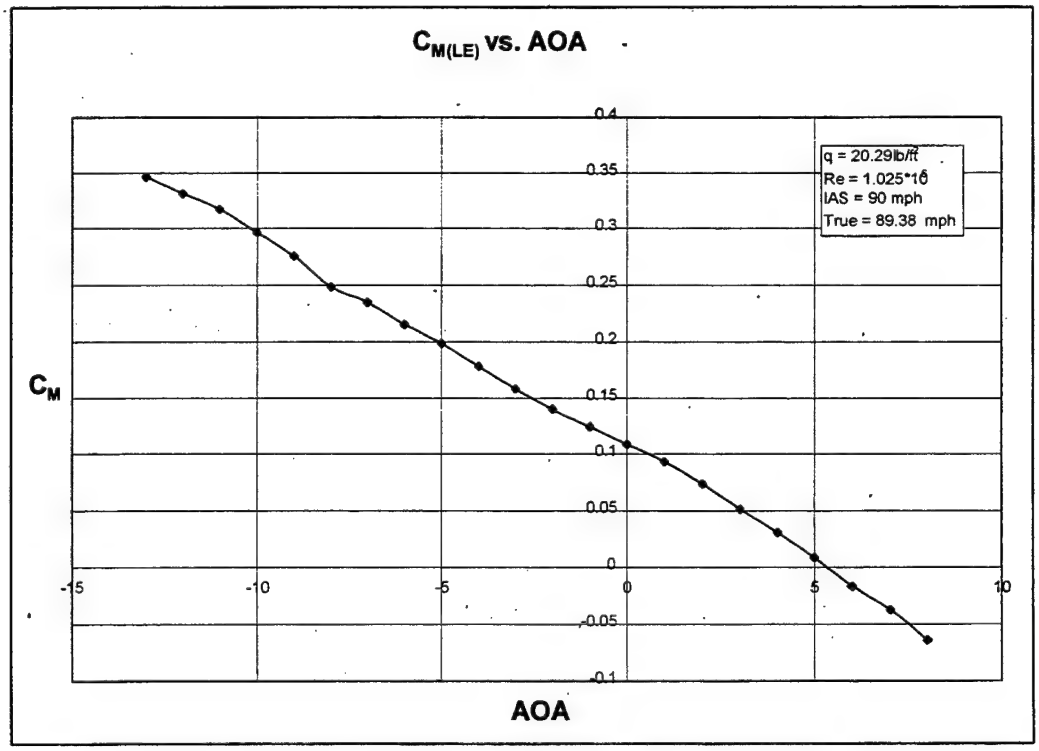

Figure 4.34 $C_{M(LE)}$ **vs. AOA, IAS = 90 mph**

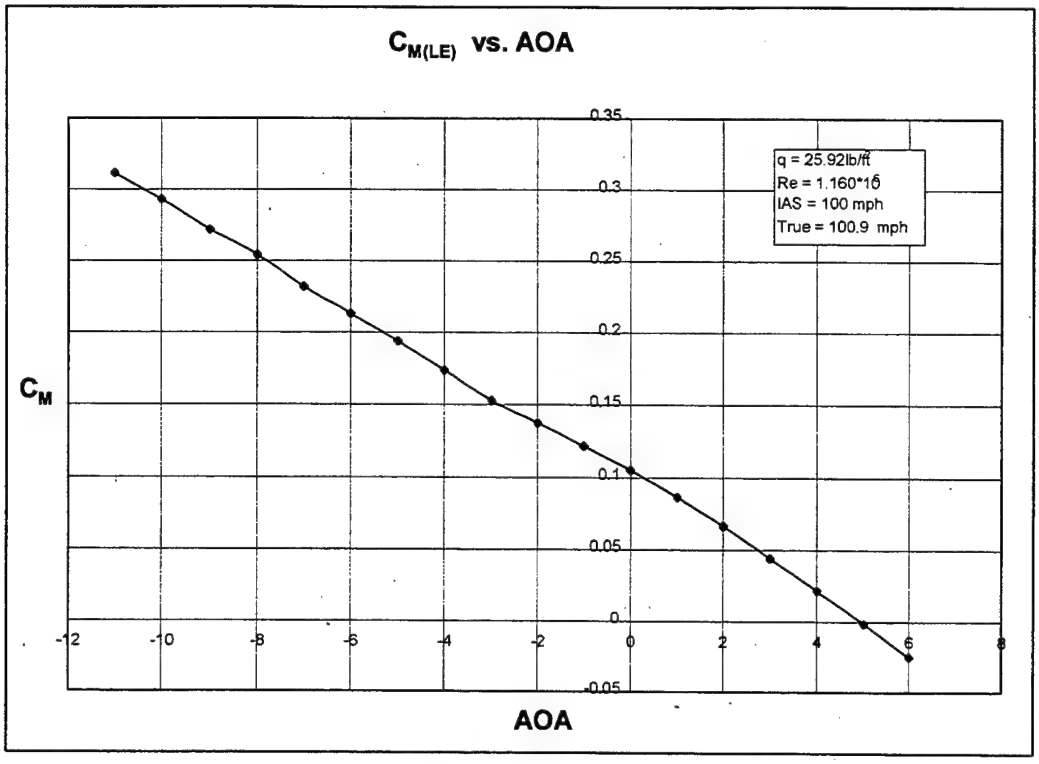

Figure 4.35 $C_{M(LE)}$ **vs. AOA, IAS = 100 mph**

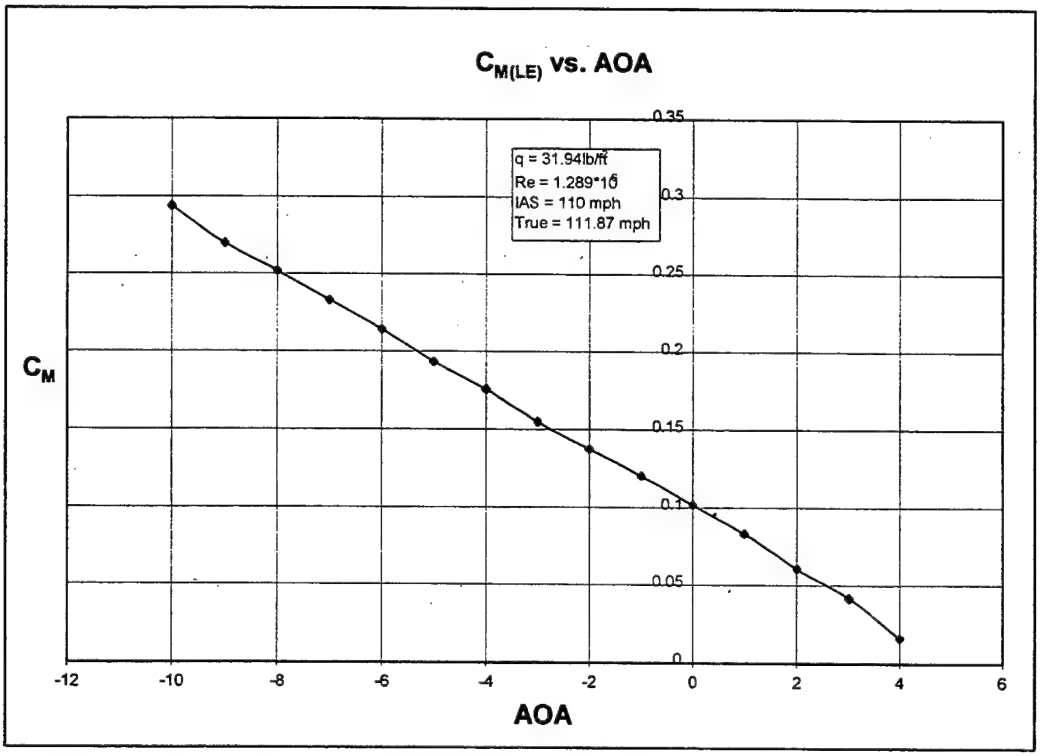

Figure 4.36 $C_{M(LE)}$ **vs. AOA, IAS = 110 mph**

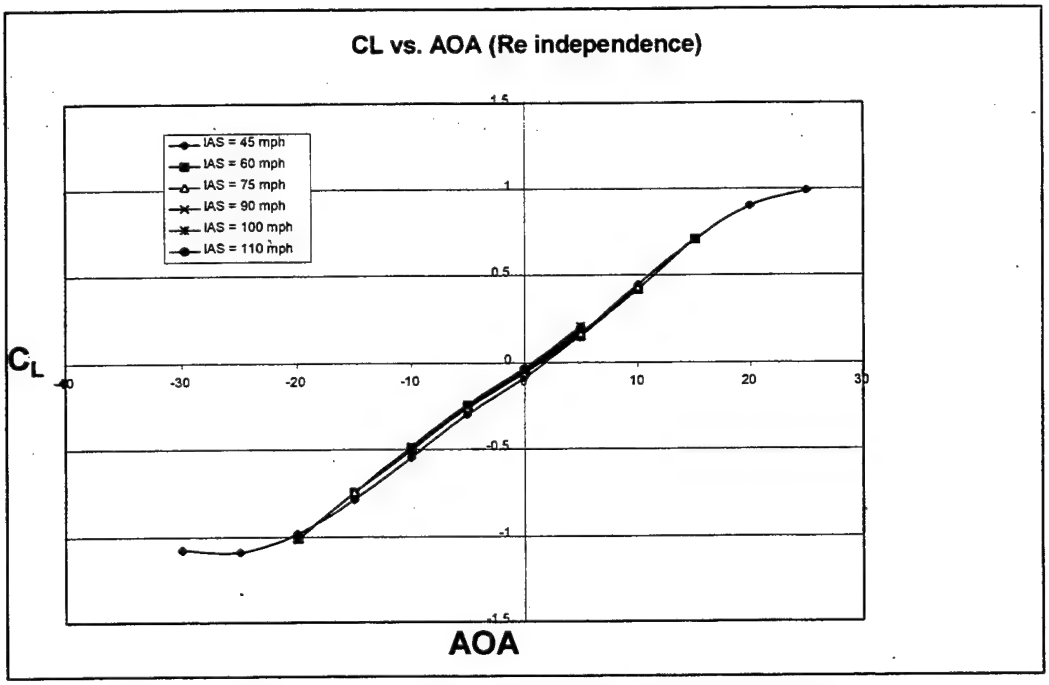

Figure 4.37 C_L vs. AOA (Reynolds Independence)

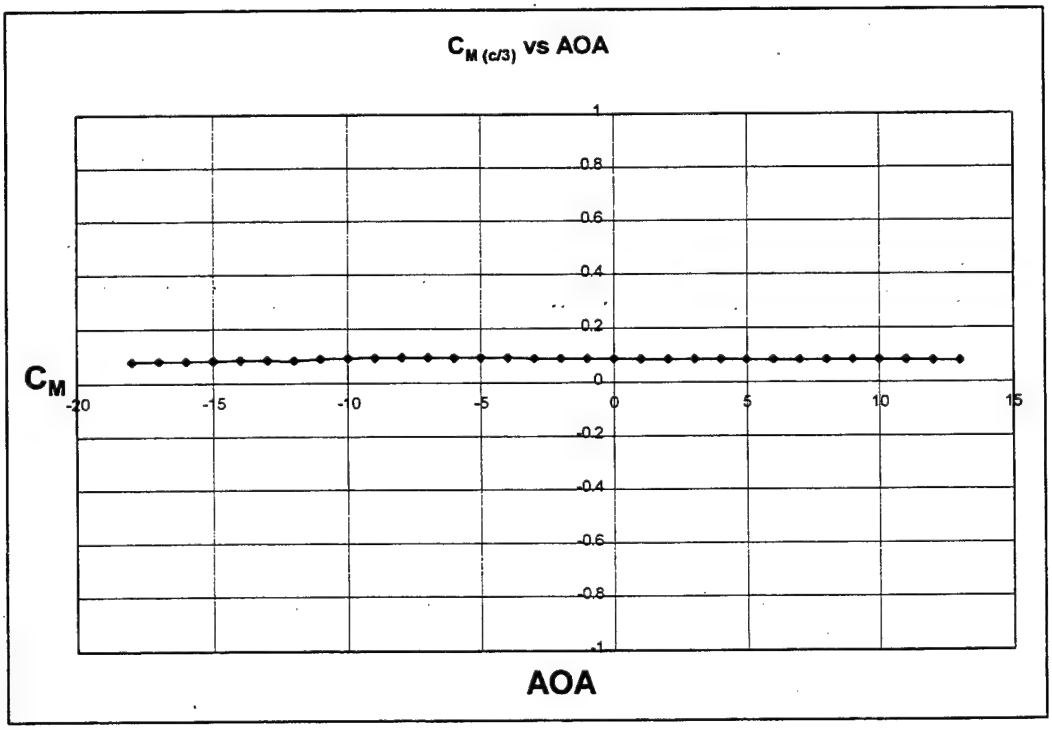

Figure 4.38 Neutral point at 1/3 of root chord

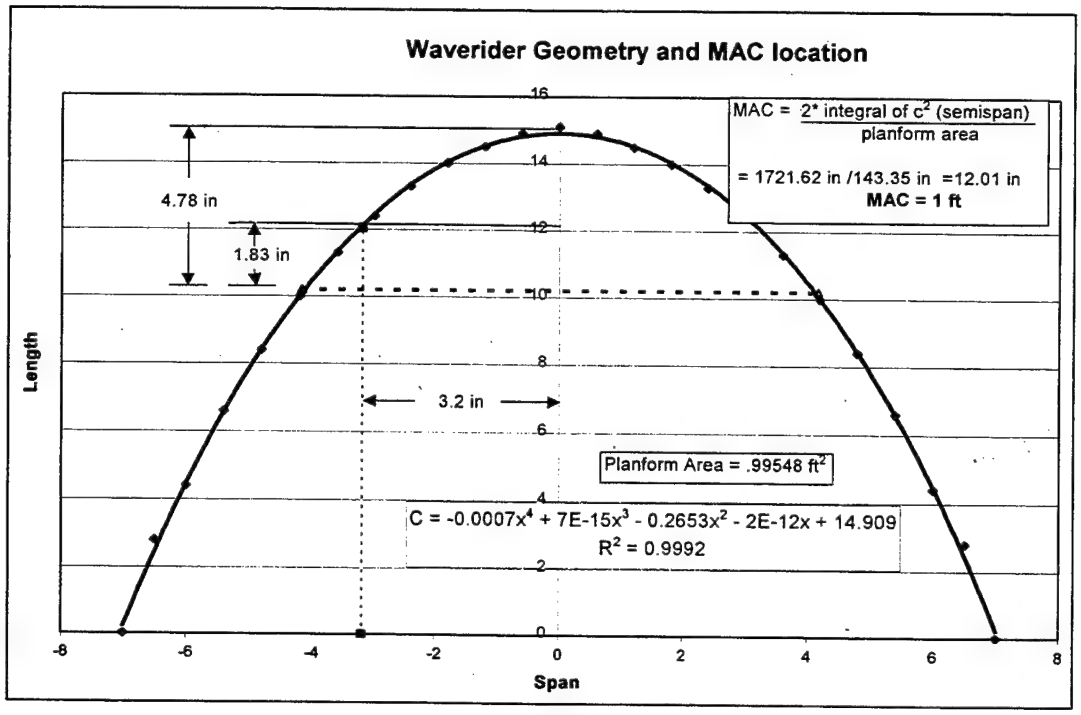

Figure 4.39 Planform Geometry, Location of Mean Aerodynamic Chord

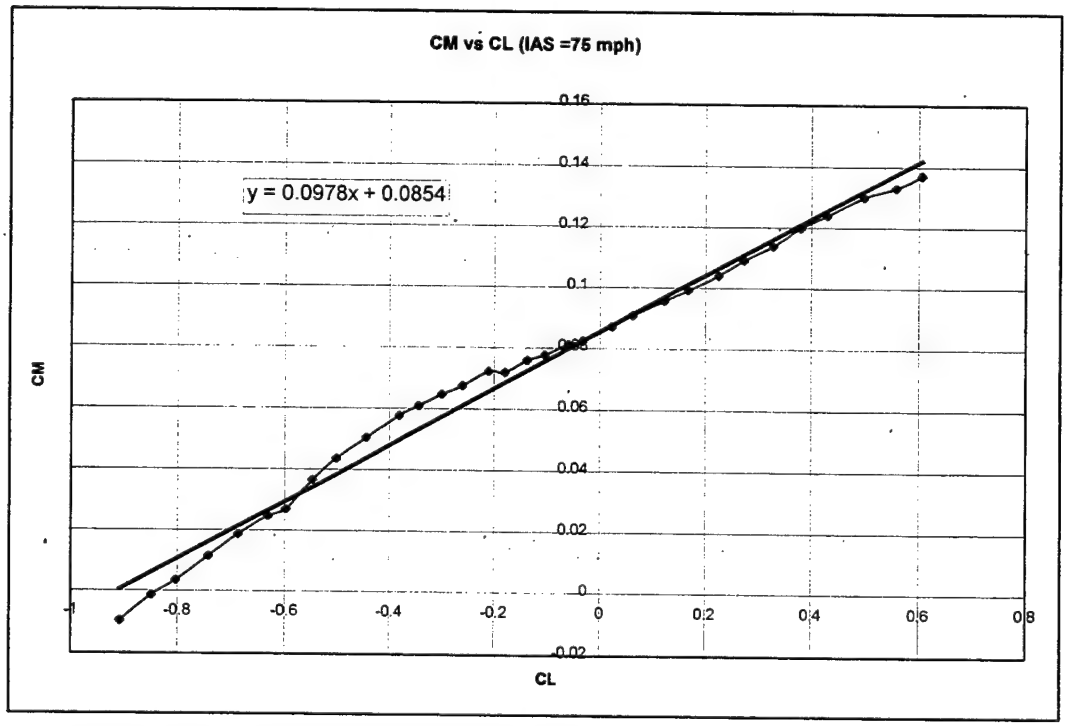

Figure 4.40 Determining slope of $C_{M(MAC)}$ vs. C_L

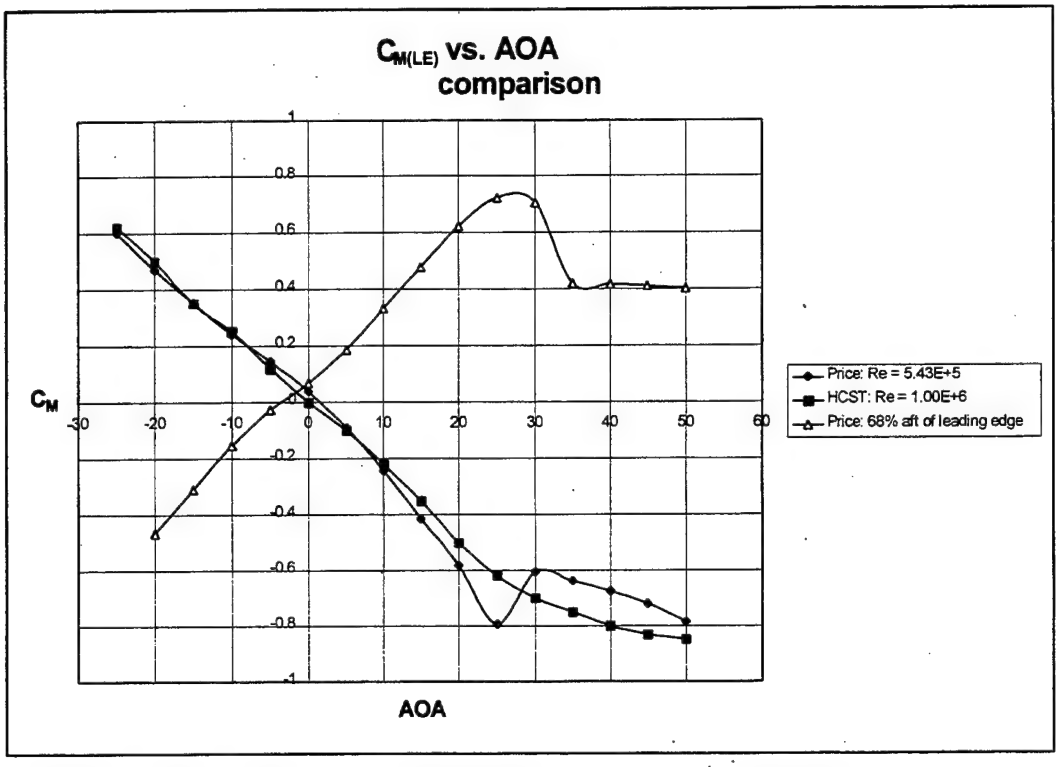

Figure 4.41 $C_{M(LE)}$ vs. AOA, Price (Tested by Huff) vs. HSCT

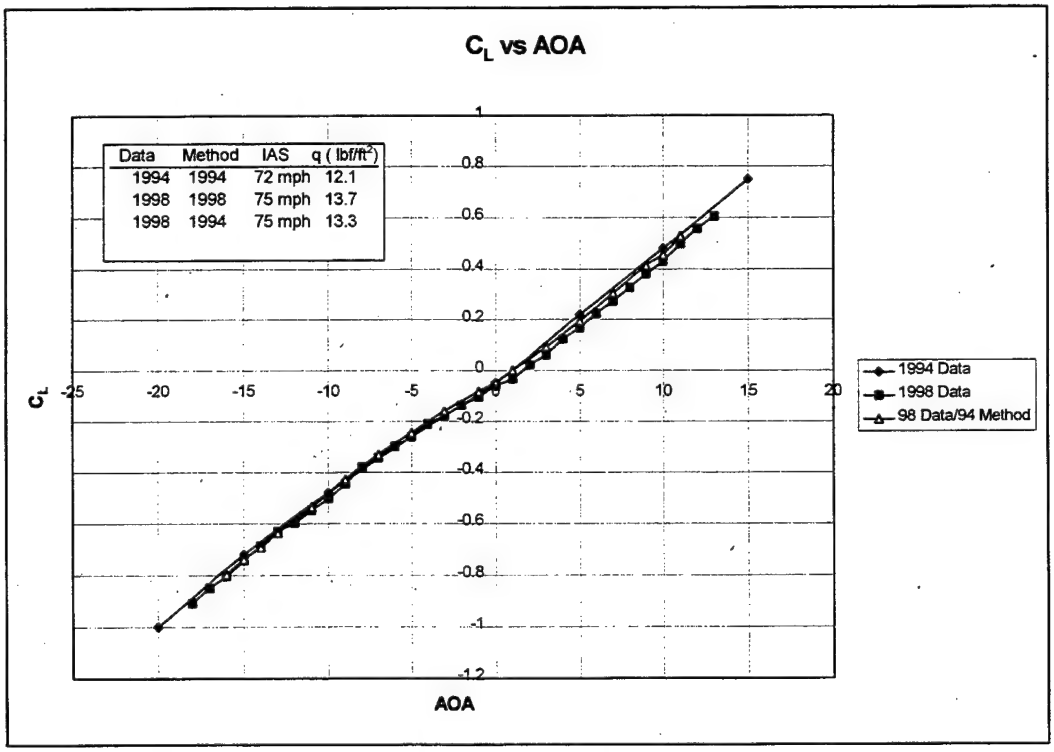

Figure 4.42 C_L vs. AOA comparison, Huff vs. Cedrun

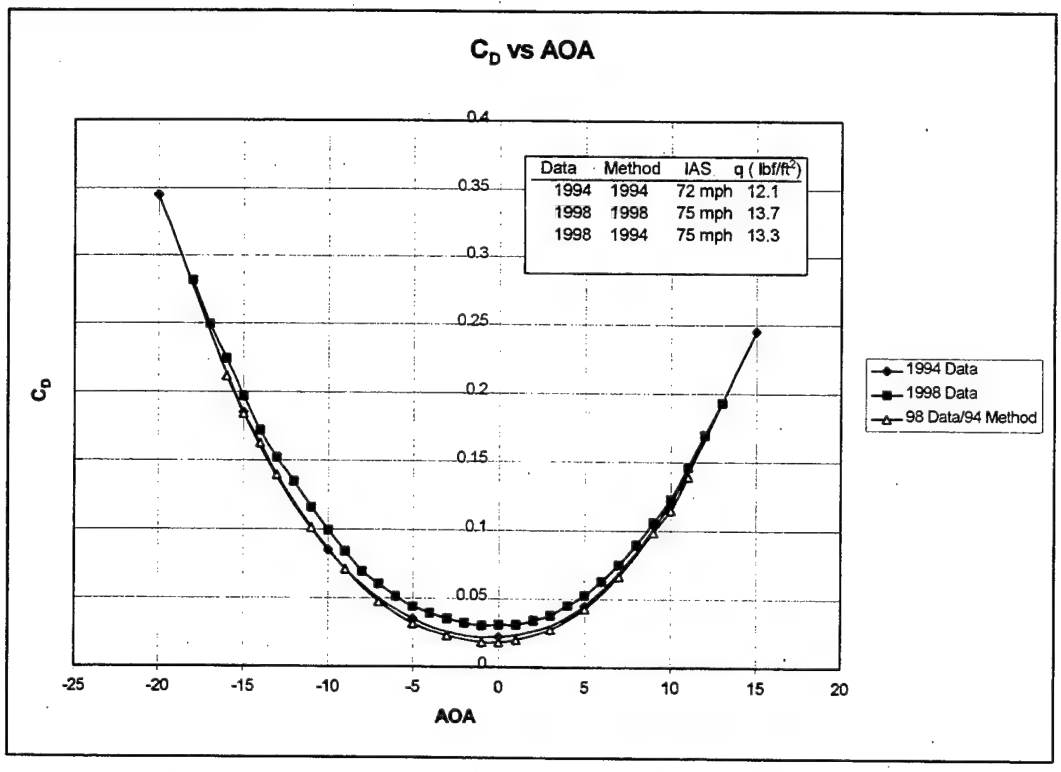

Figure 4.43 C_D vs. AOA comparison, Huff vs. Cedrun

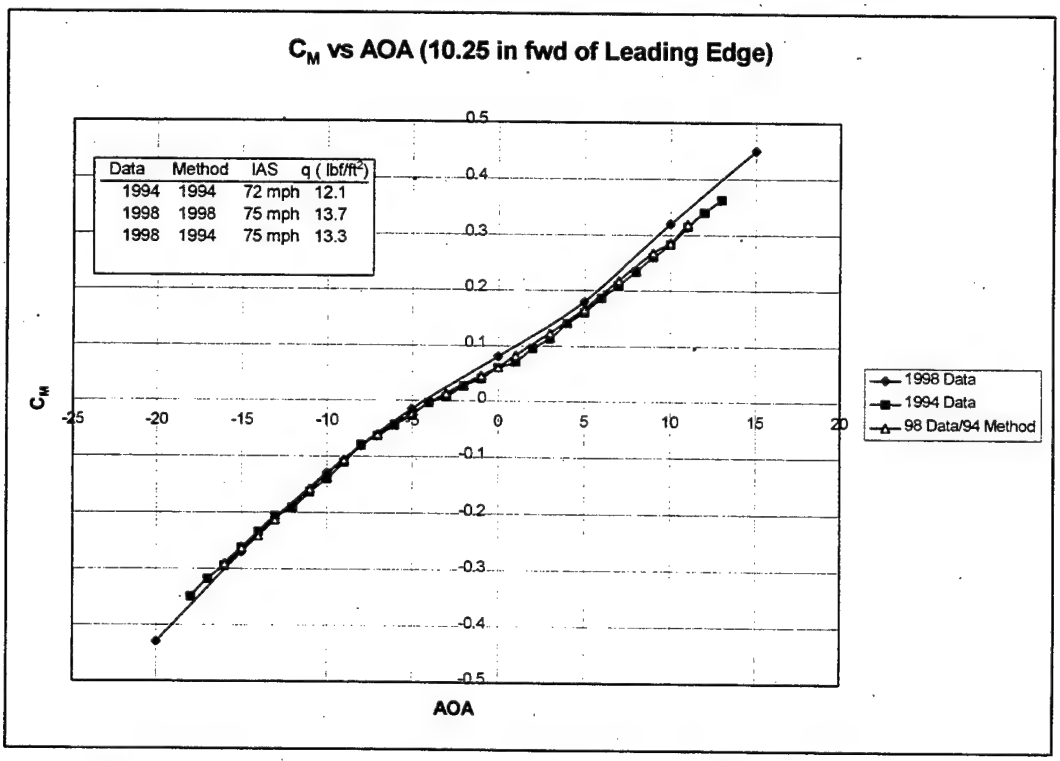

Figure 4.44 C_M vs. AOA comparison, Huff vs. Cedrun

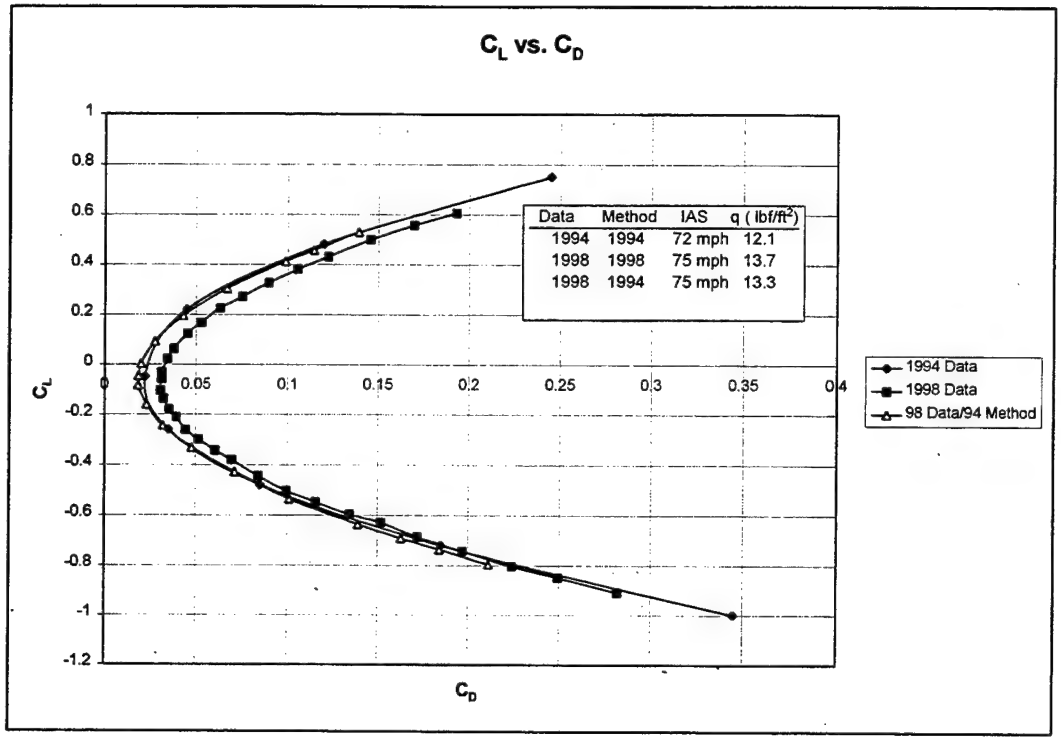

Figure 4.45 C_L vs. C_D, Huff vs. Cedrun

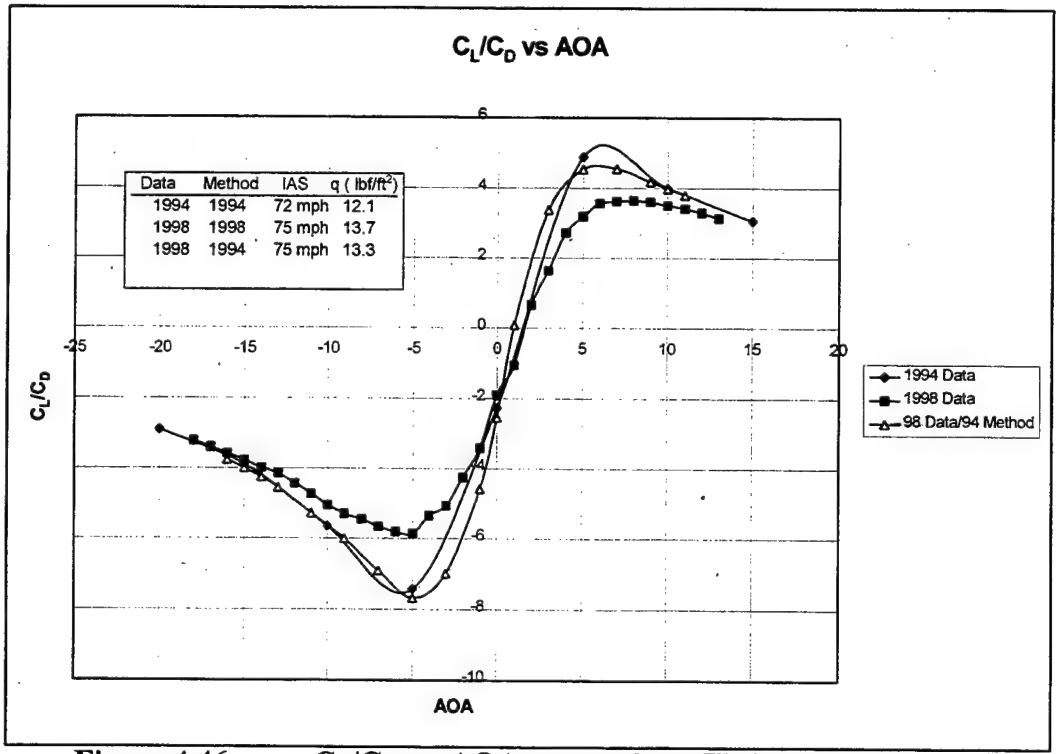

Figure 4.46 C_L/C_D vs. AOA comparison, Huff vs. Cedrun

V. CONCLUSION AND RECOMMENDATIONS

A. CONCLUSIONS

The use of a modern data acquisition system such as LabVIEW© has significantly improved the capability of the NPS Low Speed Wind Tunnel. When combined with the strain gauge balance, the aerodynamic forces on any sting-mounted model can be quickly and accurately determined. Several additional benefits are realized. First, data is acquired and processed online so results can be analyzed while testing is taking place. Second, modifications to the program can be made easily, allowing a greater variety of testing to be accomplished in a shorter amount of time. Third, the user can monitor the data processing on the front panel through all the intermediate steps as well as simply viewing the final result. Finally, the program's scan rate can be adjusted from the front panel instantly, allowing the user to choose between static testing for single run program execution or dynamic testing on a continuous running cycle.

The use of a PC based system has other inherent advantages. Post processing, if desired for future use, is made easier by compatibility with existing spreadsheet and word processing programs. The data can be easily archived on the hard drive and accessed through Windows© Explorer. Processed data, including all intermediate calculations as well as final results, can be saved automatically to floppy, zip or any other portable media with later retrieval on any other PC. The entire strain gauge program, due to its modularity and method of calling VIs from the built in software library, is also easily portable and can be saved on a single floppy diskette.

Testing performed on the Price Waverider model accomplished several purposes. Data obtained during current testing validated previous research performed by LT

Cedrun. Current testing also resolved questions regarding longitudinal stability of the Price waverider and the location of its neutral point. Perhaps most important, using a model that had been previously tested served as a verification process for the LabVIEW© program, paving the way for future wind tunnel analysis of other models.

B. RECOMMENDATIONS

1. The Price waverider has been evaluated so far with an emphasis on static testing. The capability exists for dynamic and oscillatory testing as well.
2. The range of AOA was quite limited above 100 mph IAS using the larger wind tunnel model. A water tunnel model of the Price waverider can be tested in the wind tunnel using the locally manufactured sting adapter. As the planform area is significantly smaller, testing can be conducted at higher speeds without fear of overloading the balance. A comparison could be made (in the wind tunnel) between the wind tunnel and water tunnel models to verify similarity of results.
3. Other water tunnel models, including another waverider, are also available for testing in the wind tunnel using the same locally manufactured adapter. Comparisons of aerodynamic qualities could be easily made between these different models.
4. The wind tunnel is capable of 200 mph, far exceeding the capabilities of the current strain gauge balance with larger models. The use of a balance with higher load ratings would allow larger changes in AOA at increased tunnel speeds.
5. Side force, Yaw and Rolling moments were not non-dimensionalized. Future modifications could easily incorporate these features into the existing program.

LIST OF REFERENCES

1. LabVIEW User Manual, National Instruments Corporation, Austin, TX, January, 1996.

2. Cedrun, M.E., Low-Speed Wind Tunnel Testing of the NPS/NASA Ames Mach 6 Optimized Waverider, Master's Thesis, Naval Postgraduate School, Monterey, CA, June, 1994.

3. Laboratory Manual for Low-Speed Wind Tunnel Testing, Department of Aeronautics and Astronautics, Naval Postgraduate School, Monterey, CA, August 1989.

4. Yuan, Chih-Chung, The Effects of Forebody Strakes on Asymmetric Vortices on a Vertically Launched Missile, Master's Thesis, Naval Postgraduate School, Monterey, CA, September 1990.

5. SC-2043-SG User Manual, National Instruments Corporation, Austin, TX, August 1996.

6. AT-MIO E series User Manual, National Instruments Corporation, Austin, TX, October 1994.

7. Anderson, J.D., Lewis, M.J. and Corda, S., "Several Families of Viscous Optimized Waveriders" Proceedings of the 1st Hypersonic Waverider Symposium, College Park, MD, October 1990.

8. Schindel, L.H., "Waveriders," Tactical Missile Aerodynamics, eds. Michael J. Hemsch and Jack N. Nielsen. (Progress in Aeronautics and Astronautics, Vol. 41), American Institute of Aeronautics and Astronautics, New York, NY, 1992.

9. Eggers, A.J. and Syvertson, C.A., "Aircraft Configurations Developing High Lift-Drag Ratios at High Supersonic Speeds," NACA RM *A55L05,* Ames Aeronautical Lab, Moffett Field, CA, March *1956.*

10. Ward, L., "Riding the Shock Wave," Skyline, North American Aviation, Vol. 19 No. 1, pp. 21-27, March 1961.

11. Nonweiler, T.R.F., "Aerodynamic Problems of Manned Space Vehicles," Journal of the Royal Aeronautical Society, Vol. 63, No. 1, pp. 521-528.

12. Seddon, J. and Spence, A., "The Use of Known Flowfields as an Approach to the Design of High Speed Aircraft", Hypersonic Boundary Layers and Flow Fields, Agard CP No. 30, May 1968, pp. 10/1-10/21.

13. Eggers, A.J., Ashley,H. and Springer, G.S., "Hypersonic Waverider Configurations from the 1950's to the 1990's," Proceedings of the 1st Hypersonic Waverider Symposium, College Park, Maryland, October 1990.

14. Vanhoy, D.L., Low-Speed Wind Tunnel Testing of a Mach 6 Viscous Optimized Waverider, Master's Thesis, University of Maryland, College Park, Maryland, May 1988.

15. Price, D.R., Optimization and Performance Analysis of a Supersonic Conical-Flow Waverider for a Deck-Launched Intercept Mission, Master's Thesis, Naval Postgraduate School, Monterey, California, June 1993.

16. Schindel, L., "Limitations of Waveriders", Proceedings of 1st Hypersonic Waverider Symposium, College Park, Maryland, October 1990.

17. Pope, A., Wind Tunnel Testing, John Wiley & Sons, Inc., New York, NY, 1954.

18. Miller, R. and Argrow, B., "Subsonic Aerodynamics of an Oscillating Cone Waverider", 35th Aerospace Sciences Meeting and Exhibit, Reno, NV, January 1997.

APPENDIX A: LABVIEW© PROGRAM

The first three pages of Appendix C comprise the front panel of the program. This is where the user makes inputs and views the results. The remainder of the appendix displays the overall block diagram and block diagrams of the preinteract and interact1 subVIs. The block diagrams show the process from acquisition to final analysis/plotting.

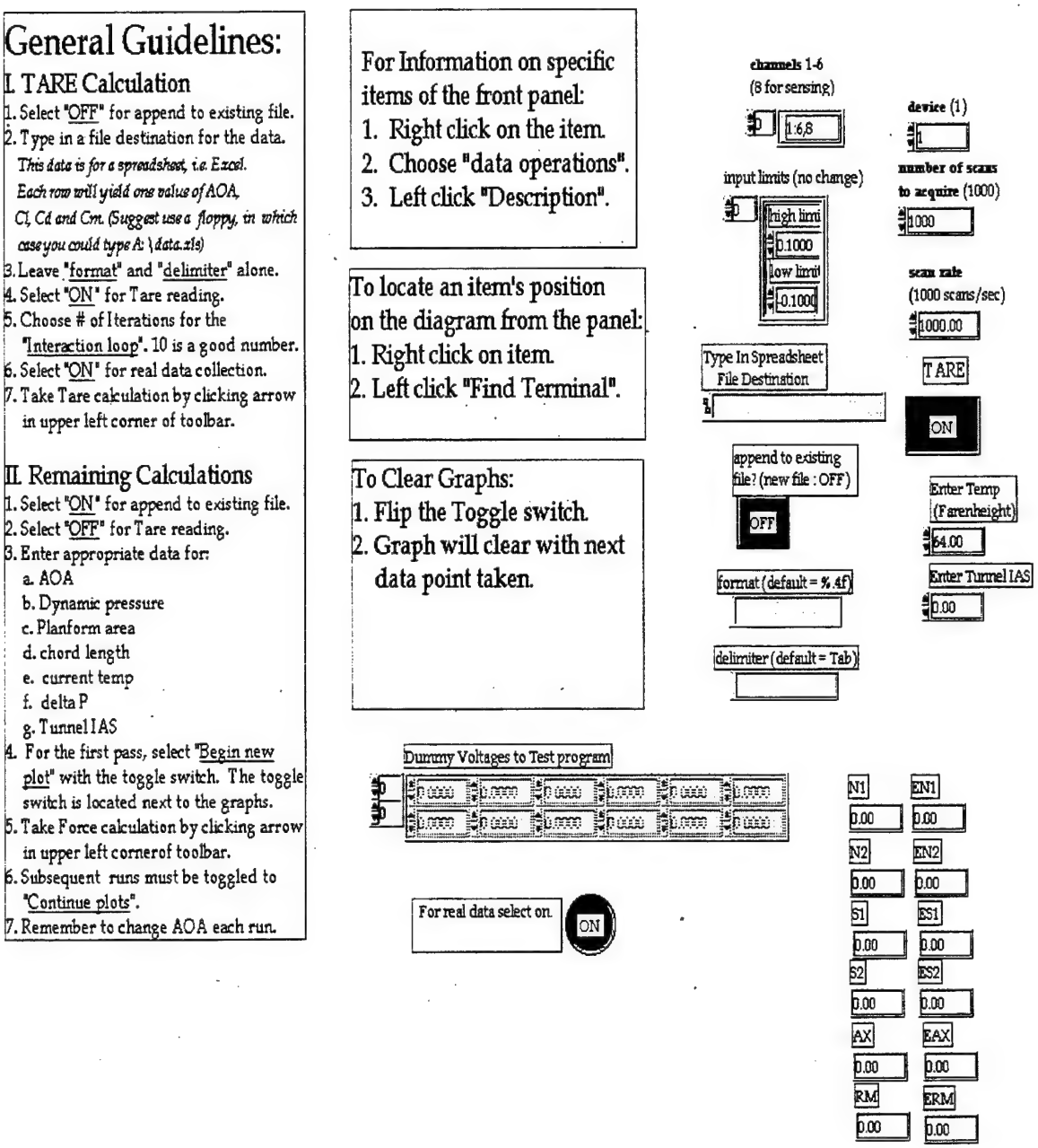

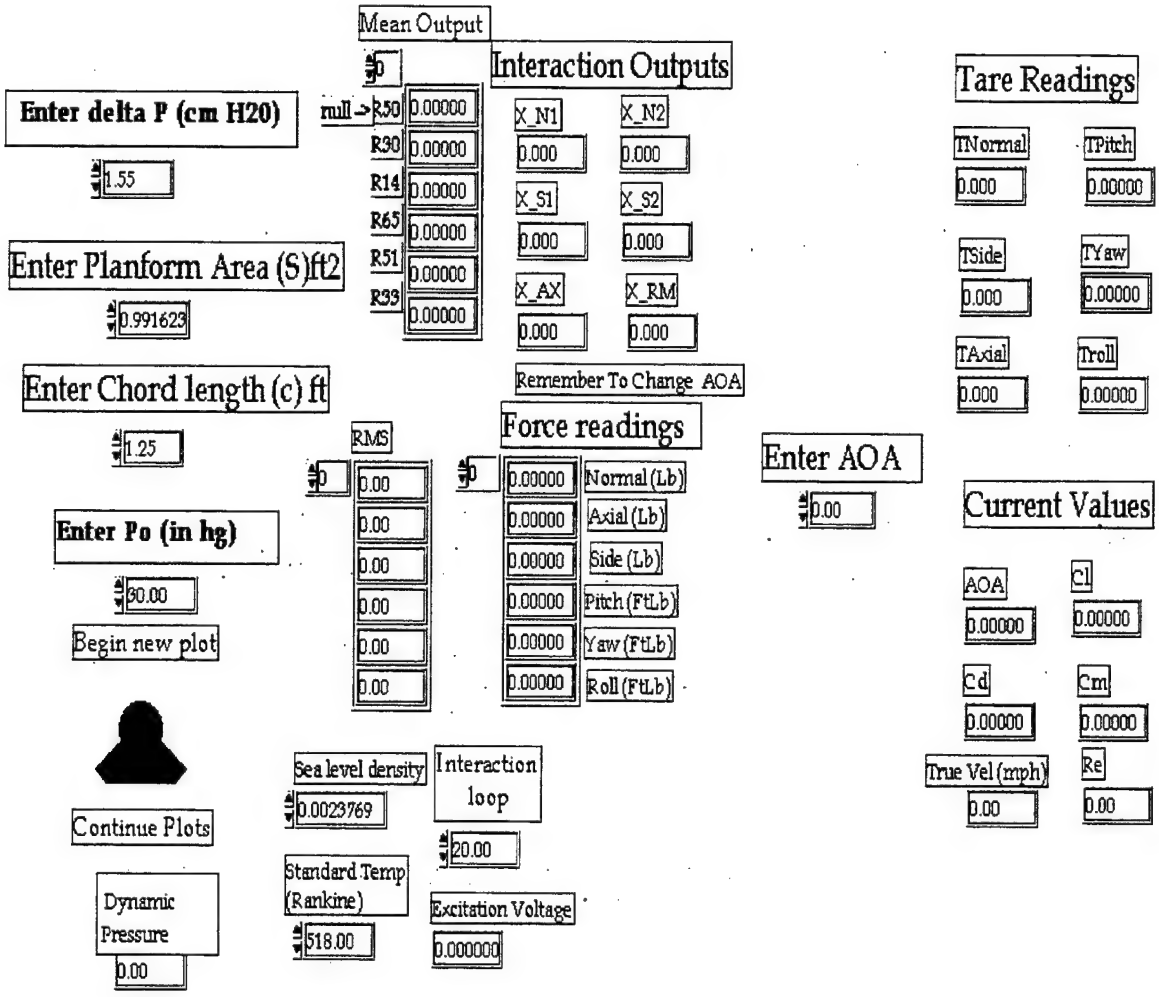
Mean Output
Interaction Outputs
Tare Readings
Enter delta P (cm H20)
1.55
null->R50
R30
R14
R65
R51
R39
0.00000
X_N1
X_N2
X_S1
X_S2
X_AX
X_RM
0.000
TNormal
TPitch
TSide
TYaw
TAxial
TRoll
Enter Planform Area (S)ft2
0.991623
Enter Chord length (c) ft
1.25
Remember To Change AOA
Force readings
RMS
Normal (Lb)
Axial (Lb)
Side (Lb)
Pitch (FtLb)
Yaw (FtLb)
Roll (FtLb)
Enter AOA
0.00
Current Values
Enter Po (in hg)
30.00
Begin new plot
AOA
Cl
Cd
Cm
True Vel (mph)
Re
Continue Plots
Sea level density
0.0023769
Interaction loop
20.00
Standard Temp (Rankine)
518.00
Excitation Voltage
0.000000
Dynamic Pressure

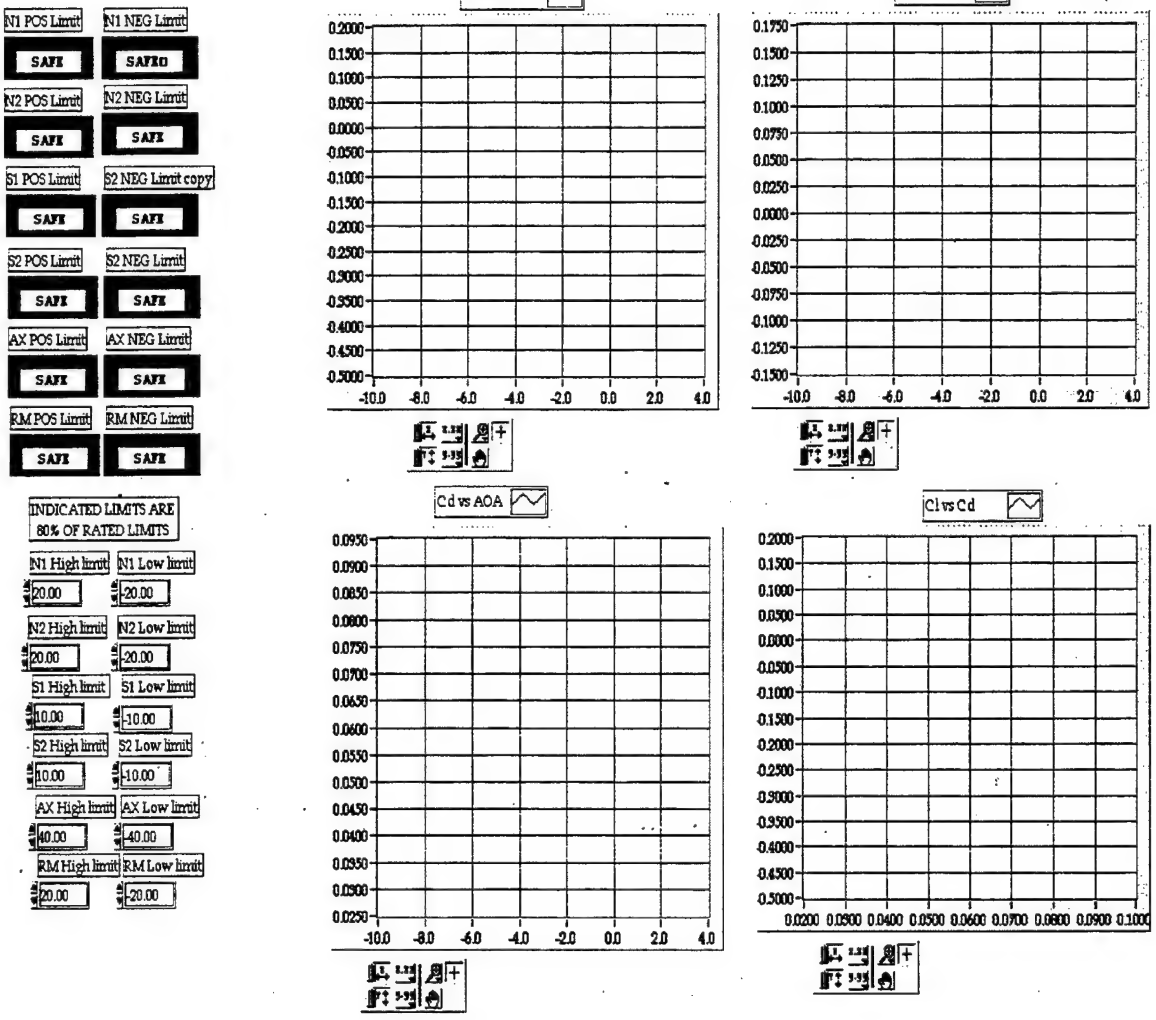
N1 POS Limit
N1 NEG Limit
SAFE
SAFE
N2 POS Limit
N2 NEG Limit
SAFE
SAFE
S1 POS Limit
S2 NEG Limit copy
SAFE
SAFE
S2 POS Limit
S2 NEG Limit
SAFE
SAFE
AX POS Limit
AX NEG Limit
SAFE
SAFE
RM POS Limit
RM NEG Limit
SAFE
SAFE
INDICATED LIMITS ARE
80% OF RATED LIMITS
N1 High limit
N1 Low limit
20.00
-20.00
N2 High limit
N2 Low limit
20.00
-20.00
S1 High limit
S1 Low limit
10.00
-10.00
S2 High limit
S2 Low limit
10.00
-10.00
AX High limit
AX Low limit
40.00
-40.00
RM High limit
RM Low limit
20.00
-20.00
Cl vs AOA
0.2000
0.1500
0.1000
0.0500
0.0000
-0.0500
-0.1000
-0.1500
-0.2000
-0.2500
-0.3000
-0.3500
-0.4000
-0.4500
-0.5000
-10.0 -8.0 -6.0 -4.0 -2.0 0.0 2.0 4.0
Cm vs AOA
0.1750
0.1500
0.1250
0.1000
0.0750
0.0500
0.0250
0.0000
-0.0250
-0.0500
-0.0750
-0.1000
-0.1250
-0.1500
-10.0 -8.0 -6.0 -4.0 -2.0 0.0 2.0 4.0
Cd vs AOA
0.0950
0.0900
0.0850
0.0800
0.0750
0.0700
0.0650
0.0600
0.0550
0.0500
0.0450
0.0400
0.0350
0.0300
0.0250
-10.0 -8.0 -6.0 -4.0 -2.0 0.0 2.0 4.0
Cl vs Cd
0.2000
0.1500
0.1000
0.0500
0.0000
-0.0500
-0.1000
-0.1500
-0.2000
-0.2500
-0.3000
-0.3500
-0.4000
-0.4500
-0.5000
0.0200 0.0300 0.0400 0.0500 0.0600 0.0700 0.0800 0.0900 0.1000

The first section of the block diagram acquires the voltage signals (waveforms) from the strain gauge and determines the average value for each channel. Output is six mean values for N1 through RM. The following page converts the voltage signals into forces (lbf) felt by each channel. It includes the Preinteract and Interact1 subVIs.

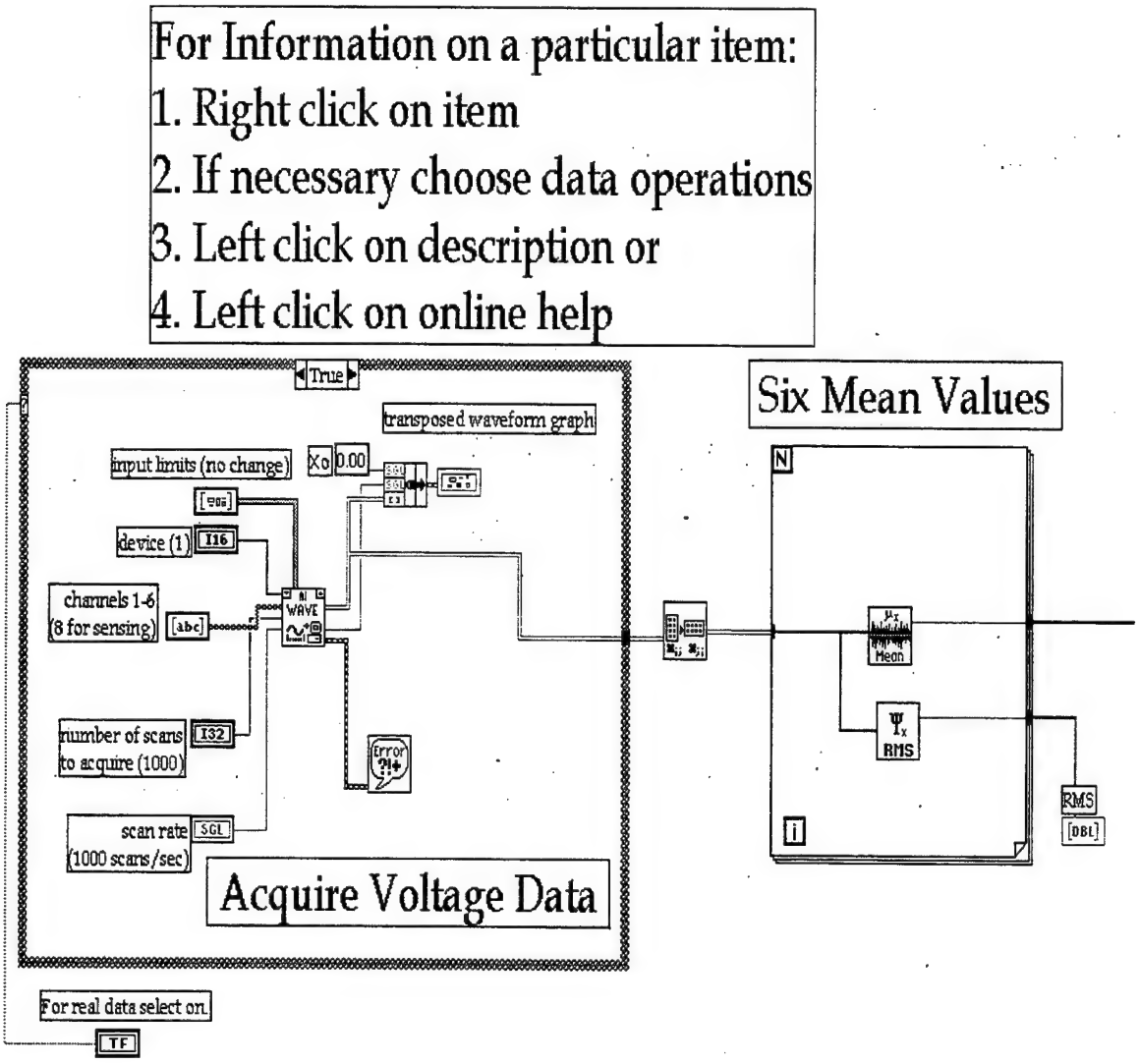

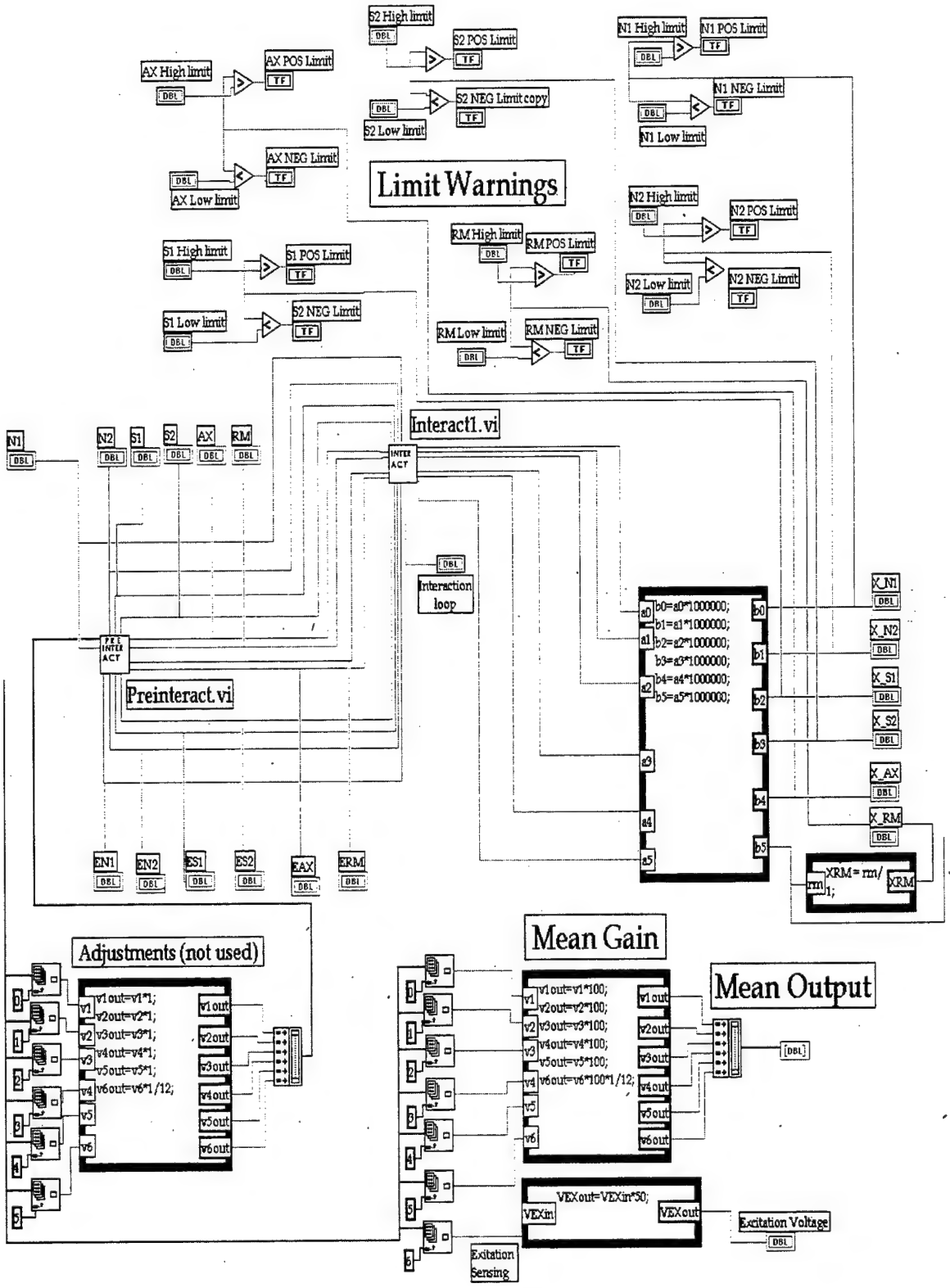
S2 High limit
S2 POS Limit
AX High limit
AX POS Limit
S2 NEG Limit copy
S2 Low limit
N1 High limit
N1 POS Limit
N1 NEG Limit
N1 Low limit
AX NEG Limit
AX Low limit
Limit Warnings
N2 High limit
N2 POS Limit
RM High limit
RM POS Limit
S1 High limit
S1 POS Limit
N2 Low limit
N2 NEG Limit
S1 Low limit
S2 NEG Limit
RM Low limit
RM NEG Limit
Interact1.vi
N1
N2
S1
S2
AX
RM
Interaction loop
Preinteract.vi
b0=a0*1000000;
b1=a1*1000000;
b2=a2*1000000;
b3=a3*1000000;
b4=a4*1000000;
b5=a5*1000000;
X_N1
X_N2
X_S1
X_S2
X_AX
X_RM
XRM = rm/ 1;
EN1
EN2
ES1
ES2
EAX
ERM
Adjustments (not used)
v1out=v1*1;
v2out=v2*1;
v3out=v3*1;
v4out=v4*1;
v5out=v5*1;
v6out=v6*1/12;
Mean Gain
v1out=v1*100;
v2out=v2*100;
v3out=v3*100;
v4out=v4*100;
v5out=v5*100;
v6out=v6*100*1/12;
Mean Output
VEXout=VEXin*50;
VEXin
VEXout
Excitation Voltage
Exitation Sensing

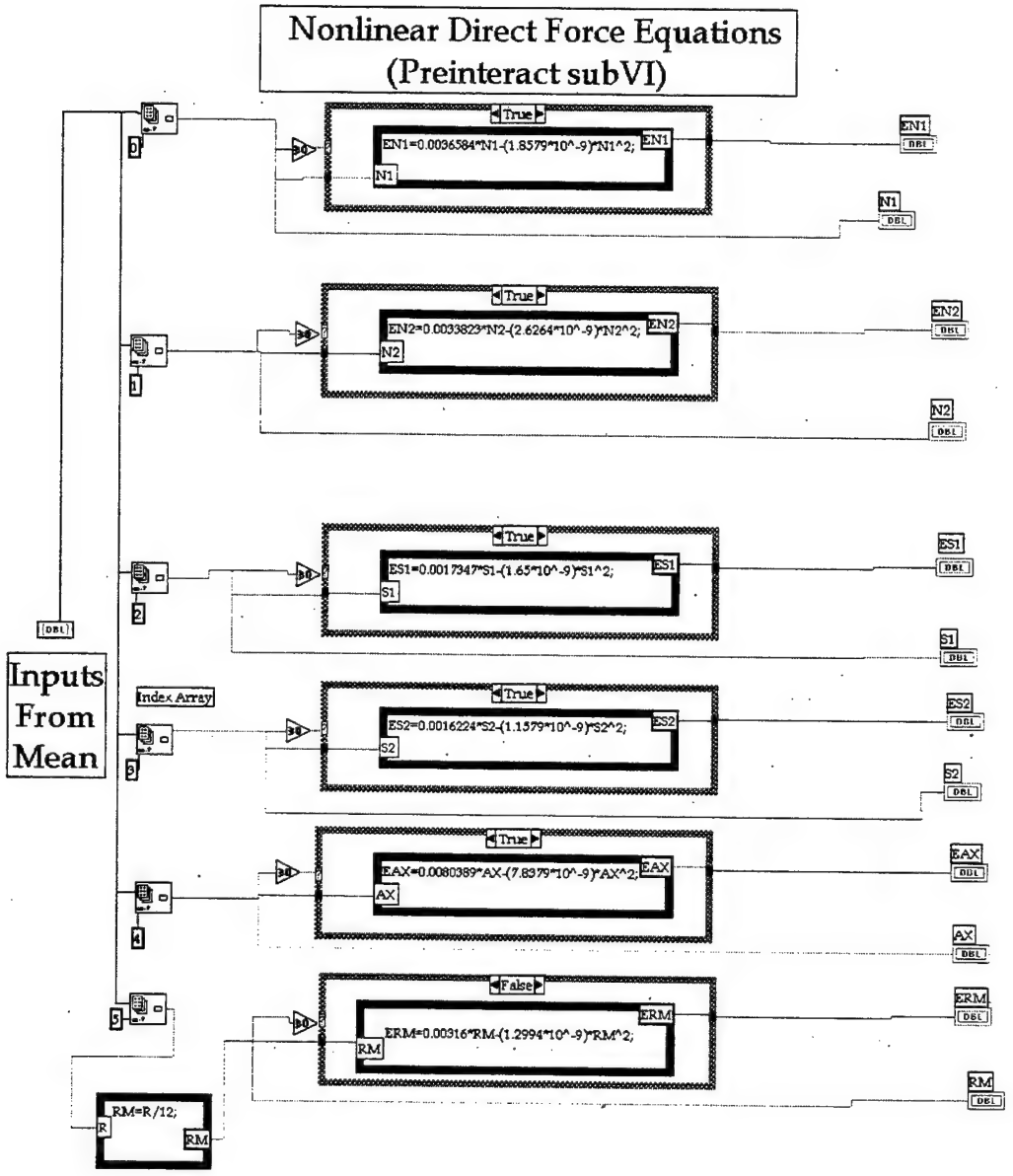
Nonlinear Direct Force Equations
(Preinteract subVI)
Inputs From Mean
Index Array
True
EN1=0.0036584*N1-(1.8579*10^-9)*N1^2;
EN1
N1
EN2=0.0033823*N2-(2.6264*10^-9)*N2^2;
EN2
N2
ES1=0.0017347*S1-(1.65*10^-9)*S1^2;
ES1
S1
ES2=0.0016224*S2-(1.1579*10^-9)*S2^2;
ES2
S2
EAX=0.0080389*AX-(7.8379*10^-9)*AX^2;
EAX
AX
False
ERM=0.00316*RM-(1.2994*10^-9)*RM^2;
ERM
RM
RM=R/12;
R
RM
DBL

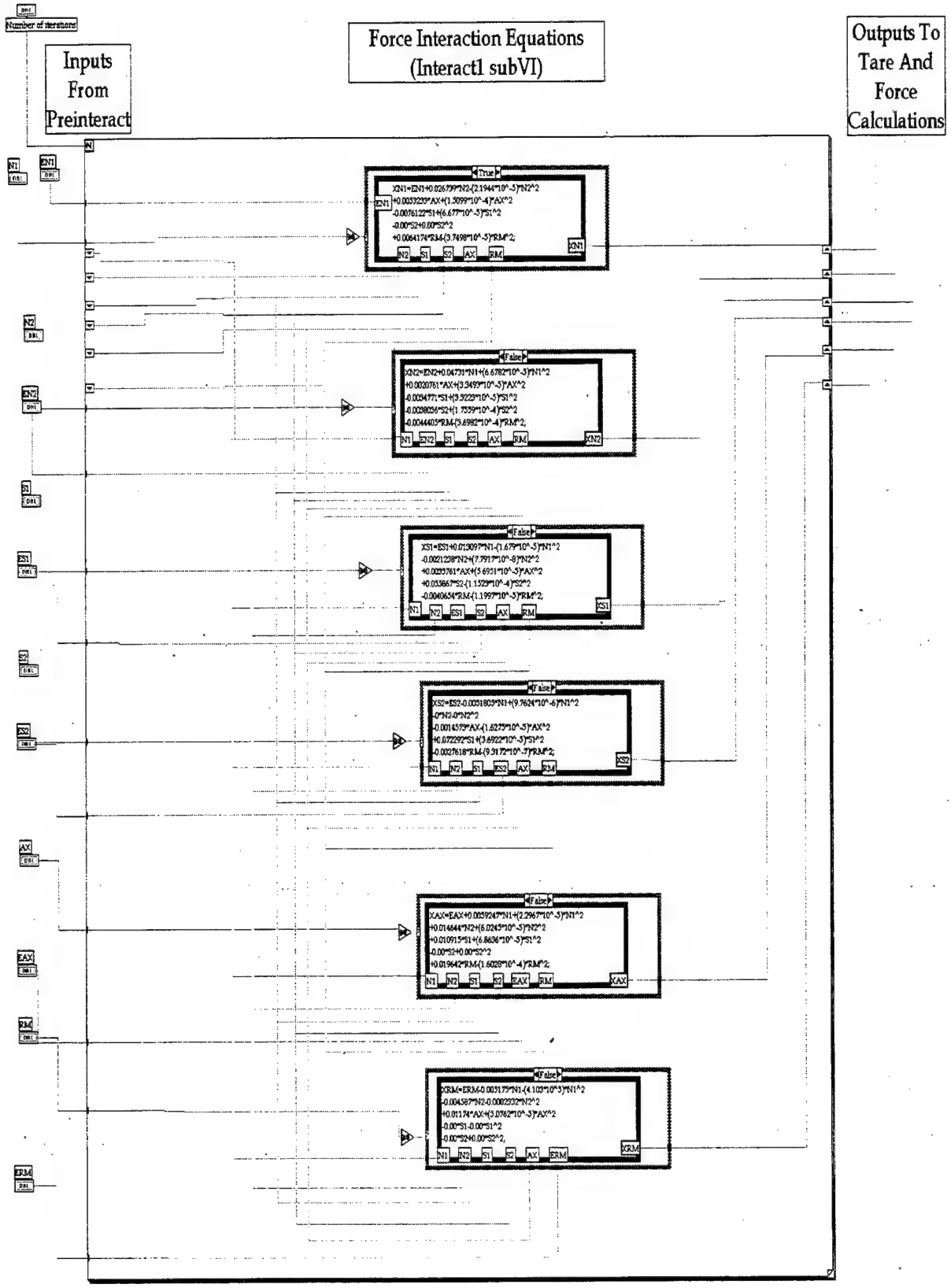
Number of iterations
Inputs From Preinteract
Force Interaction Equations (Interact1 subVI)
Outputs To Tare And Force Calculations
True
XN1=EN1+0.026739*N2-(2.1944*10^-5)*N2^2
+0.0059229*AX+(1.5099*10^-4)*AX^2
-0.0076122*S1+(6.677*10^-5)*S1^2
-0.00*S2+0.00*S2^2
+0.0064174*RM-(3.7498*10^-5)*RM^2;
N2 S1 S2 AX RM XN1
False
XN2=EN2+0.04731*N1+(6.6782*10^-5)*N1^2
+0.0020761*AX+(3.3495*10^-5)*AX^2
-0.005477*S1+(3.9223*10^-5)*S1^2
-0.0038036*S2+(1.7559*10^-4)*S2^2
-0.0044405*RM-(3.6982*10^-4)*RM^2;
N1 EN2 S1 S2 AX RM XN2
False
XS1=ES1+0.013097*N1-(1.679*10^-5)*N1^2
-0.0021238*N2+(7.7917*10^-8)*N2^2
+0.0205761*AX+(5.6951*10^-5)*AX^2
+0.053667*S2-(1.1529*10^-4)*S2^2
-0.0040654*RM-(1.1997*10^-5)*RM^2;
N1 N2 ES1 S2 AX RM XS1
False
XS2=ES2-0.0051805*N1+(9.7624*10^-6)*N1^2
-0*N2-0*N2^2
-0.0014579*AX-(1.6275*10^-5)*AX^2
+0.072292*S1+(3.6922*10^-5)*S1^2
-0.0027618*RM-(9.9172*10^-7)*RM^2;
N1 N2 S1 ES2 AX RM XS2
False
XAX=EAX+0.0059247*N1+(2.2967*10^-5)*N1^2
+0.014644*N2+(6.0245*10^-5)*N2^2
+0.010915*S1+(6.8636*10^-5)*S1^2
-0.00*S2+0.00*S2^2
+0.019642*RM-(1.6029*10^-4)*RM^2;
N1 N2 S1 S2 EAX RM XAX
False
XRM=ERM-0.005175*N1-(4.105*10^-5)*N1^2
-0.004587*N2-0.0002332*N2^2
+0.01174*AX+(3.0762*10^-5)*AX^2
-0.00*S1-0.00*S1^2
-0.00*S2+0.00*S2^2,
N1 N2 S1 S2 AX ERM XRM
N
N1
EN1
N2
EN2
S1
ES1
S2
ES2
AX
EAX
RM
ERM

Results of individual force calculations are routed to the Tare case if the Tare button is selected on the front panel. Otherwise they go to the diagram on the next page.

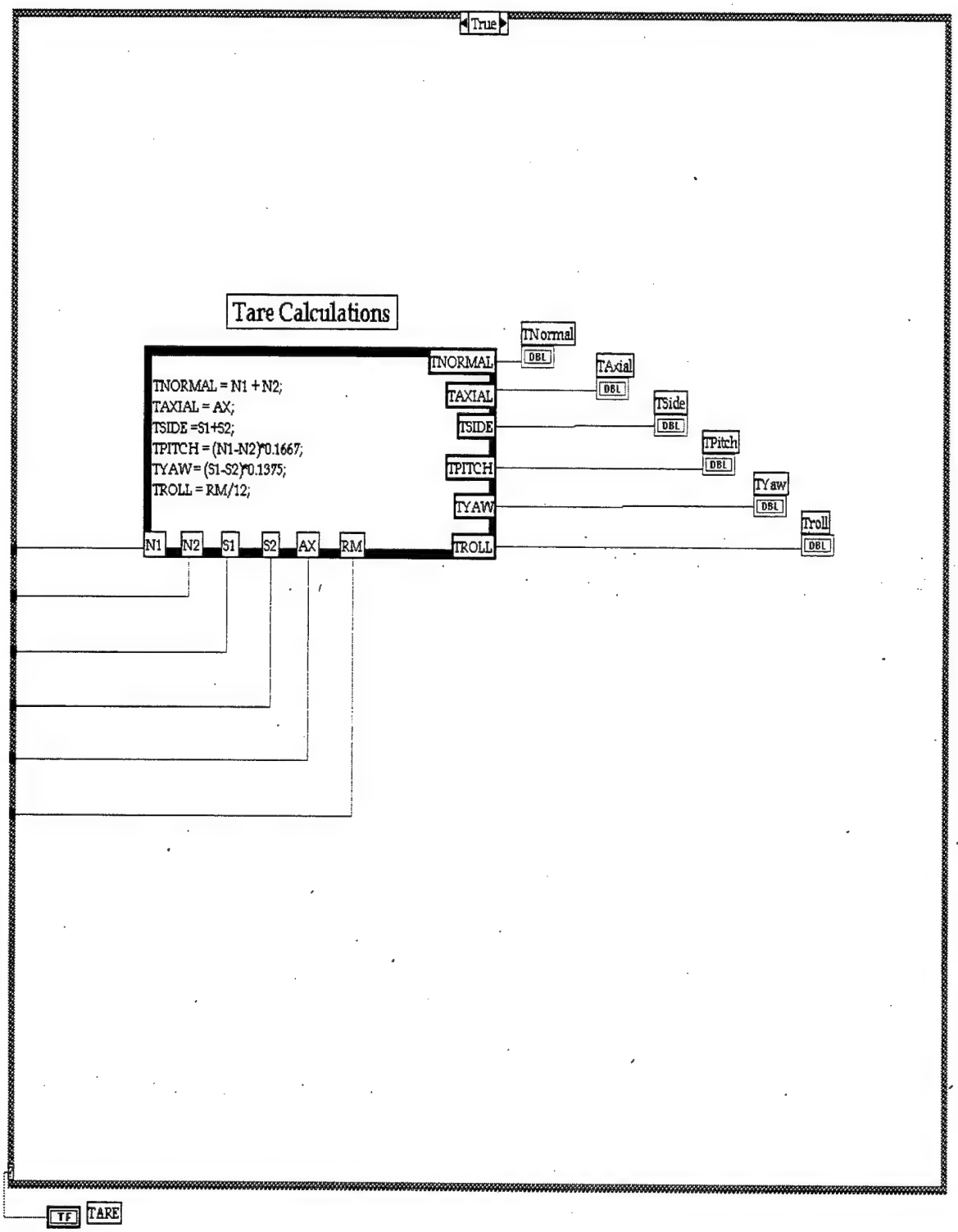

Remaining calculations, including plotting and appending to spreadsheet file, take place in this portion of the block diagram. Due to the amount of information displayed, it has been split into three sections in the three pages that follow.

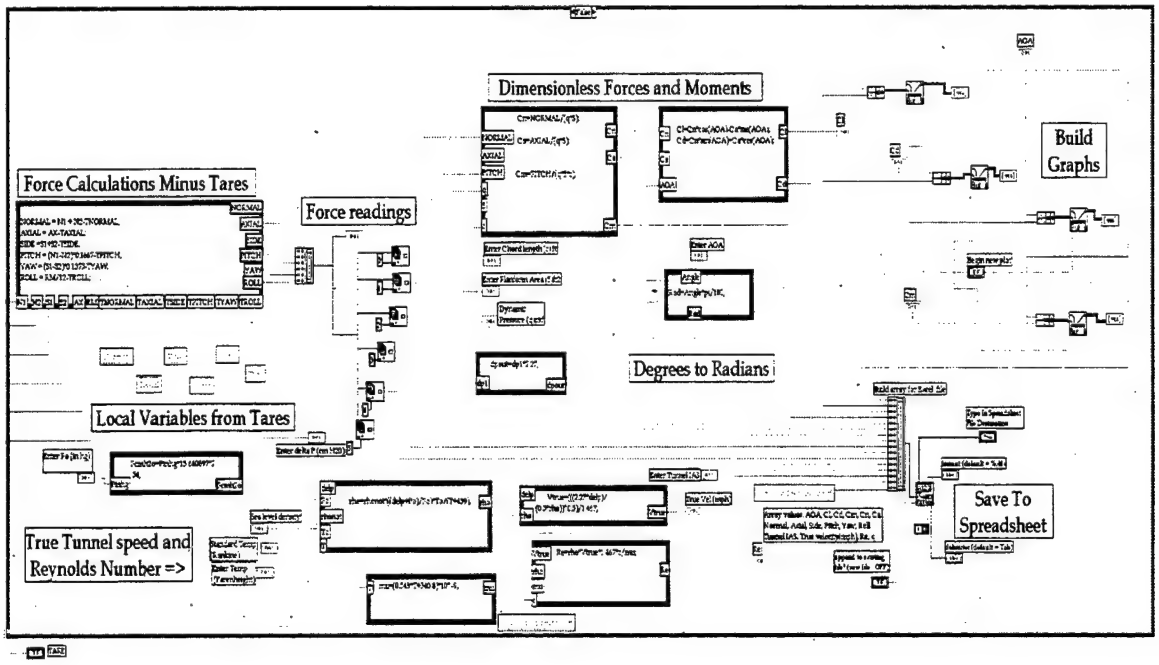

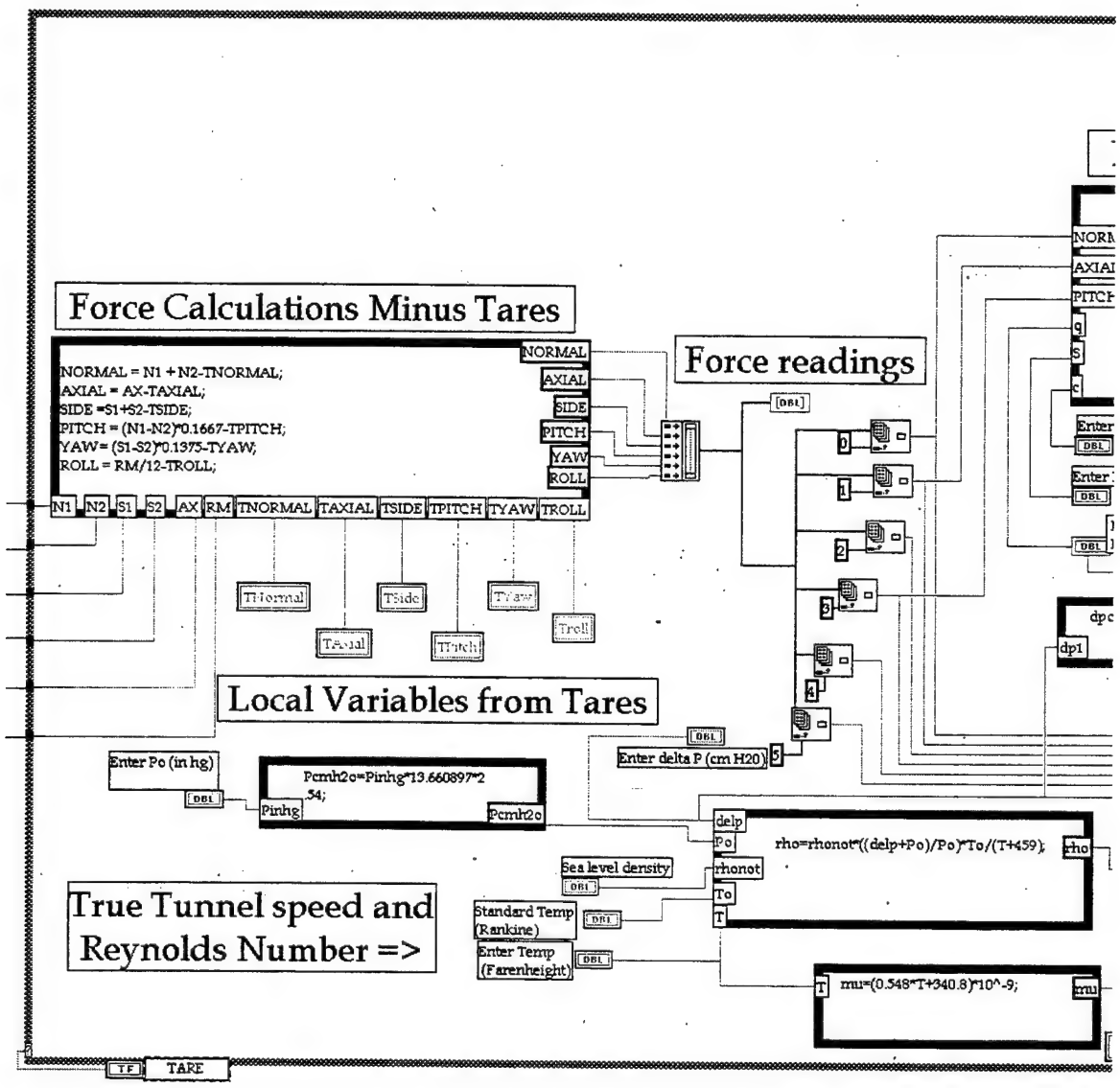
Force Calculations Minus Tares
NORMAL = N1 + N2-TNORMAL;
AXIAL = AX-TAXIAL;
SIDE =S1+S2-TSIDE;
PITCH = (N1-N2)*0.1667-TPITCH;
YAW= (S1-S2)*0.1375-TYAW;
ROLL = RM/12-TROLL;
NORMAL
AXIAL
SIDE
PITCH
YAW
ROLL
N1
N2
S1
S2
AX
RM
TNORMAL
TAXIAL
TSIDE
TPITCH
TYAW
TROLL
Force readings
Local Variables from Tares
Enter Po (in hg)
DBL
Pcmh2o=Pinhg*13.660897*2.54;
Pinhg
Pcmh2o
Enter delta P (cm H20)
delp
Po
rho=rhonot*((delp+Po)/Po)*To/(T+459);
rho
Sea level density
rhonot
To
T
Standard Temp (Rankine)
Enter Temp (Farenheight)
True Tunnel speed and Reynolds Number =>
mu=(0.548*T+340.8)*10^-9;
mu
TF
TARE

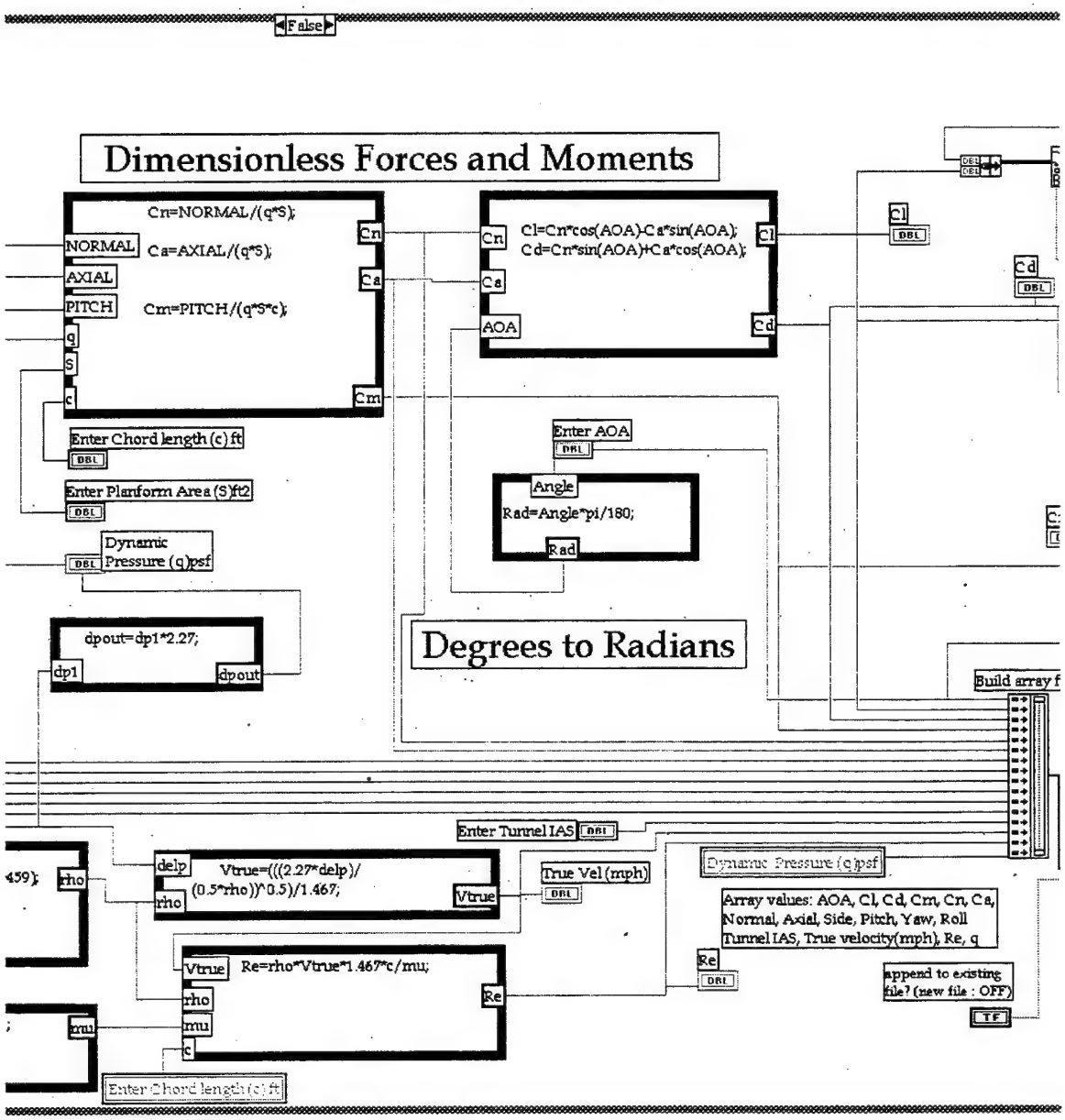
False
Dimensionless Forces and Moments
Cn=NORMAL/(q*S);
NORMAL
Ca=AXIAL/(q*S);
AXIAL
PITCH
Cm=PITCH/(q*S*c);
q
S
c
Cn
Ca
Cm
Cl=Cn*cos(AOA)-Ca*sin(AOA);
Cd=Cn*sin(AOA)+Ca*cos(AOA);
AOA
Cl
Cd
DBL
Enter Chord length (c) ft
Enter Planform Area (S)ft2
Dynamic Pressure (q)psf
Enter AOA
Angle
Rad=Angle*pi/180;
Rad
Degrees to Radians
dpout=dp1*2.27;
dp1
dpout
Build array f
Enter Tunnel IAS
delp
Vtrue=(((2.27*delp)/
(0.5*rho))^0.5)/1.467;
rho
Vtrue
True Vel (mph)
Dynamic Pressure (q)psf
Array values: AOA, Cl, Cd, Cm, Cn, Ca,
Normal, Axial, Side, Pitch, Yaw, Roll
Tunnel IAS, True velocity(mph), Re, q
Re=rho*Vtrue*1.467*c/mu;
Re
mu
append to existing
file? (new file : OFF)
TF
Enter Chord length (c) ft

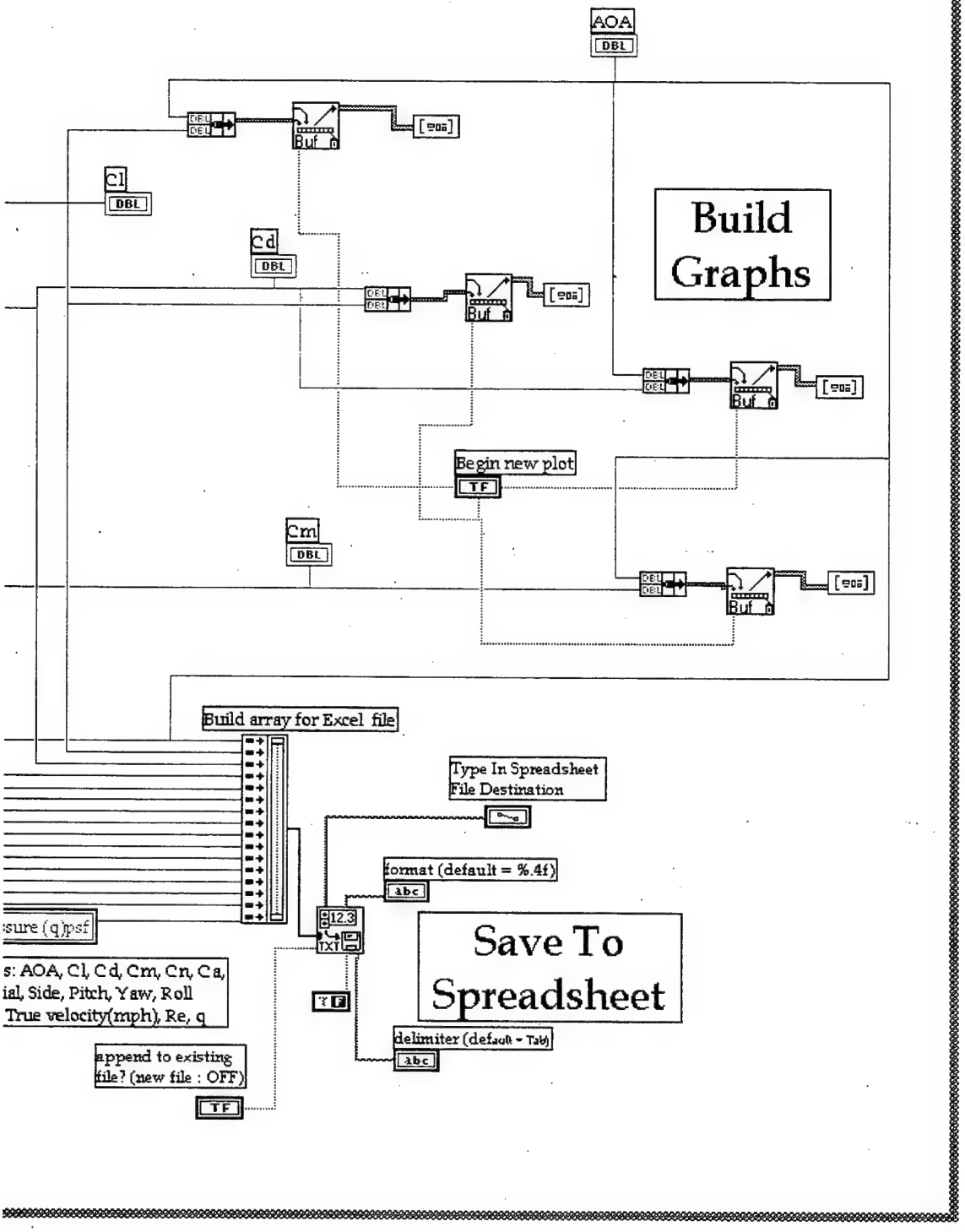
AOA
DBL
Cl
DBL
Cd
DBL
Cm
DBL
Build
Graphs
Begin new plot
TF
Build array for Excel file
Type In Spreadsheet
File Destination
format (default = %.4f)
abc
Save To
Spreadsheet
delimiter (default = Tab)
abc
append to existing
file? (new file : OFF)
TF
s: AOA, Cl, Cd, Cm, Cn, Ca,
ial, Side, Pitch, Yaw, Roll
True velocity(mph), Re, q

APPENDIX B: STING BALANCE CALIBRATION

A. Sting Balance Calibration Constants

Balance Calibration

Performed by: NASA Ames Calibration Laboratory

Cal Date:	8283	Size	0.75
Comp. Date:	8313	Make	Task/Able
Invoice No.:	440528	pin No	1
Type:	Force	Rig No.:	2

Gage	Capacity	Maximum load	Ohms	X Gage	Calibration Shunt	Calibration Reading
N1	25.00	25.00	350	0.0854	80K	5725
N2	25.00	25.00	350	0.0854	80K	5738
AX	50.00	50.00	350	N/A	80K	5752
S1	12.50	12.00	350	0.0698	80K	5732
S2	12.50	12.00	350	0.0698	80K	5736
RM	25.00	25.00	350	N/A	70K	6575

Gage	K Pos(1)	K Pos(2)	K Neg(1)	K Neg(2)	Maximum Deviation	% ACC
N1	3.6584E-03	-1.8579E-09	3.6748E-03	-1.8922E-09	-0.054	0.217
N2	3.3823E-03	-2.6264E-09	3.3785E-03	-5.5067E-09	-0.048	0.191
AX	8.0389E-03	-7.8379E-09	8.0496E-03	-8.8894E-09	-0.027	0.054
S1	1.7347E-03	-1.6500E-09	1.7463E-03	-1.3754E-09	-0.021	0.171
S2	1.6224E-03	-1.1579E-09	1.6353E-03	-8.5641E-10	-0.023	0.188
RM	3.1732E-03	1.0253E-09	3.1600E-03	-1.2994E-09	0.032	0.128

Degree of Fit: 2 Accuracy: 15 Int. Degree of Fit: 2

Interaction Coefficients

Coefficient	Positive Value	Negative Value
Nl/N2	-2.6739E-02	-2.8717E-02
N1/AX	-5.3233E-03	-2.2093E-03
N1/S1	7.6 122E-03	6.9447E-03
N1/S2	0.0000E+00	0.0000E+00
N1/RM	-6.4174E-03	0.0000E+00
N2/N1	-4.3853E-02	-4.73 1OE-02
N2/AX	6.2273E-03	-2.O761E-03
N2/S1	4.4658E-03	3.4771E-03
N2/S2	-4.8747E-03	3.8036E-03
N2/RM	-6.1 509E-03	4.4405E-03
AX/N1	0.0000E+00	-5.9247E-03
AX/N2	-9.2497E-03	-1.4644E-02
AX/S1	0.0000E+00	-1.0915E-02
AX/S2	0.0000E+00	0.0000E+00
AX/RM	-2.1O34E-02	-1.9642E-02
S1/N1	-1.0939E-02	-1.3097E-02
S1/N2	1.5093E-03	2.1238E-03
S1/AX	-1.7751E-02	-3.3761E-03
S1/S2	-5.5009E-02	-5.5867E-02
S1/RM	9.0376E-03	4.0654E-03
S2/N1	5.5317E-03	5.18O5E-03
S2/N2	-2.7958E-04	0.0000E+00
S2/AX	8.4602E-03	1 .4573E-03
S2/S1	-6.7550E-02	-7.2292E-02
S2/RM	6.4729E-03	2.7618E-03
RM/N1	2.2569E-03	5.1750E-03
RM/N2	0.0000E+00	4.5870E-03
RM/AX	-8.4466E-03	-1.174OE-02
RM/S1	0.0000E+00	0.0000E+00
RM/S2	0.0000E+00	0.0000E+00

Interaction Coefficients (cont.)

Coefficient	Positive Value	Negative Value
$N1/N2^2$	2.1944E-05	3.1064E-05
$N1/AX^2$	-1.5099E-04	-8.1729E-05
$N1/S1^2$	-6.6779E-05	2.0633E-05
$N1/S2^2$	0.0000E+00	0.0000E+00
$N1/RM^2$	3.7498E-05	0.0000E+00
$N2/N1^2$	1.7830E-05	-6.6782E-05
$N2/AX^2$	1.7338E-04	-3.3493E-05
$N2/S1^2$	-7.4991E-05	-3.3223E-05
$N2/S2^2$	-5.8651E-05	-1.7559E-04
$N2/RM^2$	3.7458E-05	3.6982E-04
$AX/N1^2$	0.0000E+00	-2.2967E-05
$AX/N2^2$	-1.4649E-05	-6.0254E-05
$AX/S1^2$	0.0000E+00	-6.8636E-05
$AX/S2^2$	0.0000E+00	0.0000E+00
AX/RM^2	1.9713E-04	1.6028E-04
$S1/N1^2$	1.6053E-05	1.6790E-05
$S1/N2^2$	-1.0662E-05	-7.7917E-08
$S1/AX^2$	4.4896E-04	-5.6951E-05
$S1/S2^2$	8.3835E-07	1.1523E-04
$S1/RM^2$	-9.2627E-05	1.1997E-05
$S2/N1^2$	-2.4811E-05	-9.7624E-06
$S2/N2^2$	-2.0669E-05	0.0000E+00
$S2/AX^2$	-1.9659E-04	1.6275E-05
$S2/S1^2$	-1.2240E-04	-3.6922E-05
$S2/RM^2$	-3.3908E-05	9.3172E-07
$RM/N1^2$	7.9926E-06	4.1030E-05
$RM/N2^2$	0.0000E+00	2.3320E-04
RM/AX^2	-8.8297E-05	-3.0762E-05
$RM/S1^2$	0.0000E+00	0.0000E+00
$RM/S2^2$	0.0000E+00	0.0000E+00

B. Sting Balance Equations

The following equations perform the direct force nonlinear corrections and the force interaction calculations using the coefficients listed in the previous section.. The first group is used by the *preinteract.vi* while the second, larger group consists of the equations used by the *interact1.vi*.

1. DIRECT NONLINEAR FORCE EQUATIONS

a. POSITIVE EQUATIONS

```
EN1 = .0036584 * N1 - 1.8579E-09 * (N1 ^ 2)
EN2 = .0033823 * N2 - 2.6264E-09 * (N2 ^ 2)
EA = .0080389 * A - 7.8379E-09 * (A ^ 2)
ES1 = .0017347 * S1 - 1.65E-09 * (S1 ^ 2)
ES2 = .0016224 * S2 - 1.1579E-09 * (S2 ^ 2)
ER = .0031732 * R + 1.0253E-09 * (R ^ 2)
```

b. NEGATIVE EQUATIONS

```
EN1 = .0036748 * N1 - 1.8922E-09 * (N1 ^ 2)
EN2 = .0033785 * N2 - 5.5067E-09 * (N2 ^ 2)
EA = .0080496 * A - 8.8894E-09 * (A ^ 2)
ES1 = .0017463 * S1 - 1.3754E-09 * (S1 ^ 2)
ES2 = .0016353 * S2 - 8.5641E-10 * (S2 ^ 2)
ER = .00316 * R - 1.2994E-09 * (R ^ 2)
```

2. FORCE INTERACTION EQUATIONS

a. POSITIVE EQUATIONS

```
XN1 = EN1 + .026739 * N2 - 2.1944E-05 * (N2 ^ 2)
          + .0053233 * A + 1.5099E-04 * (A ^ 2)
          - .0076122 * S1 + 6.677E-05 * (S1 ^ 2)
          - 0 * S2 - 0 * (S2 ^ 2)
          + 6.4174E-03* R - 3.7498E-05 * (R ^ 2)

XN2 = EN2 + .043853 * N1 - 1.783E-05 * (N1 ^ 2)
          - .0062273 * A - 1.7338E-04 * (A ^ 2)
          - .0044658 * S1 + 7.4991E-05 * (S1 ^ 2)
          + .0048747 * S2 + 5.8651E-05 * (S2 ^ 2)
          + .0061509 * R - 3.7458E-05 * (R ^ 2)

XA = EA + 0 * N1 - 0 * (N1 ^ 2)
          + .0092497 * N2 + 1.4649E-05 * (N2 ^ 2)
          - 0 * S1 - 0 * (S1 ^ 2)
          - 0 * S2 - 0 * (S2 ^ 2)
          + .021034 * R - 1.9713E-04 * (R ^ 2)
```

XS1 = ES1 + .010939 * N1 - 1.6053E-05 * (N1 ^ 2)
- .0015093 * N2 + 1.0662E-05 * (N2 ^ 2)
+ .017751 * A - 4.4896E-04 * (A ^ 2)
+ .055009 * S2 - 8.3835E-07 * (S2 ^ 2)
- .0090376 * R + 9.2627E-05 * (R ^ 2)

XS2 = ES2 - .0055317 * N1 + 2.4811E-05 * (N1 ^ 2)
+ 2.7958E-04 * N2 + 2.0669E-05 * (N2 ^ 2)
-.0084602 * A + 1.9659E-04 * (A ^ 2)
+ .06755 * S1 + .0001224 * (S1 ^ 2)
- .0064729 * R + 3.3908E-05 * (R ^ 2)

XR = ER - .0022569 * N1 - 7.9926E-06 * (N1 ^ 2)
- 0 * N2 - 0 * (N2 ^ 2)
+ .0084466 * A + 8.8297E-05 * (A ^ 2)
- 0 * S1 - 0 * (S1 ^ 2)
- 0 * S2 - 0 * (S2 ^ 2)

b. NEGATIVE EQUATIONS

XN1 = EN1 + .028717 * N2 - 3.1064E-05 * (N2 ^ 2)
+ .0022093 * A + 8.1729E-05 * (A ^ 2)
- .0069447 * S1 - 2.0633E-05 * (S1 ^ 2)
- 0 * S2 - 0 * (S2 ^ 2)
- 0 * R - 0 * (R ^ 2)

XN2 = EN2 + .04731 * N1 + 6.6782E-05 * (N1 ^ 2)
+ .0020761 * A + 3.3493E-05 * (A ^ 2)
- .0034771 * S1 + 3.3223E-05 * (S1 ^ 2)
- .0038036 * S2 + 1.7559E-04 * (S2 ^ 2)
- .0044405 * R - 3.6982E-04 * (R ^ 2)

XA = EA + .0059247 * N1 + 2.2967E-05 * (N1 ^ 2)
+ .014644 * N2 + 6.0245E-05 * (N2 ^ 2)
+ .010915 * S1 + 6.8636E-05 * (S1 ^ 2)
- 0 * S2 - 0 * (S2 ^ 2)
+ .019642 * R - 1.6028E-04 * (R ^ 2)

XS1 = ES1 + .013097 * N1 - 1.679E-05 * (N1 ^ 2)
- .0021238 * N2 + 7.7917E-08 * (N2 ^ 2)
+ .0033761 * A + 5.6951E-05 * (A ^ 2)
+ .055867 * S2 - 1.1523E-04 * (S2 ^ 2)
- .0040654 * R - 1.1997E-05 * (R ^ 2)

XS2 = ES2 - .0051805 * N1 + 9.7624E-06 * (N1 ^ 2)
- 0 * N2 - 0 * (N2 ^ 2)
- .0014573 * A - 1.6275E-05 * (A ^ 2)
+ .072292 * S1 + 3.6922E-05 * (S1 ^ 2)
- .0027618 * R - 9.3172E-07 * (R ^ 2)

XR = ER - .005175 * N1 - 4.103E-05 * (N1 ^ 2)
- .004587 * N2 - .0002332 * (N2 ^ 2)
+ .01174 * A + 3.0762E-05 * (A ^ 2)
- 0 * S1 - 0 * (S1 ^ 2)
- 0 * S2 - 0 * (S2 ^ 2)

C. Outputs using NASA Ames calibration constants only

Table A.1

Weight	load point	N1 POS	N2 POS	N TOTAL	N1 NEG	N2 NEG	N TOTAL
1.212	Front	1.226	-0.028	1.198	-1.32	-0.101	-1.421
1.212	Middle	0.59	0.59	1.18	-0.772	-0.696	-1.468
1.212	Back	0	1.194	1.194	-0.722	-0.696	-1.418
2.212	Front	2.22	-0.011	2.209	-2.375	-0.076	-2.451
2.212	Middle	1.079	1.094	2.173	-1.25	-1.18	-2.43
2.212	Back	-0.023	2.212	2.189	-0.12	-2.289	-2.409
4.217	Front	4.219	0.013	4.232	-4.391	-0.085	-4.476
4.217	Middle	2.094	2.05	4.144	-2.256	-2.183	-4.439
4.217	Back	0.04	4.155	4.195	-0.135	-4.307	-4.442
10.228	Front	10.46	-0.112	10.348	-10.239	-0.279	-10.518
10.228	Middle	5.1	4.95	10.05	-5.28	-5.196	-10.476
10.228	Back	0.018	10.221	10.239	-0.07	-10.386	-10.456
Weight	load point	S1 POS	S2 POS	S TOTAL	S1 NEG	S2 NEG	S TOTAL
1.212	Front	1.327	0.08	1.407	-1.201	-0.012	-1.213
1.212	Middle	0.713	0.674	1.387	-0.583	-0.625	-1.208
1.212	Back	0.106	1.288	1.394	0.012	-1.215	-1.203
2.212	Front	2.342	0.074	2.416	-2.214	-0.008	-2.222
2.212	Middle	1.235	1.145	2.38	-1.104	-1.107	-2.211
2.212	Back	0.141	2.243	2.384	0	-2.198	-2.198
4.217	Front	4.381	0.048	4.429	-4.148	-0.094	-4.242
4.217	Middle	2.205	2.158	4.363	-2.026	-2.204	-4.23
4.217	Back	0.212	4.173	4.385	0.023	-4.243	-4.22
10.228	Front	10.366	0.128	10.494	-10.002	-0.267	-10.269
10.228	Middle	5.247	5.094	10.341	-5.071	-5.203	-10.274
10.228	Back	0.238	10.15	10.388	0.156	-10.438	-10.282

D. Local sting Balance Calibration

Fine-tuning of the Task Mark XX sting balance was difficult to achieve. Previous local calibration efforts involved adjusting the individual excitation voltages to each channel. This method was not available as the signal conditioning board uses a single excitation voltage for all channels. In addition, it is not well known how the adjusting the voltage for one channel effects the interactions of the other five channels. It was possible to mimic changing the voltages however, by adjusting the voltage output of each channel by a linear gain in LabVIEW. This could be done before and/or after the interactions were performed to improve results, and each method was attempted. As during the verification of the NASA calibration, weights from one to ten lbs. were used.

The procedure chosen was somewhat different though, as forces were loaded along the span of the balance rather than loading each individual channel. This was accomplished by using the adapter sleeve that attaches other models to the balance. Since it surrounds the balance with a "smooth friction" fit, an entire force, e.g. Normal, Side, or Axial, could be loaded all at once. This was thought to best duplicate how loads would be imparted on the balance by the model during testing.

The balance was first loaded with the adapter sleeve and sling that held the weights. The weight of these components was 0.456 lbs. but by using the nulling potentiometers on the signal conditioning board the weight was nulled to zero. With the gain set to equal values on all six channels, the balance was then loaded in the S-direction with weights of one to ten lbs. A gentle finger tapping on the balance prior to each measurement improved results by minimizing any possible hysteresis from the

previous load. Similar measurements were taken for the S+, N+, N- and AX+ directions. The final average value between applied and measured load differed by 0.059 lbs. The largest amount of error occurred at the lower weights in the N+ and AX directions.

Adjusting the gain on any of the channels appeared to have only negative effects on the results. Small improvements could be gained on the channel of interest, but would adversely change the values of the other five channels. Another consequence was a possible adverse effect on the channel being adjusted when loaded in the opposite direction. In conclusion, without an actual laboratory calibration it is doubtful that overall results could be improved from the initial settings. Table A.2 presents a listing of the applied loads and resultant forces read in each direction measured.

Table A.2

Weight	S +	S -	N +	N -	AX +
1.001	1.020	1.027	1.101	1.079	1.078
2.001	1.992	2.002	2.113	2.004	2.036
3.001	3.005	3.050	3.141	2.941	3.140
4.006	4.016	4.037	4.172	4.078	4.001
5.011	5.011	4.992	5.163	4.969	5.103
6.012	6.028	6.031	6.164	5.957	6.172
7.012	7.033	7.015	7.151	7.072	7.063
8.017	8.029	8.010	8.106	8.005	8.171
9.017	9.024	9.028	9.150	9.003	9.020
10.018	10.018	10.006	10.120	10.03	10.180

APPENDIX C: WIND TUNNEL WALL CORRECTIONS

A. WALL CORRECTION DESCRIPTIONS

In an effort to increase the accuracy of the data collected, tunnel wall corrections were applied to the raw data. Applying tunnel wall corrections is necessary because the conditions under which a model is tested in a wind tunnel are not the same as those in free air. The walls of a closed test section produce changes in flow patterns that influence the aerodynamic results. When applying these corrections the following areas should be considered [Ref. 21].

- Solid and Wake Blocking
- Horizontal Bouyancy
- Streamline Curvature
- Downwash Corrections

1. Solid Blocking:

The presence of a model in the test section reduces the flow area and thereby increases the velocity of the air through the test section around the model. The solid blocking velocity increment at the model is much less than that which would be calculated from a direct area reduction since the streamlines near the tunnel walls are displaced more than those near the model. Solid blocking causes an increase in local dynamic pressure which in turn increases all measured forces and moments.

2. Wake Blocking:

All models tested in a wind tunnel will have a wake behind them caused by the detachment of the models' boundary layer. This wake has a mean velocity lower than that of the freestream. In order to keep the mass flow constant from the test section entrance to exit the velocity outside the wake must be higher than the freestream velocity. This higher velocity results in a lower wake pressure and hence a lower model base pressure than would occur in free air. The wake blocking effect increases with wake size hence is highest when large flow separations occur. Wake blocking also creates an increase in dynamic pressure on the model.

3. Horizontal Bouyancy:

Almost all wind tunnels with closed test sections have a variation in static pressure along the axis of the test section (even with no model present). A thickening of the wall boundary layer causes a decrease in the effective test section flow area. Test section pressure normally decreases as the end of the test section is approached and the resulting pressure variation over the model produces an additional drag force. The NPS tunnel test section is slightly divergent to help counteract this. In addition, the amount of horizontal buoyancy is usually insignificant for thin bodies like wings, and will therefore not be considered.

4. Streamline Curvature:

The natural free air streamline curvature that exists about any foil or lifting body is effected by the ceiling and floor of the tunnel. These tunnel surfaces induce a chordwise variation in upwash and the model acts as if it had extra camber. Thus, tests of a foil or lifting body in a closed jet tunnel will show too much lift as well as too great a moment about the quarter chord. Furthermore, the effective angle of attack will be increased.

5. Downwash Corrections:

The effect of the sidewalls of the tunnel is only applicable to 3-D models where trailing vortices exist. In this case the tunnel walls induce a spanwise variation in upwash which decreases the normal downwash. Thus, tests of a wing or lifting body will have too little induced drag and the wing will appear to have a larger effective aspect ratio than it would if tested in free air. These effects are small if the span is much less than the tunnel width (if mounted sideways, height) and in any case will be neglected here.

B. CORRECTIONS FOR TWO DIMENSIONAL TESTING

All uncorrected coefficients are defined in terms of an uncorrected dynamic pressure (q_u) which is the q that would exist if no model were present in the test section. Neglecting horizontal bouyancy, these are the same outputs calculated previously using the LabVIEW program. The coefficients will first be modified by the solid and wake blocking corrections (ε_{sb} and ε_{wb}).

1. Solid Blocking:

The solid blocking correction is defined in terms of the velocity increment produced (ΔV) and the uncorrected test section velocity (Vu).

$$\varepsilon_{sb} = \frac{\Delta V}{V_u} = \frac{K_1(Model\_volume)}{C^{3/2}}$$

where: $K_1 = 0.74$ for a wing spanning the tunnel width.

$K_1 = 0.52$ for a wing spanning the tunnel height.

C = tunnel test section area.

The volume of an airfoil is often approximated by the relation: 0.7(max thickness)(chord)(span)[Ref. 21]. Due to its unique shape the waverider tested was estimated as 0.5(max thickness)(planform area) = .0862 ft^3. Wind tunnel geometric area = 8.75 ft^2, hence $\varepsilon_{sb} = 0.001732$.

2. Wake Blocking:

For a model which spans the test section width (wall to wall) the following equation is normally used:

$$\varepsilon_{wb} = \frac{\Delta V}{V_u} = \frac{cC_{du}}{2h}$$

For a model which spans the test section height (which is the setup used):

$$\varepsilon_{wb} = \frac{\Delta V}{V_u} = \frac{cC_{du}}{2w}$$

where: c = model chord

h = test section height

w = test section width

C_{du} = uncorrected drag coefficient

The coefficient for wake blocking is a function of C_{du}, hence a function of AOA. Therefore, a different value is obtained for each data point.

3. Aerodynamic Corrections:

The total blockage correction (ε) is found by summing the solid and wake blockage corrections. Once the blockage factors have been calculated the following expressions may be used to determine the corrected aerodynamic performance parameters, providing the chord to tunnel height ratio (c/h) is less than 0.7. The subscript "u" denotes uncorrected values.

Velocity: $V = V_u (1 + \varepsilon)$

Dynamic Pressure: $q = q_u (1 + 2\varepsilon)$

Reynolds Number: $Re_{EFF} = Re_u (1 + \varepsilon)$

Drag Coefficient: $C_d = C_{du} (1 - 3\varepsilon_{sb} - 2\varepsilon_{wb})$

AOA, C_L and C_M require correction for streamline curvature, introducing a new parameter (σ).

Curvature Coeff: $$\sigma = \frac{\pi^2}{48}\left(\frac{c}{h}\right)^2$$ (h = test section height)

Angle of attack: $$\alpha = \alpha_u + \frac{57.3\sigma}{2\pi}\left(C_{l_u} + C_{m_{c/4u}}\right)$$

Lift Coefficient: $$C_l = C_{lu}\,(1 - \sigma - 2\varepsilon)$$

Moment coefficient: $$C_{m_{c/4}} = C_{m_{c/4u}}(1-2\varepsilon) + \frac{\sigma C_l}{4}$$

APPENDIX D: WIND TUNNEL DATA

IAS = 45 mph

del_p (cm H20)	patm (in-Hg)	IAS (mph)	Vel True (mph)	q (lbf/ft2)	T (deg F)	Re	S (ft2)	chord © ft
1.61	30.5	45	37.99	3.65	66	$4.355*10^5$	0.991623	1.25

AOA (deg)	CL	CD	CL/CD	CM	CN	CA	Normal Force (lbf)	Axial Force (lbf)	Side Force (lbf)	Pitch Moment (ft-lbf)	Yaw Moment (ft-lbf)	Roll Moment (ft-lbf)
-90	0.0228	1.2949	0.0176	-0.226	-1.295	0.0228	-4.693	0.0828	0.2736	-1.022	0.0553	0.002
-85	-0.088	1.2935	-0.068	-0.243	-1.296	0.0247	-4.698	0.0894	0.273	-1.103	0.0597	0.0021
-80	-0.202	1.2703	-0.159	-0.259	-1.286	0.022	-4.66	0.0798	0.2707	-1.171	0.0632	0.0021
-75	-0.315	1.2542	-0.251	-0.274	-1.293	0.0206	-4.686	0.0747	0.2746	-1.243	0.0678	0.0021
-70	-0.419	1.2177	-0.344	-0.287	-1.287	0.0232	-4.666	0.0841	0.2713	-1.302	0.0712	0.0021
-65	-0.613	1.3692	-0.447	-0.352	-1.5	0.0234	-5.436	0.0846	0.313	-1.595	0.0868	0.0024
-60	-0.724	1.282	-0.564	-0.36	-1.472	0.0144	-5.335	0.0521	0.3147	-1.63	0.0905	0.0024
-55	-0.79	1.1647	-0.679	-0.36	-1.407	0.0206	-5.1	0.0748	0.2897	-1.631	0.0887	0.0023
-50	-0.876	1.0748	-0.815	-0.364	-1.387	0.0195	-5.026	0.0707	0.2914	-1.65	0.0888	0.0023
-45	-0.966	0.993	-0.973	-0.37	-1.385	0.0188	-5.021	0.068	0.2901	-1.676	0.0915	0.0023
-40	-1.368	1.1317	-1.209	-0.527	-1.775	-0.012	-6.434	-0.045	0.3635	-2.387	0.1304	0.0028
-35	-1.546	1.0423	-1.484	-0.698	-1.865	-0.033	-6.757	-0.12	0.3848	-3.161	0.1707	0.0029
-30	-1.562	0.8671	-1.802	-0.719	-1.786	-0.03	-6.474	-0.11	0.363	-3.258	0.1767	0.0028
-25	-1.428	0.6467	-2.209	-0.624	-1.568	-0.018	-5.682	-0.064	0.321	-2.827	0.1521	0.0025
-20	-1.177	0.4275	-2.754	-0.466	-1.253	-9E-04	-4.54	-0.003	0.2581	-2.11	0.1141	0.002
-15	-0.879	0.2493	-3.524	-0.308	-0.913	0.0134	-3.31	0.0486	0.1932	-1.395	0.0741	0.0015
-10	-0.582	0.1214	-4.799	-0.153	-0.595	0.0184	-2.155	0.0666	0.13	-0.692	0.0361	0.0006
-5	-0.311	0.0569	-5.459	-0.028	-0.314	0.0296	-1.14	0.1073	0.074	-0.126	0.0049	0.0003
0	-0.091	0.0458	-1.987	0.0675	-0.091	0.0458	-0.33	0.1662	0.0257	0.3058	-0.017	-2E-05
5	0.1685	0.0715	2.3569	0.1855	0.1741	0.0565	0.631	0.2049	-0.027	0.8405	-0.046	-4E-04
10	0.478	0.1524	3.1368	0.3321	0.4972	0.0671	1.8019	0.2431	-0.091	1.5042	-0.082	-8E-04
15	0.7983	0.2938	2.7172	0.4781	0.8471	0.0772	3.0701	0.2797	-0.155	2.1658	-0.115	-0.001
20	1.1115	0.5022	2.2134	0.6214	1.2162	0.0917	4.4076	0.3324	-0.236	2.815	-0.153	-0.002
25	1.3499	0.7323	1.8433	0.722	1.5329	0.0932	5.5553	0.3378	-0.294	3.2707	-0.177	-0.002
30	1.4712	0.9704	1.516	0.7049	1.7593	0.1048	6.3758	0.3799	-0.334	3.1931	-0.171	-0.002
35	0.9117	0.7984	1.142	0.4196	1.2048	0.131	4.3662	0.4749	-0.228	1.9007	-0.101	-0.001
40	0.8607	0.902	0.9542	0.4163	1.2391	0.1377	4.4906	0.4992	-0.235	1.8859	-0.101	-0.001
45	0.8017	1.0015	0.8006	0.4098	1.2751	0.1412	4.6209	0.5118	-0.242	1.8563	-0.099	-0.001
50	0.7434	1.0956	0.6785	0.402	1.3171	0.1347	4.7732	0.4883	-0.244	1.8212	-0.097	-0.001
55	0.6731	1.2235	0.5501	0.3959	1.3883	0.1504	5.0313	0.5451	-0.265	1.7935	-0.097	-0.001
60	0.6029	1.3219	0.4561	0.3862	1.4463	0.1388	5.2415	0.5031	-0.274	1.7494	-0.094	-0.001
65	0.5076	1.4093	0.3602	0.3711	1.4918	0.1356	5.4062	0.4913	-0.282	1.6812	-0.09	-0.001
70	0.3981	1.4734	0.2702	0.3516	1.5207	0.1299	5.5113	0.4706	-0.284	1.5928	-0.086	-0.001
75	0.2743	1.4907	0.184	0.3245	1.5109	0.1209	5.4758	0.4381	-0.282	1.4698	-0.079	-1E-03
80	0.1524	1.5619	0.0975	0.3048	1.5647	0.1212	5.6705	0.4392	-0.295	1.3807	-0.074	-9E-04
85	0.023	1.5571	0.0148	0.2741	1.5532	0.1128	5.629	0.4089	-0.297	1.2415	-0.067	-8E-04
90	-0.103	1.5395	-0.067	0.244	1.5395	0.1029	5.5793	0.373	-0.29	1.1052	-0.06	-8E-04

45 mph Boundary Layer Corrections Corrected values = "new"

σ	0.0201
V new	37.382
Re new	4277262

ε_{sb} =0.00104
ε_{wb} varies with C_D
$\varepsilon = \varepsilon_{sb} + \varepsilon_{wb}$

εwb	ε	q new	AOAu (deg)	AOA new	CL	CL new	CD	CD new	CM	CM(1/4c)	CM new (1/4 c)	CN
0.2158	0.2169	5.2330	-90.00	-89.9087	0.0228	0.0125	1.2949	0.7319	-0.2257	0.4757	0.2694	-1.2949
0.2156	0.2166	5.2314	-85.00	-84.9322	-0.0884	-0.0483	1.2935	0.7318	-0.2434	0.4588	0.2598	-1.2963
0.2117	0.2127	5.2031	-80.00	-79.9567	-0.2016	-0.1118	1.2703	0.7284	-0.2586	0.4380	0.2511	-1.2860
0.2090	0.2101	5.1836	-75.00	-74.9796	-0.3147	-0.1762	1.2542	0.7260	-0.2744	0.4259	0.2461	-1.2930
0.2030	0.2040	5.1392	-70.00	-70.0016	-0.4185	-0.2394	1.2177	0.7196	-0.2873	0.4100	0.2416	-1.2874
0.2006	0.2017	5.1221	-65.00	-65.0279	-0.6127	-0.3533	1.2037	0.7170	-0.3520	0.4604	0.2729	-1.4998
0.1971	0.1982	5.0967	-60.00	-60.0524	-0.7236	-0.4222	1.1828	0.7128	-0.3598	0.4375	0.2620	-1.4720
0.1941	0.1951	5.0746	-55.00	-55.0710	-0.7903	-0.4660	1.1647	0.7089	-0.3600	0.4023	0.2430	-1.4073
0.1791	0.1802	4.9653	-50.00	-50.0896	-0.8764	-0.5430	1.0748	0.6864	-0.3642	0.3869	0.2448	-1.3867
0.1655	0.1665	4.8657	-45.00	-45.1073	-0.9664	-0.6251	0.9930	0.6612	-0.3699	0.3805	0.2507	-1.3855
0.1886	0.1897	5.0345	-40.00	-40.1709	-1.3679	-0.8216	1.1317	0.7013	-0.5268	0.4348	0.2657	-1.7753
0.1737	0.1748	4.9258	-35.00	-35.2260	-1.5464	-0.9748	1.0423	0.6769	-0.6978	0.3122	0.1982	-1.8646
0.1445	0.1456	4.7125	-30.00	-30.2406	-1.5623	-1.0761	0.8671	0.6138	-0.7192	0.2484	0.1707	-1.7865
0.1078	0.1088	4.4444	-25.00	-25.2203	-1.4284	-1.0889	0.6467	0.5053	-0.6240	0.2252	0.1708	-1.5679
0.0713	0.0723	4.1778	-20.00	-20.1766	-1.1774	-0.9835	0.4275	0.3653	-0.4658	0.2127	0.1770	-1.2526
0.0416	0.0426	3.9609	-15.00	-15.1267	-0.8787	-0.7862	0.2493	0.2278	-0.3080	0.1867	0.1669	-0.9133
0.0202	0.0213	3.8053	-10.00	-10.0756	-0.5824	-0.5460	0.1214	0.1161	-0.1527	0.1694	0.1595	-0.5947
0.0095	0.0105	3.7268	-5.00	-5.0308	-0.3107	-0.2979	0.0569	0.0557	-0.0278	0.1426	0.1381	-0.3145
0.0076	0.0087	3.7134	0.00	0.0047	-0.0911	-0.0877	0.0458	0.0450	0.0675	0.1168	0.1144	-0.0911
0.0119	0.0130	3.7446	5.00	5.0476	0.1685	0.1608	0.0715	0.0696	0.1855	0.0912	0.0897	0.1741
0.0254	0.0264	3.8430	10.00	10.0990	0.4780	0.4431	0.1524	0.1442	0.3321	0.0627	0.0616	0.4972
0.0490	0.0500	4.0150	15.00	15.1497	0.7983	0.7024	0.2938	0.2641	0.4781	0.0192	0.0208	0.8471
0.0837	0.0847	4.2686	20.00	20.1967	1.1115	0.9008	0.5022	0.4165	0.6214	-0.0374	-0.0265	1.2162
0.1220	0.1231	4.5486	25.00	25.2273	1.3499	0.9904	0.7323	0.5513	0.7220	-0.1083	-0.0767	1.5329
0.1617	0.1628	4.8383	30.00	30.2240	1.4712	0.9627	0.9704	0.6535	0.7049	-0.2481	-0.1625	1.7593
0.1331	0.1341	4.6289	35.00	35.1243	0.9117	0.6489	0.7984	0.5834	0.4196	-0.2330	-0.1673	1.2048
0.1503	0.1514	4.7550	40.00	40.1109	0.8607	0.5828	0.9020	0.6280	0.4163	-0.2549	-0.1748	1.2391
0.1669	0.1679	4.8760	45.00	45.0954	0.8017	0.5163	1.0015	0.6640	0.4098	-0.2809	-0.1839	1.2751
0.1826	0.1836	4.9905	50.00	50.0791	0.7434	0.4554	1.0956	0.6921	0.4020	-0.3114	-0.1947	1.3171
0.2039	0.2050	5.1462	55.00	55.0580	0.6731	0.3837	1.2235	0.7207	0.3959	-0.3561	-0.2082	1.3883
0.2203	0.2214	5.2660	60.00	60.0377	0.6029	0.3239	1.3219	0.7353	0.3862	-0.3972	-0.2197	1.4463
0.2349	0.2359	5.3722	65.00	65.0129	0.5076	0.2579	1.4093	0.7429	0.3711	-0.4369	-0.2295	1.4918
0.2456	0.2466	5.4503	70.00	69.9864	0.3981	0.1938	1.4734	0.7452	0.3516	-0.4721	-0.2383	1.5207
0.2485	0.2495	5.4713	75.00	74.9598	0.2743	0.1319	1.4907	0.7453	0.3245	-0.4940	-0.2468	1.5109
0.2603	0.2614	5.5580	80.00	79.9285	0.1524	0.0697	1.5619	0.7438	0.3048	-0.5427	-0.2587	1.5647
0.2595	0.2606	5.5521	85.00	84.9003	0.0230	0.0105	1.5571	0.7441	0.2741	-0.5673	-0.2716	1.5532
0.2566	0.2576	5.5307	90.00	89.8731	-0.1029	-0.0478	1.5395	0.7447	0.2440	-0.5899	-0.2862	1.5395

IAS = 60 mph

del_p (cm H20)	patm (in-Hg)	IAS (mph)	Vel True (mph)	q (lbf/ft2)	T (deg F)	Re	S (ft2)	chord © ft
3.41	30.5	60	55.24	7.74	66	$6.343*10^5$	0.991623	1.25

AOA (deg)	CL	CD	CL/CD	CM	CN	CA	Normal Force (lbf)	Axial Force (lbf)	Side Force (lbf)	Pitch Moment (ft-lbf)	Yaw Moment (ft-lbf)	Roll Moment (ft-lbf)
-25	-1.222	0.5341	-2.287	-0.539	-1.333	-0.032	-10.23	-0.247	0.5506	-5.168	0.2791	0.0045
-24	-1.175	0.492	-2.388	-0.505	-1.273	-0.028	-9.773	-0.218	0.5239	-4.845	0.2617	0.0043
-23	-1.135	0.4557	-2.49	-0.48	-1.222	-0.024	-9.383	-0.183	0.5101	-4.602	0.2489	0.004
-22	-1.103	0.4241	-2.601	-0.46	-1.182	-0.02	-9.071	-0.154	0.4953	-4.413	0.2375	0.004
-21	-1.042	0.3836	-2.717	-0.425	-1.11	-0.015	-8.524	-0.118	0.4623	-4.077	0.2181	0.0038
-20	-1.013	0.3562	-2.843	-0.406	-1.073	-0.012	-8.239	-0.089	0.4469	-3.891	0.2098	0.0037
-19	-0.973	0.3251	-2.994	-0.385	-1.026	-0.009	-7.876	-0.073	0.4263	-3.692	0.1976	0.0036
-18	-0.9	0.2885	-3.119	-0.342	-0.945	-0.004	-7.253	-0.028	0.3969	-3.281	0.1778	0.0031
-18	-0.843	0.2716	-3.104	-0.314	-0.886	-0.002	-6.799	-0.017	0.3718	-3.013	0.162	0.003
-17	-0.838	0.2536	-3.304	-0.31	-0.875	-0.002	-6.718	-0.019	0.3678	-2.973	0.1579	0.0031
-16	-0.787	0.2262	-3.478	-0.284	-0.818	0.0006	-6.282	0.0045	0.3435	-2.724	0.1463	0.0028
-15	-0.744	0.2055	-3.621	-0.262	-0.772	0.0059	-5.926	0.0453	0.3237	-2.515	0.1332	0.0028
-14	-0.682	0.1783	-3.826	-0.231	-0.705	0.008	-5.412	0.061	0.3006	-2.219	0.1177	0.0025
-13	-0.636	0.156	-4.079	-0.209	-0.655	0.0089	-5.027	0.0681	0.2774	-2.007	0.1062	0.0023
-12	-0.59	0.136	-4.339	-0.185	-0.606	0.0103	-4.649	0.0793	0.2584	-1.772	0.0947	0.0021
-11	-0.547	0.1174	-4.658	-0.163	-0.559	0.0109	-4.293	0.0837	0.2348	-1.564	0.0816	0.0014
-10	-0.487	0.1002	-4.856	-0.13	-0.497	0.0142	-3.814	0.1089	0.2101	-1.246	0.0659	0.0018
-9	-0.436	0.0851	-5.123	-0.106	-0.444	0.0159	-3.406	0.1217	0.1876	-1.013	0.0531	0.0016
-8	-0.396	0.0728	-5.439	-0.087	-0.402	0.017	-3.086	0.1303	0.1706	-0.834	0.0434	0.0009
-7	-0.346	0.0614	-5.64	-0.065	-0.351	0.0187	-2.696	0.1439	0.1491	-0.622	0.0323	0.0007
-6	-0.31	0.0535	-5.794	-0.048	-0.314	0.0208	-2.41	0.1597	0.1331	-0.462	0.0237	0.0006
-5	-0.248	0.0458	-5.413	-0.019	-0.251	0.024	-1.926	0.1843	0.1034	-0.187	0.0087	0.0004
-4	-0.208	0.0409	-5.094	-0.003	-0.211	0.0263	-1.617	0.2017	0.089	-0.029	0.0007	0.0008
-3	-0.167	0.0377	-4.438	0.0158	-0.169	0.0289	-1.296	0.2215	0.0652	0.1513	-0.01	0.0002
-2	-0.128	0.0356	-3.602	0.0334	-0.129	0.0311	-0.993	0.2386	0.053	0.3203	-0.018	0.0006
-1	-0.1	0.0343	-2.918	0.0436	-0.101	0.0326	-0.773	0.25	0.0427	0.4188	-0.024	0.0005
0	-0.057	0.0341	-1.679	0.0622	-0.057	0.0341	-0.439	0.2615	0.0217	0.5965	-0.034	-7E-05
1	-0.023	0.0357	-0.642	0.078	-0.022	0.0361	-0.171	0.2773	0.0093	0.7483	-0.041	-2E-04
2	0.01	0.0371	0.2704	0.0924	0.0113	0.0367	0.0869	0.282	-3E-04	0.8869	-0.048	9E-05
3	0.0569	0.0406	1.4011	0.1131	0.059	0.0376	0.4527	0.2886	-0.022	1.0847	-0.059	-4E-04
4	0.0948	0.0458	2.0712	0.1296	0.0978	0.0391	0.7505	0.2997	-0.039	1.2431	-0.068	-5E-04
5	0.1534	0.0547	2.8053	0.1564	0.1576	0.0411	1.2098	0.3156	-0.063	1.5005	-0.082	-7E-04
6	0.2078	0.0647	3.2135	0.1826	0.2134	0.0426	1.6383	0.3269	-0.085	1.7519	-0.095	-9E-04
7	0.2619	0.0773	3.3873	0.2063	0.2694	0.0448	2.0677	0.3441	-0.106	1.9795	-0.105	-8E-04
8	0.3168	0.0914	3.4645	0.2318	0.3264	0.0465	2.5055	0.3566	-0.127	2.224	-0.119	-0.001
9	0.3533	0.1043	3.3865	0.2492	0.3653	0.0478	2.8037	0.3667	-0.153	2.3914	-0.128	-0.001
10	0.4195	0.1257	3.3374	0.2827	0.435	0.0509	3.3389	0.3911	-0.173	2.7122	-0.146	-0.002
11	0.4817	0.1478	3.2589	0.3125	0.501	0.0532	3.8458	0.4082	-0.207	2.9982	-0.16	-0.002
12	0.5482	0.1724	3.179	0.3426	0.5721	0.0547	4.3911	0.4198	-0.236	3.287	-0.176	-0.002
13	0.6011	0.1976	3.0418	0.3665	0.6302	0.0573	4.8371	0.4401	-0.257	3.5168	-0.189	-0.002
14	0.6543	0.2237	2.9253	0.39	0.689	0.0587	5.2887	0.4508	-0.284	3.7424	-0.2	-0.002
15	0.7074	0.2524	2.803	0.4146	0.7486	0.0607	5.7461	0.4658	-0.307	3.9781	-0.214	-0.002
16	0.7571	0.2821	2.6842	0.4365	0.8055	0.0625	6.1831	0.4794	-0.331	4.188	-0.225	-0.003
17	0.8148	0.3158	2.58	0.4632	0.8716	0.0638	6.6901	0.4897	-0.37	4.4439	-0.24	-0.003
18	0.8669	0.35	2.4769	0.4867	0.9327	0.065	7.1589	0.4987	-0.386	4.6703	-0.251	-0.003
19	0.9194	0.3862	2.3807	0.5092	0.995	0.0658	7.6374	0.5052	-0.413	4.8854	-0.264	-0.003
20	0.9793	0.4276	2.2904	0.5373	1.0665	0.0668	8.186	0.5131	-0.447	5.1548	-0.279	-0.003
21	1.0285	0.4675	2.2002	0.5579	1.1278	0.0678	8.6565	0.5206	-0.468	5.3534	-0.289	-0.003
22	1.071	0.5085	2.1061	0.5769	1.1835	0.0703	9.0844	0.5395	-0.491	5.5354	-0.298	-0.003

60 mph Boundary Layer Corrections Corrected values = "new"

σ	0.0201
V new	55.627
Re new	636245

ε_{sb} =0.00104
ε_{wb} varies with C_D
$\varepsilon = \varepsilon_{sb} + \varepsilon_{wb}$

εwb	ε	q new	AOAu (deg)	AOA new	CL	CL new	CD	CD new	CM	CM(1/4c)	CM new (1/4 c)	CN
0.07344	0.0745	8.8929	-25.0	-25.1901	-1.2216	-1.0151	0.5341	0.4540	-0.5386	0.1834	0.1510	-1.3328
0.06764	0.0687	8.8032	-24.0	-24.1813	-1.1747	-0.9898	0.4920	0.4239	-0.5050	0.1848	0.1544	-1.2733
0.06265	0.0637	8.7260	-23.0	-23.1743	-1.1345	-0.9672	0.4557	0.3971	-0.4797	0.1825	0.1544	-1.2224
0.05831	0.0594	8.6588	-22.0	-22.1690	-1.1032	-0.9501	0.4241	0.3733	-0.4599	0.1802	0.1540	-1.1817
0.05275	0.0538	8.5726	-21.0	-21.1585	-1.0422	-0.9092	0.3836	0.3420	-0.4249	0.1766	0.1530	-1.1105
0.04898	0.0500	8.5144	-20.0	-20.1532	-1.0127	-0.8910	0.3562	0.3202	-0.4056	0.1759	0.1538	-1.0734
0.04470	0.0457	8.4480	-19.0	-19.1469	-0.9732	-0.8646	0.3251	0.2950	-0.3848	0.1710	0.1510	-1.0260
0.03967	0.0407	8.3701	-18.0	-18.1337	-0.8998	-0.8084	0.2885	0.2647	-0.3419	0.1699	0.1520	-0.9449
0.03486	0.0359	8.2958	-17.0	-17.1233	-0.8376	-0.7607	0.2536	0.2351	-0.3099	0.1642	0.1486	-0.8752
0.03110	0.0321	8.2375	-16.0	-16.1148	-0.7866	-0.7202	0.2262	0.2114	-0.2839	0.1594	0.1456	-0.8184
0.02826	0.0293	8.1936	-15.0	-15.1077	-0.7442	-0.6857	0.2055	0.1933	-0.2621	0.1561	0.1435	-0.7721
0.02451	0.0256	8.1356	-14.0	-14.0973	-0.6822	-0.6336	0.1783	0.1690	-0.2313	0.1506	0.1397	-0.7050
0.02144	0.0225	8.0881	-13.0	-13.0898	-0.6361	-0.5947	0.1560	0.1488	-0.2092	0.1456	0.1360	-0.6549
0.01870	0.0197	8.0457	-12.0	-12.0818	-0.5903	-0.5551	0.1360	0.1305	-0.1847	0.1434	0.1349	-0.6057
0.01615	0.0172	8.0061	-11.0	-11.0745	-0.5470	-0.5172	0.1174	0.1133	-0.1630	0.1400	0.1326	-0.5593
0.01378	0.0148	7.9695	-10.0	-10.0636	-0.4868	-0.4626	0.1002	0.0972	-0.1298	0.1393	0.1329	-0.4968
0.01170	0.0127	7.9372	-9.0	-9.0551	-0.4358	-0.4159	0.0851	0.0828	-0.1056	0.1347	0.1292	-0.4437
0.01000	0.0110	7.9110	-8.0	-8.0485	-0.3957	-0.3790	0.0728	0.0711	-0.0869	0.1309	0.1261	-0.4020
0.00844	0.0095	7.8868	-7.0	-7.0405	-0.3463	-0.3328	0.0614	0.0602	-0.0649	0.1254	0.1213	-0.3512
0.00736	0.0084	7.8700	-6.0	-6.0344	-0.3100	-0.2986	0.0535	0.0526	-0.0481	0.1219	0.1184	-0.3139
0.00630	0.0073	7.8536	-5.0	-5.0241	-0.2479	-0.2393	0.0458	0.0451	-0.0195	0.1165	0.1135	-0.2509
0.00562	0.0067	7.8432	-4.0	-4.0178	-0.2084	-0.2014	0.0409	0.0403	-0.0030	0.1111	0.1086	-0.2107
0.00518	0.0062	7.8363	-3.0	-3.0110	-0.1671	-0.1617	0.0377	0.0372	0.0158	0.1072	0.1051	-0.1689
0.00489	0.0059	7.8318	-2.0	-2.0045	-0.1282	-0.1241	0.0356	0.0351	0.0334	0.1034	0.1016	-0.1293
0.00472	0.0058	7.8292	-1.0	-1.0004	-0.1002	-0.0970	0.0343	0.0339	0.0436	0.0982	0.0966	-0.1008
0.00468	0.0057	7.8286	0.0	0.0066	-0.0572	-0.0554	0.0341	0.0336	0.0622	0.0932	0.0918	-0.0572
0.00491	0.0060	7.8321	1.0	1.0123	-0.0230	-0.0222	0.0357	0.0353	0.0780	0.0901	0.0889	-0.0223
0.00510	0.0061	7.8351	2.0	2.0176	0.0100	0.0097	0.0371	0.0366	0.0924	0.0863	0.0853	0.0113
0.00559	0.0066	7.8426	3.0	3.0253	0.0569	0.0550	0.0406	0.0400	0.1131	0.0811	0.0803	0.0590
0.00629	0.0073	7.8535	4.0	4.0314	0.0948	0.0915	0.0458	0.0451	0.1296	0.0766	0.0759	0.0978
0.00752	0.0086	7.8725	5.0	5.0411	0.1534	0.1477	0.0547	0.0537	0.1564	0.0710	0.0705	0.1576
0.00889	0.0099	7.8938	6.0	6.0503	0.2078	0.1995	0.0647	0.0633	0.1826	0.0670	0.0666	0.2134
0.01063	0.0117	7.9207	7.0	7.0590	0.2619	0.2505	0.0773	0.0754	0.2063	0.0604	0.0602	0.2694
0.01257	0.0136	7.9507	8.0	8.0681	0.3168	0.3018	0.0914	0.0888	0.2318	0.0550	0.0550	0.3264
0.01434	0.0154	7.9782	9.0	9.0741	0.3533	0.3353	0.1043	0.1010	0.2492	0.0514	0.0515	0.3653
0.01728	0.0183	8.0237	10.0	10.0854	0.4195	0.3957	0.1257	0.1210	0.2827	0.0470	0.0473	0.4350
0.02032	0.0214	8.0707	11.0	11.0957	0.4817	0.4514	0.1478	0.1413	0.3125	0.0411	0.0416	0.5010
0.02371	0.0248	8.1231	12.0	12.1064	0.5482	0.5101	0.1724	0.1637	0.3426	0.0327	0.0336	0.5721
0.02717	0.0282	8.1767	13.0	13.1147	0.6011	0.5551	0.1976	0.1863	0.3665	0.0252	0.0265	0.6302
0.03076	0.0318	8.2322	14.0	14.1229	0.6543	0.5996	0.2237	0.2092	0.3900	0.0168	0.0187	0.6890
0.03470	0.0357	8.2933	15.0	15.1312	0.7074	0.6426	0.2524	0.2341	0.4146	0.0091	0.0117	0.7486
0.03878	0.0398	8.3565	16.0	16.1387	0.7571	0.6816	0.2821	0.2593	0.4365	0.0001	0.0035	0.8055
0.04343	0.0445	8.4283	17.0	17.1476	0.8148	0.7260	0.3158	0.2874	0.4632	-0.0090	-0.0045	0.8716
0.04813	0.0492	8.5011	18.0	18.1554	0.8669	0.7643	0.3500	0.3152	0.4867	-0.0185	-0.0128	0.9327
0.05310	0.0541	8.5781	19.0	19.1629	0.9194	0.8014	0.3862	0.3440	0.5092	-0.0298	-0.0226	0.9950
0.05879	0.0598	8.6662	20.0	20.1719	0.9793	0.8424	0.4276	0.3760	0.5373	-0.0405	-0.0314	1.0665
0.06428	0.0653	8.7511	21.0	21.1786	1.0285	0.8735	0.4675	0.4059	0.5579	-0.0530	-0.0417	1.1278
0.06992	0.0710	8.8385	22.0	22.1844	1.0710	0.8975	0.5085	0.4358	0.5769	-0.0642	-0.0506	1.1835

IAS = 75 mph

del_p (cm H20)	patm (in-Hg)	IAS (mph)	Vel calc (mph)	q (lbf/ft2)	T (deg F)	Re	S (ft2)	chord © ft
6.05	30.5	75	73.56	13.74	66	8.439*105	0.991623	1.25

AOA (deg)	CL	CD	CL/CD	CM	CM(1/4c)	CN	CA	Normal Force (lbf)	Axial Force (lbf)	Side Force (lbf)	Pitch Moment (ft-lbf)	Yaw Moment (ft-lbf)	Roll Moment (ft-lbf)
-18	-0.908	0.2819	-3.22	-0.349	-0.052	-0.9504	-0.012	-12.94	-0.169	0.7059	-5.944	0.32	0.006
-17	-0.848	0.2493	-3.403	-0.317	-0.041	-0.8842	-0.01	-12.04	-0.131	0.6658	-5.403	0.285	0.005
-16	-0.803	0.2242	-3.581	-0.294	-0.034	-0.8335	-0.006	-11.35	-0.079	0.6257	-5.01	0.267	0.005
-15	-0.741	0.1969	-3.765	-0.263	-0.023	-0.7671	-0.002	-10.45	-0.023	0.5821	-4.472	0.241	0.005
-14	-0.686	0.1717	-3.994	-0.234	-0.013	-0.7071	0.0007	-9.629	0.0096	0.542	-3.984	0.212	0.004
-13	-0.63	0.1519	-4.147	-0.207	-0.004	-0.6478	0.0063	-8.822	0.0858	0.4944	-3.522	0.187	0.004
-12	-0.597	0.1348	-4.427	-0.192	-5E-04	-0.6118	0.0078	-8.332	0.1061	0.472	-3.263	0.174	0.004
-11	-0.548	0.116	-4.723	-0.163	0.0115	-0.5600	0.0093	-7.627	0.1271	0.4356	-2.783	0.149	0.003
-10	-0.502	0.0996	-5.046	-0.139	0.0207	-0.5120	0.0108	-6.973	0.1473	0.3892	-2.372	0.125	0.003
-9	-0.445	0.084	-5.297	-0.111	0.0302	-0.4526	0.0134	-6.164	0.1819	0.35	-1.894	0.1	0.003
-8	-0.38	0.0696	-5.456	-0.08	0.0404	-0.3859	0.0161	-5.255	0.219	0.3022	-1.365	0.071	0.003
-7	-0.343	0.0606	-5.661	-0.063	0.0453	-0.3477	0.0183	-4.735	0.2497	0.274	-1.078	0.056	0.002
-6	-0.299	0.0515	-5.811	-0.044	0.051	-0.3028	0.0199	-4.123	0.2713	0.2397	-0.742	0.039	0.002
-5	-0.26	0.0443	-5.87	-0.026	0.0558	-0.2629	0.0215	-3.581	0.2924	0.2091	-0.45	0.022	0.002
-4	-0.21	0.0393	-5.347	-0.004	0.0628	-0.2122	0.0245	-2.89	0.334	0.1659	-0.06	1E-04	0.001
-3	-0.179	0.0354	-5.069	0.0073	0.0639	-0.1809	0.0259	-2.463	0.3532	0.1436	0.1248	-0.01	0.001
-2	-0.137	0.0322	-4.25	0.0267	0.0698	-0.1379	0.0274	-1.878	0.3733	0.1091	0.4542	-0.03	0.001
-1	-0.104	0.0305	-3.412	0.0403	0.073	-0.1047	0.0287	-1.426	0.391	0.0864	0.6866	-0.04	0.001
0	-0.059	0.0311	-1.901	0.06	0.0785	-0.0592	0.0311	-0.807	0.4242	0.0503	1.0209	-0.06	0.000
1	-0.033	0.0311	-1.049	0.0709	0.0809	-0.0321	0.0317	-0.437	0.4314	0.0355	1.2065	-0.07	0.000
2	0.0223	0.0342	0.6512	0.0954	0.0881	0.0235	0.0334	0.3196	0.4552	-0.006	1.6245	-0.09	-0.001
3	0.0617	0.0379	1.6304	0.1135	0.0936	0.0636	0.0346	0.8662	0.4708	-0.034	1.932	-0.1	-0.001
4	0.1229	0.0453	2.7153	0.1406	0.1013	0.1258	0.0366	1.713	0.4983	-0.083	2.3929	-0.13	-0.001
5	0.1681	0.0528	3.1865	0.1606	0.1068	0.1721	0.0379	2.3434	0.5162	-0.119	2.7333	-0.15	-0.001
6	0.2247	0.0631	3.5633	0.1862	0.1143	0.2301	0.0392	3.1333	0.5343	-0.155	3.1692	-0.17	-0.002
7	0.2724	0.0752	3.6244	0.2089	0.1216	0.2796	0.0414	3.8071	0.5638	-0.194	3.5568	-0.19	-0.002
8	0.3267	0.0895	3.65	0.2338	0.1288	0.3360	0.0432	4.5761	0.588	-0.226	3.9807	-0.21	-0.002
9	0.38	0.1055	3.6032	0.2598	0.1374	0.3918	0.0447	5.3363	0.609	-0.27	4.4231	-0.24	-0.003
10	0.4302	0.1227	3.506	0.2829	0.1438	0.4449	0.0461	6.0595	0.6283	-0.311	4.8157	-0.26	-0.003
11	0.4985	0.1458	3.4188	0.3148	0.1531	0.5171	0.048	7.0426	0.6538	-0.371	5.358	-0.29	-0.003
12	0.5574	0.1694	3.2907	0.3404	0.159	0.5804	0.0498	7.9041	0.6781	-0.43	5.7942	-0.31	-0.003
13	0.6055	0.1928	3.1397	0.3634	0.1655	0.6333	0.0517	8.6252	0.7041	-0.473	6.1864	-0.34	-0.004

75 mph Tunnel Wall Corrections Corrected values = "new"

σ	0.0201
V new	73.681
Renew	846331

ε_{sb} =0.00104
ε_{wb} varies with C_D
$\varepsilon = \varepsilon_{sb} + \varepsilon_{wb}$

εwb	ε	q new	AOAu (deg)	AOA new	CL	CL new	CD	CD new	CM	CM(1/4c)	CM(1/4c) new	CN
0.0470	0.0480	15.0597	-18.000	-18.1359	-0.9077	-0.8023	0.2819	0.2416	-0.3492	0.1657	0.1457	-0.9504
0.0416	0.0426	14.9105	-17.000	-17.1258	-0.8484	-0.7591	0.2493	0.2177	-0.3174	0.1616	0.1440	-0.8842
0.0374	0.0384	14.7954	-16.000	-16.1182	-0.8028	-0.7251	0.2242	0.1986	-0.2943	0.1572	0.1415	-0.8335
0.0328	0.0339	14.6704	-15.000	-15.1078	-0.7414	-0.6763	0.1969	0.1771	-0.2627	0.1528	0.1391	-0.7671
0.0286	0.0297	14.5551	-14.000	-14.0983	-0.6859	-0.6314	0.1717	0.1566	-0.2341	0.1490	0.1370	-0.7071
0.0253	0.0263	14.4641	-13.000	-13.0889	-0.6297	-0.5839	0.1519	0.1400	-0.2069	0.1440	0.1335	-0.6478
0.0225	0.0235	14.3861	-12.000	-12.0837	-0.5968	-0.5568	0.1348	0.1255	-0.1917	0.1398	0.1304	-0.6118
0.0193	0.0204	14.2999	-11.000	-11.0747	-0.5480	-0.5146	0.1160	0.1090	-0.1635	0.1399	0.1316	-0.5600
0.0166	0.0176	14.2246	-10.000	-10.0667	-0.5024	-0.4746	0.0996	0.0944	-0.1393	0.1380	0.1308	-0.5120
0.0140	0.0150	14.1533	-9.000	-9.0570	-0.4450	-0.4226	0.0840	0.0803	-0.1113	0.1339	0.1278	-0.4526
0.0116	0.0126	14.0875	-8.000	-8.0460	-0.3799	-0.3626	0.0696	0.0671	-0.0802	0.1289	0.1238	-0.3859
0.0101	0.0111	14.0460	-7.000	-7.0399	-0.3429	-0.3284	0.0606	0.0586	-0.0633	0.1250	0.1206	-0.3477
0.0086	0.0096	14.0043	-6.000	-6.0327	-0.2990	-0.2873	0.0515	0.0500	-0.0436	0.1204	0.1167	-0.3028
0.0074	0.0084	13.9715	-5.000	-5.0264	-0.2601	-0.2505	0.0443	0.0432	-0.0264	0.1160	0.1128	-0.2629
0.0065	0.0076	13.9484	-4.000	-4.0180	-0.2100	-0.2026	0.0393	0.0384	-0.0035	0.1114	0.1087	-0.2122
0.0059	0.0069	13.9306	-3.000	-3.0135	-0.1793	-0.1732	0.0354	0.0347	0.0073	0.1053	0.1030	-0.1809
0.0054	0.0064	13.9161	-2.000	-2.0065	-0.1369	-0.1324	0.0322	0.0316	0.0267	0.1014	0.0994	-0.1379
0.0051	0.0061	13.9084	-1.000	-1.0013	-0.1042	-0.1008	0.0305	0.0300	0.0403	0.0970	0.0953	-0.1047
0.0052	0.0062	13.9112	0.000	0.0060	-0.0592	-0.0573	0.0311	0.0306	0.0600	0.0921	0.0906	-0.0592
0.0052	0.0062	13.9111	1.000	1.0102	-0.0327	-0.0316	0.0311	0.0306	0.0709	0.0883	0.0870	-0.0321
0.0057	0.0067	13.9253	2.000	2.0192	0.0223	0.0215	0.0342	0.0336	0.0954	0.0827	0.0817	0.0235
0.0063	0.0073	13.9419	3.000	3.0258	0.0617	0.0596	0.0379	0.0371	0.1135	0.0790	0.0782	0.0636
0.0075	0.0086	13.9759	4.000	4.0358	0.1229	0.1183	0.0453	0.0442	0.1406	0.0724	0.0718	0.1258
0.0088	0.0098	14.0102	5.000	5.0431	0.1681	0.1614	0.0528	0.0513	0.1606	0.0673	0.0668	0.1721
0.0105	0.0116	14.0574	6.000	6.0524	0.2247	0.2150	0.0631	0.0609	0.1862	0.0615	0.0612	0.2301
0.0125	0.0136	14.1128	7.000	7.0604	0.2724	0.2596	0.0752	0.0722	0.2089	0.0575	0.0572	0.2796
0.0149	0.0160	14.1786	8.000	8.0693	0.3267	0.3098	0.0895	0.0853	0.2338	0.0518	0.0517	0.3360
0.0176	0.0186	14.2516	9.000	9.0783	0.3800	0.3582	0.1055	0.0997	0.2598	0.0476	0.0476	0.3918
0.0204	0.0215	14.3305	10.000	10.0864	0.4302	0.4030	0.1227	0.1149	0.2829	0.0419	0.0421	0.4449
0.0243	0.0253	14.4364	11.000	11.0976	0.4985	0.4632	0.1458	0.1349	0.3148	0.0346	0.0352	0.5171
0.0282	0.0293	14.5443	12.000	12.1068	0.5574	0.5135	0.1694	0.1547	0.3404	0.0260	0.0270	0.5804
0.0321	0.0332	14.6518	13.000	13.1146	0.6055	0.5531	0.1928	0.1739	0.3634	0.0203	0.0218	0.6333

IAS = 90 mp

del_p (cm H20)	patm (in-Hg)	IAS (mph)	Vel calc (mph)	q (lbf/ft2)	T (deg F)	Re	S (ft2)	chord © ft
8.93	30.05	90	89.38	20.29	66	$1.025*10^6$	0.991623	1.25

AOA (deg)	CL	CD	CL/CD	CM	CM(1/4c)	CN	CA	Normal Force (lbf)	Axial Force (lbf)	Side Force (lbf)	Pitch Moment (ft-lbf)	Yaw Moment (ft-lbf)	Roll Moment (ft-lbf)
-13	-0.6294	0.15015	-4.1921	-0.2061	-0.0039	-0.647086	0.00471	-13.022	0.09473	0.73164	-5.1837	0.276	0.0059
-12	-0.591	0.13192	-4.4797	-0.1855	0.00367	-0.605496	0.00617	-12.185	0.12414	0.67832	-4.6673	0.25	0.0055
-11	-0.5429	0.11385	-4.7691	-0.1565	0.01684	-0.554695	0.00816	-11.163	0.16414	0.62738	-3.9369	0.21	0.0050
-10	-0.4926	0.09719	-5.0681	-0.1323	0.02452	-0.501983	0.01018	-10.102	0.20486	0.56447	-3.3291	0.176	0.0047
-9	-0.4377	0.08276	-5.2891	-0.1051	0.03403	-0.445255	0.01327	-8.9602	0.26695	0.51528	-2.644	0.14	0.0040
-8	-0.3738	0.06851	-5.4565	-0.076	0.04261	-0.379691	0.01582	-7.6408	0.31828	0.43895	-1.9128	0.101	0.0035
-7	-0.3413	0.05932	-5.7526	-0.061	0.04712	-0.345942	0.01729	-6.9617	0.34797	0.39997	-1.534	0.08	0.0033
-6	-0.2937	0.05072	-5.7904	-0.0391	0.05387	-0.297393	0.01974	-5.9847	0.39732	0.34439	-0.9828	0.047	0.0029
-5	-0.2528	0.044	-5.7459	-0.0198	0.06008	-0.255665	0.0218	-5.1449	0.43859	0.29978	-0.4983	0.023	0.0024
-4	-0.2085	0.03786	-5.5075	-0.0018	0.06408	-0.210663	0.02323	-4.2393	0.46737	0.24414	-0.0442	-0.003	0.0008
-3	-0.1646	0.03384	-4.8645	0.01631	0.06823	-0.16615	0.02518	-3.3436	0.50665	0.19046	0.41019	-0.027	0.0017
-2	-0.1224	0.03024	-4.0483	0.03467	0.07323	-0.123384	0.02595	-2.483	0.52213	0.14842	0.87213	-0.052	0.0014
-1	-0.0894	0.02961	-3.02	0.04778	0.07589	-0.089936	0.02805	-1.8099	0.56445	0.11339	1.202	-0.067	0.0011
0	-0.0515	0.02916	-1.7673	0.06496	0.08106	-0.051539	0.02916	-1.0372	0.58685	0.06658	1.63398	-0.091	-0.0004
1	-0.0185	0.02961	-0.6243	0.07797	0.08358	-0.017964	0.02992	-0.3615	0.60218	0.03223	1.96129	-0.109	-0.0006
2	0.03002	0.03236	0.92748	0.09998	0.09025	0.031126	0.0313	0.62637	0.62977	-0.0127	2.51485	-0.136	0.0000
3	0.08381	0.03761	2.22849	0.12401	0.09724	0.085661	0.03317	1.72382	0.66749	-0.077	3.1195	-0.168	-0.0014
4	0.13217	0.04388	3.01178	0.14554	0.10338	0.134908	0.03456	2.71486	0.69542	-0.1336	3.6611	-0.196	-0.0018
5	0.18097	0.05213	3.47152	0.16632	0.10856	0.184822	0.03616	3.71932	0.72764	-0.1864	4.18371	-0.222	-0.0021
6	0.24128	0.06298	3.83087	0.19398	0.11693	0.246542	0.03742	4.96136	0.75299	-0.2572	4.87943	-0.263	-0.0026
7	0.29572	0.07615	3.88342	0.22093	0.1263	0.30279	0.03954	6.09329	0.79572	-0.3124	5.55733	-0.298	-0.0031
8	0.35454	0.09188	3.85873	0.24683	0.13311	0.363877	0.04164	7.32259	0.83802	-0.3823	6.20885	-0.333	-0.0036

90 mph Tunnel Wall Corrections Corrected values = "new"

σ	0.0201
V new	90.27
Renew	1029982

ε_{sb} =0.00104 0.00104

ε_{wb} varies with C_D

$\varepsilon = \varepsilon_{sb} + \varepsilon_{wb}$

ε_{wb}	ε	q new	AOAu (deg)	AOA new	CL	CL new	CD	CD new	CM	CM(1/4c)	CM(1/4c) new	CN
0.0250	0.0261	20.99	-13.00	-13.089	-0.6294	-0.5840	0.1501	0.1386	-0.2061	0.1445	0.1340	-0.6471
0.0220	0.0230	20.87	-12.00	-12.082	-0.5910	-0.5519	0.1319	0.1229	-0.1855	0.1425	0.1331	-0.6055
0.0190	0.0200	20.75	-11.00	-11.073	-0.5429	-0.5103	0.1138	0.1071	-0.1565	0.1440	0.1356	-0.5547
0.0162	0.0172	20.64	-10.00	-10.065	-0.4926	-0.4657	0.0972	0.0923	-0.1323	0.1396	0.1324	-0.5020
0.0138	0.0148	20.54	-9.00	-9.0552	-0.4377	-0.4159	0.0828	0.0792	-0.1051	0.1361	0.1300	-0.4453
0.0114	0.0125	20.45	-8.00	-8.0447	-0.3738	-0.3570	0.0685	0.0660	-0.0760	0.1296	0.1246	-0.3797
0.0099	0.0109	20.39	-7.00	-7.0393	-0.3413	-0.3269	0.0593	0.0574	-0.0610	0.1264	0.1220	-0.3459
0.0085	0.0095	20.33	-6.00	-6.0314	-0.2937	-0.2822	0.0507	0.0493	-0.0391	0.1220	0.1183	-0.2974
0.0073	0.0084	20.28	-5.00	-5.0246	-0.2528	-0.2435	0.0440	0.0429	-0.0198	0.1187	0.1155	-0.2557
0.0063	0.0074	20.24	-4.00	-4.0176	-0.2085	-0.2013	0.0379	0.0371	-0.0018	0.1124	0.1097	-0.2107
0.0056	0.0067	20.22	-3.00	-3.0107	-0.1646	-0.1591	0.0338	0.0332	0.0163	0.1063	0.1041	-0.1662
0.0050	0.0061	20.19	-2.00	-2.0038	-0.1224	-0.1185	0.0302	0.0297	0.0347	0.1015	0.0997	-0.1234
0.0049	0.0060	20.19	-1.00	-0.9987	-0.0894	-0.0866	0.0296	0.0291	0.0478	0.0965	0.0949	-0.0899
0.0049	0.0059	20.19	0.00	0.0076	-0.0515	-0.0499	0.0292	0.0287	0.0650	0.0929	0.0915	-0.0515
0.0049	0.0060	20.19	1.00	1.0127	-0.0185	-0.0179	0.0296	0.0291	0.0780	0.0877	0.0866	-0.0180
0.0054	0.0064	20.21	2.00	2.0207	0.0300	0.0290	0.0324	0.0318	0.1000	0.0831	0.0822	0.0311
0.0063	0.0073	20.24	3.00	3.0296	0.0838	0.0809	0.0376	0.0368	0.1240	0.0776	0.0769	0.0857
0.0073	0.0084	20.28	4.00	4.0375	0.1322	0.1273	0.0439	0.0428	0.1455	0.0725	0.0719	0.1349
0.0087	0.0097	20.34	5.00	5.0453	0.1810	0.1738	0.0521	0.0507	0.1663	0.0662	0.0658	0.1848
0.0105	0.0115	20.41	6.00	6.0552	0.2413	0.2309	0.0630	0.0609	0.1940	0.0604	0.0602	0.2465
0.0127	0.0137	20.50	7.00	7.0646	0.2957	0.2817	0.0761	0.0731	0.2209	0.0569	0.0568	0.3028
0.0153	0.0164	20.60	8.00	8.0740	0.3545	0.3358	0.0919	0.0875	0.2468	0.0497	0.0498	0.3639

IAS = 100 mph

del_p (cm H20)	patm (in-Hg)	IAS (mph)	Vel calc (mph)	q (lbf/ft2)	T (deg F)	Re	S (ft2)	chord © ft
11.42	30.05	100	100.9	25.92	66	$1.160*10^6$	0.991623	1.25

AOA (deg)	CL	CD	CL/CD	CM	CM(1/4c)	CN	CA	Normal Force (lbf)	Axial Force (lbf)	Side Force (lbf)	Pitch Moment (ft-lbf)	Yaw Moment (ft-lbf)	Roll Moment (ft-lbf)
-11	-0.5325	0.11063	-4.8135	-0.1532	0.01679	-0.5438	0.00699	-13.98	0.17962	0.77527	-4.9214	0.261	0.0064
-10	-0.4859	0.09517	-5.1054	-0.1299	0.02479	-0.4950	0.00935	-12.725	0.24036	0.71334	-4.174	0.222	0.0057
-9	-0.4316	0.0806	-5.355	-0.103	0.03417	-0.4389	0.01209	-11.282	0.31072	0.63991	-3.3094	0.176	0.0050
-8	-0.3903	0.06869	-5.6818	-0.084	0.03974	-0.3960	0.0137	-10.18	0.35228	0.57384	-2.6996	0.141	0.0047
-7	-0.3348	0.05714	-5.8591	-0.058	0.04803	-0.3392	0.01591	-8.7206	0.40906	0.49485	-1.863	0.095	0.0040
-6	-0.2905	0.04902	-5.9255	-0.0381	0.05374	-0.2940	0.01839	-7.5574	0.4727	0.43054	-1.2253	0.058	0.0036
-5	-0.2419	0.04177	-5.7916	-0.0152	0.06123	-0.2447	0.02053	-6.2893	0.52771	0.35741	-0.4892	0.02	0.0030
-4	-0.1987	0.03615	-5.4962	0.00198	0.06471	-0.2007	0.0222	-5.1604	0.57078	0.29671	0.06355	-0.009	0.0025
-3	-0.1519	0.03148	-4.8249	0.02166	0.06957	-0.1533	0.02349	-3.9411	0.60373	0.22531	0.69596	-0.044	0.0020
-2	-0.118	0.02898	-4.071	0.03577	0.07292	-0.1189	0.02484	-3.0563	0.63856	0.17853	1.14923	-0.069	0.0016
-1	-0.0831	0.02813	-2.9531	0.04992	0.07604	-0.0836	0.02668	-2.148	0.68584	0.13455	1.60421	-0.09	0.0012
0	-0.0444	0.02781	-1.5976	0.06726	0.08114	-0.0444	0.02781	-1.1421	0.7149	0.0816	2.16118	-0.12	0.0008
1	-0.001	0.02891	-0.0332	0.08615	0.0863	-0.0005	0.02892	-0.0117	0.74344	0.02117	2.76836	-0.154	0.0003
2	0.04501	0.03175	1.4174	0.1061	0.0917	0.0461	0.03016	1.18477	0.77541	-0.0445	3.40933	-0.187	-0.0002
3	0.09719	0.03717	2.61477	0.12892	0.09799	0.0990	0.03203	2.545	0.82344	-0.1172	4.14269	-0.222	-0.0009
4	0.15111	0.04408	3.42808	0.1531	0.10503	0.1538	0.03343	3.95412	0.85942	-0.1946	4.91945	-0.263	-0.0025
5	0.20441	0.05296	3.85949	0.17637	0.1113	0.2082	0.03495	5.35327	0.89834	-0.2801	5.65738	-0.304	-0.0029
6	0.26	0.06397	4.0644	0.20159	0.11869	0.2653	0.03644	6.81901	0.93681	-0.3595	6.47756	-0.345	-0.0035

100 mph Tunnel Wall Corrections Corrected values = "new"

σ	0.0201
V new	101.37
Renew	1165070

ε_{sb} =0.00104
ε_{wb} varies with C_D
$\varepsilon = \varepsilon_{sb} + \varepsilon_{wb}$

εwb	ε	q new	AOAu (deg)	AOA new	CL	CL new	CD	CD new	CM	CM(1/4c)	CM(1/4c) new	εwb
0.0184	0.0195	20.73	-11.00	-11.072	-0.5325	-0.5011	0.1106	0.1043	-0.1532	0.1414	0.1334	-0.5438
0.0159	0.0169	20.62	-10.00	-10.064	-0.4859	-0.4597	0.0952	0.0904	-0.1299	0.1382	0.1313	-0.4950
0.0134	0.0145	20.53	-9.00	-9.0544	-0.4316	-0.4104	0.0806	0.0772	-0.1030	0.1348	0.1288	-0.4389
0.0114	0.0125	20.45	-8.00	-8.0476	-0.3903	-0.3727	0.0687	0.0662	-0.0840	0.1305	0.1254	-0.3960
0.0095	0.0106	20.37	-7.00	-7.0383	-0.3348	-0.3210	0.0571	0.0554	-0.0580	0.1258	0.1215	-0.3392
0.0082	0.0092	20.32	-6.00	-6.0310	-0.2905	-0.2793	0.0490	0.0477	-0.0381	0.1211	0.1175	-0.2940
0.0070	0.0080	20.27	-5.00	-5.0228	-0.2419	-0.2332	0.0418	0.0408	-0.0152	0.1173	0.1143	-0.2447
0.0060	0.0071	20.23	-4.00	-4.0161	-0.1987	-0.1919	0.0362	0.0354	0.0020	0.1107	0.1082	-0.2007
0.0052	0.0063	20.20	-3.00	-3.0086	-0.1519	-0.1469	0.0315	0.0309	0.0217	0.1047	0.1027	-0.1533
0.0048	0.0059	20.18	-2.00	-2.0033	-0.1180	-0.1142	0.0290	0.0285	0.0358	0.1002	0.0984	-0.1189
0.0047	0.0057	20.18	-1.00	-0.9978	-0.0831	-0.0805	0.0281	0.0277	0.0499	0.0952	0.0937	-0.0836
0.0046	0.0057	20.18	0.00	0.0086	-0.0444	-0.0430	0.0278	0.0274	0.0673	0.0913	0.0901	-0.0444
0.0048	0.0059	20.18	1.00	1.0156	-0.0010	-0.0009	0.0289	0.0284	0.0862	0.0864	0.0854	-0.0005
0.0053	0.0063	20.20	2.00	2.0231	0.0450	0.0435	0.0318	0.0312	0.1061	0.0811	0.0803	0.0461
0.0062	0.0072	20.24	3.00	3.0316	0.0972	0.0938	0.0372	0.0364	0.1289	0.0753	0.0747	0.0990
0.0073	0.0084	20.28	4.00	4.0404	0.1511	0.1455	0.0441	0.0430	0.1531	0.0698	0.0693	0.1538
0.0088	0.0099	20.34	5.00	5.0491	0.2044	0.1963	0.0530	0.0515	0.1764	0.0636	0.0633	0.2082
0.0107	0.0117	20.42	6.00	6.0582	0.2600	0.2487	0.0640	0.0618	0.2016	0.0579	0.0578	0.2653

IAS = 110

del_p (cm H20)	patm (in-Hg)	IAS (mph)	Vel calc (mph)	q (lbf/ft2)	T (deg F)	Re	S (ft2)	chord© ft
14.07	30.05	110	111.87	31.94	66	$1.289*10^6$	0.991623	1.25

AOA (deg)	CL	CD	CL/CD	CM	CM(1/4c)	CN	CA	Normal Force (lbf)	Axial Force (lbf)	Side Force (lbf)	Pitch Moment (ft-lbf)	Yaw Moment (ft-lbf)	Roll Moment (ft-lbf)
-10	-0.4874	0.09442	-5.1622	-0.1303	0.02483	-0.4964	0.00835	-15.721	0.26435	0.87302	-5.1581	0.273	0.0070
-9	-0.4285	0.07914	-5.4151	-0.1025	0.03363	-0.4356	0.01113	-13.798	0.35236	0.77407	-4.0584	0.214	0.0062
-8	-0.3846	0.06733	-5.7117	-0.0813	0.04064	-0.3902	0.01315	-12.357	0.41656	0.70082	-3.2182	0.17	0.0055
-7	-0.3387	0.0571	-5.9313	-0.0598	0.04742	-0.3431	0.0154	-10.867	0.48772	0.62009	-2.3677	0.123	0.0050
-6	-0.2912	0.04845	-6.0102	-0.0374	0.05466	-0.2946	0.01775	-9.3315	0.56199	0.53537	-1.4812	0.071	0.0043
-5	-0.243	0.04101	-5.9253	-0.0164	0.06035	-0.2456	0.01967	-7.7794	0.62311	0.44786	-0.6497	0.028	0.0037
-4	-0.2037	0.03538	-5.7582	5.8E-06	0.06428	-0.2057	0.02108	-6.5137	0.66762	0.38019	0.00023	-0.006	0.0031
-3	-0.1563	0.03087	-5.0642	0.01987	0.06916	-0.1577	0.02265	-4.9953	0.71719	0.28457	0.7868	-0.05	0.0025
-2	-0.1171	0.02794	-4.1898	0.03652	0.07339	-0.1180	0.02384	-3.7367	0.75509	0.21839	1.44574	-0.085	0.0020
-1	-0.08	0.02707	-2.956	0.05128	0.07643	-0.0805	0.02567	-2.549	0.813	0.16089	2.03013	-0.118	0.0014
0	-0.0356	0.02702	-1.316	0.07122	0.08233	-0.0356	0.02702	-1.1262	0.85575	0.08978	2.81962	-0.158	0.0007
1	0.00563	0.02811	0.20028	0.08833	0.08642	0.0061	0.028	0.19378	0.8869	0.01296	3.49683	-0.195	0.0002
2	0.05978	0.03191	1.87342	0.11239	0.09338	0.0609	0.0298	1.92733	0.94387	-0.0725	4.4495	-0.24	-0.0006
3	0.10611	0.037	2.86757	0.13388	0.10016	0.1079	0.0314	3.41726	0.99441	-0.1644	5.30032	-0.29	-0.0026
4	0.16211	0.04466	3.63037	0.15574	0.10523	0.1648	0.03324	5.22052	1.05267	-0.2571	6.20534	-0.331	-0.0021

110 mph Tunnel Wall Corrections Corrected values = "new"

σ	0.0201
V new	112.37
Renew	1294501

ε_{sb} =0.00104 0.00104

ε_{wb} varies with C_D

$\varepsilon = \varepsilon_{sb} + \varepsilon_{wb}$

εwb	ε	q new	AOAu (deg)	AOA new	CL	CL new	CD	CD new	CM	CM(1/4c)	CM(1/4c) new	CN
0.0157	0.0168	33.0013	-10.00	-10.0639	-0.4874	-0.4612	0.0944	0.0898	-0.1303	0.1386	0.1316	-0.4964
0.0132	0.0142	32.8387	-9.00	-9.0540	-0.4285	-0.4077	0.0791	0.0758	-0.1025	0.1335	0.1276	-0.4356
0.0112	0.0123	32.7130	-8.00	-8.0466	-0.3846	-0.3674	0.0673	0.0649	-0.0813	0.1301	0.1250	-0.3902
0.0095	0.0106	32.6042	-7.00	-7.0389	-0.3387	-0.3247	0.0571	0.0554	-0.0598	0.1261	0.1218	-0.3431
0.0081	0.0091	32.5121	-6.00	-6.0309	-0.2912	-0.2800	0.0484	0.0472	-0.0374	0.1222	0.1186	-0.2946
0.0068	0.0079	32.4329	-5.00	-5.0231	-0.2430	-0.2343	0.0410	0.0401	-0.0164	0.1166	0.1136	-0.2456
0.0059	0.0069	32.3729	-4.00	-4.0169	-0.2037	-0.1968	0.0354	0.0347	0.0000	0.1114	0.1089	-0.2057
0.0051	0.0062	32.3250	-3.00	-3.0093	-0.1563	-0.1512	0.0309	0.0303	0.0199	0.1053	0.1033	-0.1577
0.0047	0.0057	32.2939	-2.00	-2.0030	-0.1171	-0.1134	0.0279	0.0275	0.0365	0.1004	0.0987	-0.1180
0.0045	0.0056	32.2846	-1.00	-0.9973	-0.0800	-0.0775	0.0271	0.0266	0.0513	0.0949	0.0934	-0.0805
0.0045	0.0055	32.2840	0.00	0.0101	-0.0356	-0.0345	0.0270	0.0266	0.0712	0.0905	0.0893	-0.0356
0.0047	0.0057	32.2956	1.00	1.0166	0.0056	0.0055	0.0281	0.0277	0.0883	0.0850	0.0841	0.0061
0.0053	0.0064	32.3360	2.00	2.0255	0.0598	0.0578	0.0319	0.0313	0.1124	0.0794	0.0787	0.0609
0.0062	0.0072	32.3903	3.00	3.0332	0.1061	0.1024	0.0370	0.0362	0.1339	0.0754	0.0749	0.1079
0.0074	0.0085	32.4717	4.00	4.0420	0.1621	0.1561	0.0447	0.0436	0.1567	0.0675	0.0671	0.1648

APPENDIX E: PRICE WAVERIDER PHOTOGRAPHS

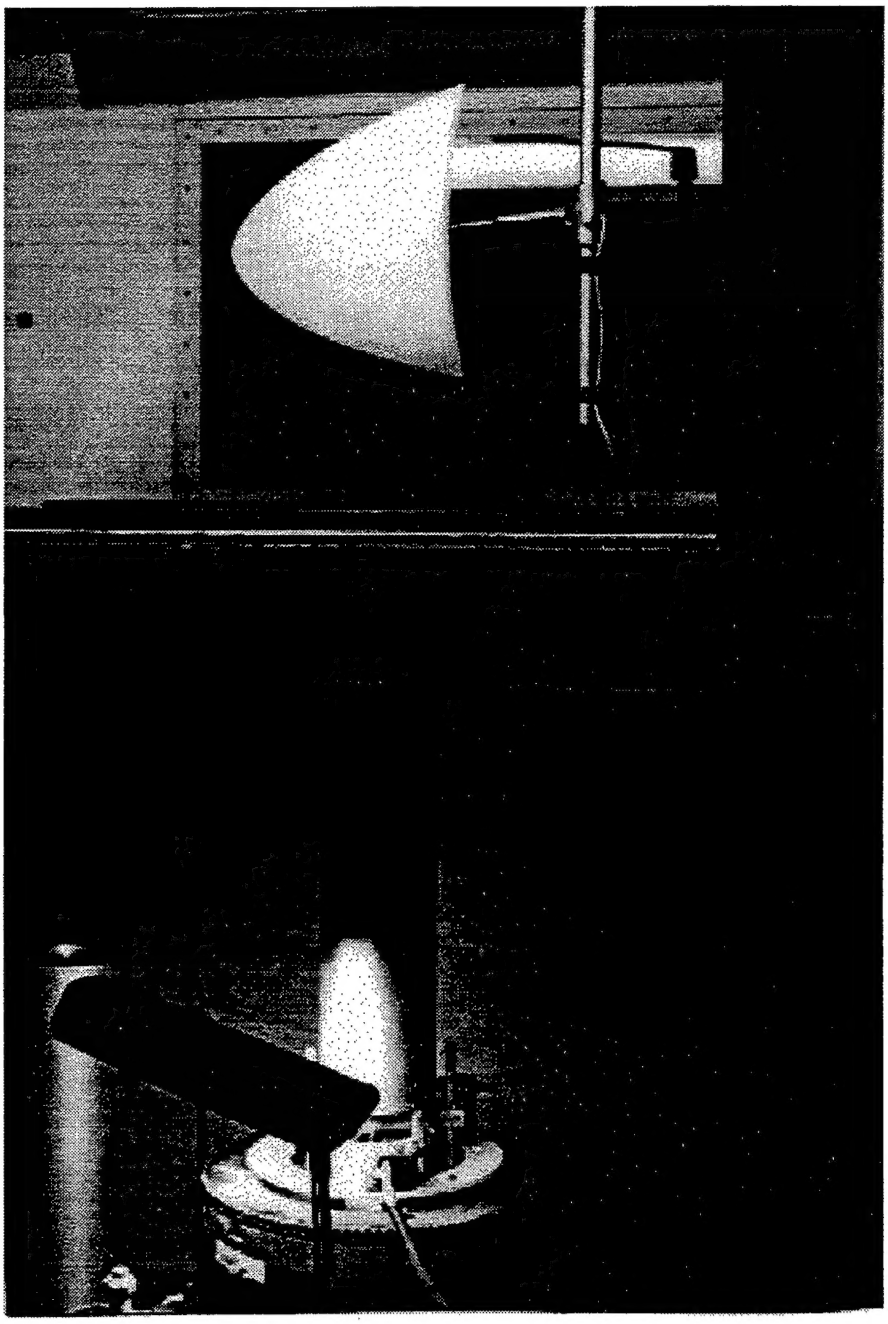

Price Waverider As Seen From Outside Wind Tunnel
Turntable Mechanism Is Visible Below

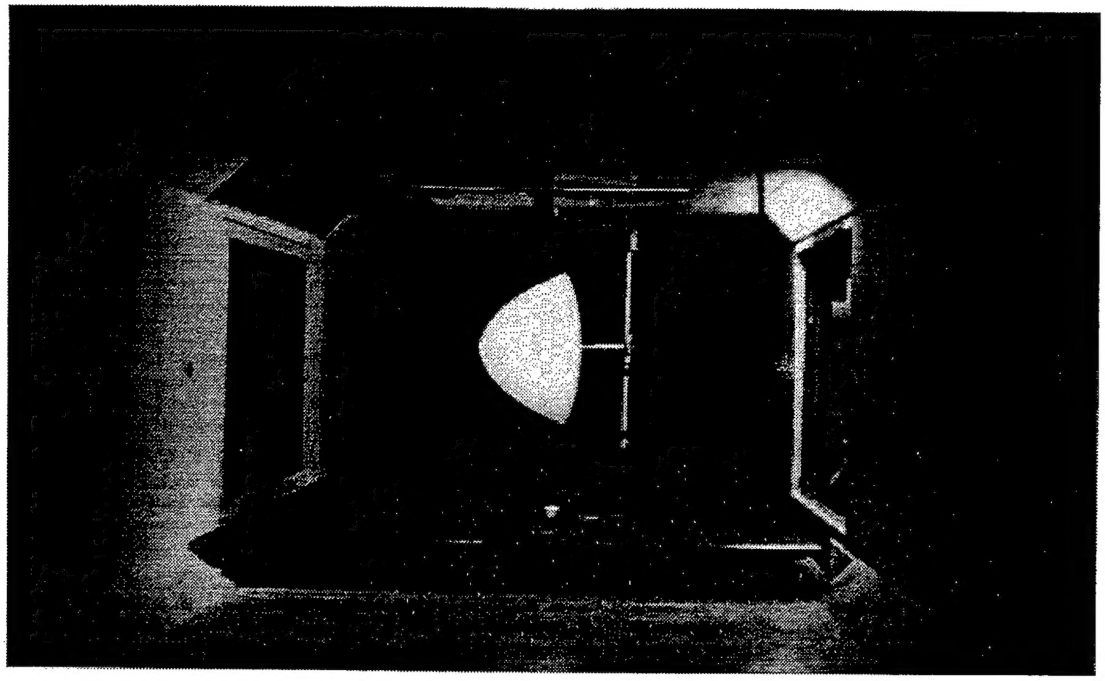

Price Waverider As Seen From Settling Chamber, Negative AOA

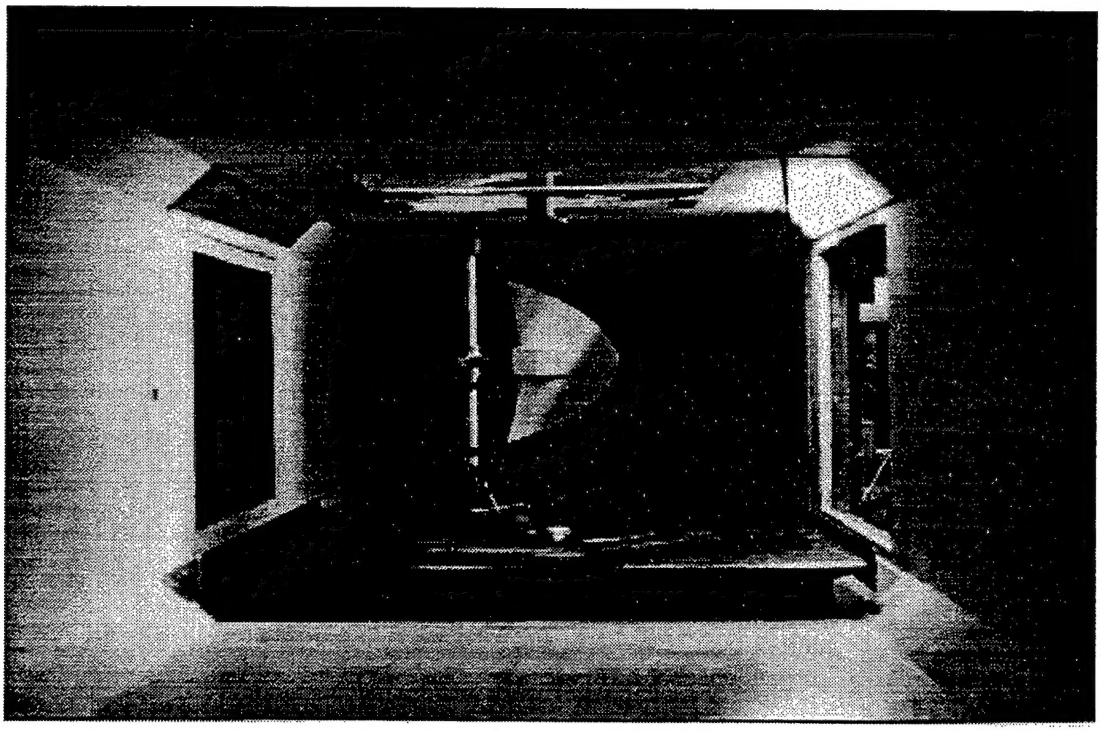

Price Waverider As Seen From Settling Chamber, Positive AOA

INITIAL DISTRIBUTION LIST

No. Copies

1. Defense Technical Information Center.....2
   8725 John J. Kingman Road, Ste 0944
   Ft. Belvoir, Virginia 22060-6218

2. Dudley Knox Library 2
   Naval Postgraduate School
   411 Dyer Road,
   Monterey, California 93943-5101

3. Dr. Conrad F. Newberry.....1
   Dept. of Aeronautics and Astronautics
   AA/Ne
   Naval Postgraduate School
   Monterey, California 93943

4. Dr. Richard M. Howard.....1
   Dept. of Aeronautics and Astronautics
   AA/Ho
   Naval Postgraduate School
   Monterey, California 93943

5 Dr. Max F. Platzer.....1
   Dept. of Aeronautics and Astronautics
   AA/PL
   Naval Postgraduate School
   Monterey, California 93943

6. Dr. M.S. Chandrasekhara.....1
   Navy-NASA Joint Institute of Aeronautics
   Fluid Mechanics Laboratory, MS 260-1
   NASA Ames Research Center
   Moffett Field, California 94035-1000

7. Dr. Anthony Dietz 1
   Senior Research Scientist, MCAT Inc.
   Fluid Mechanics Laboratory, MS 260-1
   NASA Ames Research Center
   Moffett Field, CA 94035-1000

8. Mr. Jeffrey V. Bowles.....1
   Systems Analysis Branch, MS 237-11
   NASA Ames Research Center
   Moffett Field, CA 94035-1000

9. Dr. John D. Anderson, Jr.....1
Professor
Aerospace Engineering Department
University of Maryland
College Park, Maryland 20742

10. Dr. Mark J. Lewis.....1
Professor
Aerospace Engineering Department
University of Maryland
College Park, Maryland 20742

11. Dr. Isaiah M. Blankson.....1
Senior Technologist
NASA Lewis Research Center
MS 5-9, Room 109
2100 Brookpark Rd.
Cleveland Ohio 44135

12. Mr. Edward L Jeter.....1
Code 4731FOD
NAWC-WD
China Lake, California 93555

13. LT Mike Huff.....1
511 Coffman St.
Pinckneyville, Illinois 62274